



2  
(1999)



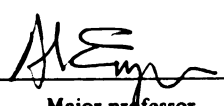
This is to certify that the  
thesis entitled  
PERFORMANCE ASSESSMENT OF RADIAL VANELESS  
DIFFUSERS FOR CENTRIFUGAL COMPRESSORS

presented by

Fahed A.N. AL-Awaidy

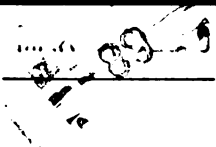
has been accepted towards fulfillment  
of the requirements for

Ph.D. degree in Mechanical Engineering

  
Major professor

Date 11-09-98

PLACE IN RETURN BOX to remove this checkout from your record.  
 TO AVOID FINES return on or before date due.  
 MAY BE RECALLED with earlier due date if requested.

DATE DUE	DATE DUE	DATE DUE
		
<del>JAN 02 2004</del>		
<del>JUN 19 2004</del> <del>JAN 25 2005</del>		

**PERFORMANCE ASSESSMENT OF RADIAL VANELESS  
DIFFUSERS FOR CENTRIFUGAL COMPRESSORS**

**By**

**Fahed A. N. AL-Awaidy**

**A DISSERTATION**

**Submitted to  
Michigan State University  
in partial fulfillment of the requirements  
for the degree of**

**DOCTOR OF PHILOSOPHY**

**Department of Mechanical Engineering**

**1998**



## **ABSTRACT**

### **PERFORMANCE ASSESSMENT OF RADIAL VANELESS DIFFUSERS FOR CENTRIFUGAL COMPRESSORS**

**By**

**Fahed A. N. AL-Awaidy**

Vaneless radial diffusers continue to be used widely with industrial centrifugal compressors, and many experimental and analytical studies have investigated their steady and unsteady effects on the compressor stage.

In vaneless diffusers of centrifugal compressors, many different flow phenomena interfere with one another and different geometric parameters influence the flow field. Variations of these parameters allow the designer to optimize the vaneless diffuser for certain applications or to use a variable geometry to control the stage over a wide range. Among the main geometrical parameters affecting the vaneless diffuser performance are the ratio of vaneless diffuser inlet width to impeller radius ( $b_3/r_2$ ) and the ratio of vaneless diffuser outlet radius to impeller radius ( $r_5/r_2$ ) which is also called radius ratio.

Two vaneless diffusers, VNLD1 and VNLD2, that differ in their passage widths (VNLD2 wider than VNLD1) are tested experimentally downstream of the same centrifugal impeller to investigate the effect of this variation on the overall compressor stage performance. Each diffuser was tested at four different impeller speeds, which are

18800 rpm, 24000 rpm, 28000 rpm, and 32000 rpm respectively. These speeds corresponds to impeller tip Mach numbers of  $M_t = 0.7, 0.89, 1.04, \text{ and } 1.19$  respectively. A theoretical analysis was carried out also from the diffuser inlet radius to the diffuser outlet radius using different values of radius ratio. The results of this theoretical analysis were compared to the measured performance curves of both vaneless diffusers.

The analysis and comparison of these two vaneless diffusers resulted in a detailed description of the actual flow mechanism in these diffusers. The influence of geometrical and aerodynamical parameters of both vaneless diffusers on the compressor stage performance was studied and investigated. Also the pressure recovery characteristics were studied and compared for both vaneless diffusers. In addition to the steady performance analysis, unsteady performance analyses of the compressor stage with both vaneless diffusers have been carried out. The results showed that the centrifugal compressor stage has better overall performance with VNLD2 than with VNLD1 at impeller speeds of 18800 rpm, 24000 rpm, and 28000 rpm. At impeller speed of 32000 rpm, VNLD1 was better. In terms of flow coefficient, the centrifugal compressor with VNLD2 showed wider range of flow operation than with VNLD1 at all impeller rotational speeds.

**To my parents, my wife, my kids, and my teachers**

## **ACKNOWLEDGMENTS**

In the beginning, I thank Allah (SWT) for the completion of this dissertation. Then, I would like to express my deepest gratitude to Professor Abraham Engeda, the chairperson of my committee, for his wise advice, understanding, encouragement, and kind support throughout my study in the department of Mechanical Engineering at Michigan State University. I am also grateful to the other members of my committee, Professor John McGrath, Professor Craig Somerton, and Professor Patricia Lamm for their encouragement, kindness, and valuable comments.

My appreciation also goes to the General Organization for Technical Education and Vocational Training in Riyadh, Saudi Arabia, which granted me a scholarship to pursue my graduate study in the USA. I would like to express my thanks to other individuals who contributed, in some way, to the completion of this research especially my colleagues in the Turbomachinery Lab., Michigan State University. I thank also Mr. Craig Gunn for his help in preparing my dissertation.

Last but certainly not the least, my thanks and deep appreciation go to my parents for their love and support at all times. Also I would like to express my indebtedness, appreciation and gratitude to great companion, my wife Badriyah Al-Jmaiaah, the most important person who stood by me and was a trusted friend and a compassionate partner in all my life. Her emotional support, understanding, love and constant encouragement made my life much happier and my work much easier. I am also grateful to my

daughters, Hessah and Lujain, and my sons, Abdullah and Mohamad, for the joy they brought into our life and for their love which have been my source of motivation.

# TABLE OF CONTENTS

<b>LIST OF TABLES.....</b>	<b>IX</b>
<b>LIST OF FIGURES.....</b>	<b>X</b>
<b>NOMENCLATURE.....</b>	<b>XIII</b>
<b>1. INTRODUCTION .....</b>	<b>1</b>
1.1 TURBOMACHINES: DEFINITION AND CATEGORIZATION .....	1
1.2 THE CENTRIFUGAL COMPRESSOR.....	2
1.2.1 <i>Steady flow in centrifugal compressor</i> .....	4
1.2.2 <i>Centrifugal Compressor Stall</i> .....	6
1.3 OBJECTIVE OF THE CURRENT WORK.....	9
<b>2. FLOW IN VANELESS DIFFUSERS .....</b>	<b>13</b>
2.1 TYPES OF RADIAL DIFFUSERS.....	13
2.1.1 <i>Vaned Diffuser</i> .....	13
2.1.2 <i>Vaneless Diffuser</i> .....	16
2.2 VANELESS DIFFUSER .....	17
2.2.1 <i>Mode of Operation</i> .....	17
2.2.2 <i>Losses in Vaneless Diffuser</i> .....	20
2.3 RESEARCH STATUS ON VANELESS DIFFUSER .....	21
<b>3. THEORY OF DIFFUSION.....</b>	<b>34</b>
3.1 DIFFUSION PHENOMENON .....	34
3.2 PERFORMANCE PARAMETERS OF DIFFUSION .....	38
3.2.1 <i>Geometric Performance Parameters</i> .....	38
3.2.1.1 Passage Width/Radius .....	39
3.2.1.2 Length to Width Ratio .....	40
3.2.1.3 Divergence Angle.....	42
3.2.1.4 Vane Leading Edge Shape.....	45
3.2.1.5 Vane Shape .....	47
3.2.1.6 Area Ratio .....	48
3.2.1.7 Radius Ratio.....	49
3.2.1.8 Vane Number .....	51
3.2.1.9 Throat Blockage.....	53
3.2.1.10 Incidence.....	54
3.2.2 <i>Aerodynamic Performance Parameters</i> .....	55
3.2.2.1 Aerodynamic Blockage .....	56
3.2.2.2 Reynolds Number.....	57

3.2.2.3	Mach Number .....	58
3.2.2.4	Inlet Velocity Profile .....	59
3.2.3	<i>Overall Performance Parameters</i> .....	60
3.2.3.1	Pressure Recovery Coefficient.....	60
3.2.3.2	Effectiveness .....	62
3.2.3.3	Total Pressure Loss .....	62
3.2.3.4	Flow Range .....	62
3.2.3.5	Distortion .....	65
3.3	FLOW ANALYSIS IN VANELESS DIFFUSER .....	65
3.3.1	<i>Incompressible and Inviscid Flow</i> .....	68
3.3.2	<i>Compressible and Inviscid Flow</i> .....	74
<b>4.</b>	<b>EXPERIMENTAL SETUP .....</b>	<b>75</b>
4.1	THE CENTRIFUGAL COMPRESSOR TEST STAND .....	75
4.2	INVESTIGATED VANELESS DIFFUSERS.....	77
4.3	MEASUREMENT POSITIONS AND MEASUREMENTS .....	77
4.4	STEADY PERFORMANCE MEASUREMENT.....	82
4.4.1	<i>Instrumentation</i> .....	82
4.4.2	<i>Data Collection and Reduction</i> .....	83
4.4.3	<i>Instrument Accuracy and Result Uncertainty</i> .....	91
4.5	UNSTEADY PERFORMANCE MEASUREMENT .....	93
4.5.1	<i>Obtaining and Storing the Pressure Signal</i> .....	93
4.5.2	<i>Signal Processing</i> .....	95
4.5.3	<i>Analysis of the Data</i> .....	97
<b>5.</b>	<b>RESULTS AND DISCUSSIONS .....</b>	<b>99</b>
5.1	OVERALL COMPRESSOR STAGE PERFORMANCE CHARACTERISTICS .....	100
5.1.1	<i>Stage Efficiency and Head Coefficient</i> .....	100
5.1.2	<i>Flow Range</i> .....	104
5.1.3	<i>At Peak Efficiency</i> .....	105
5.2	PRESSURE RISE IN THE COMPRESSOR STAGE.....	107
5.3	OVERALL VANELESS DIFFUSER PERFORMANCE CHARACTERISTICS .....	110
5.3.1	<i>Vaneless Diffuser Efficiency</i> .....	110
5.3.2	<i>Pressure Recovery of the Vaneless Diffusers</i> .....	114
5.3.2.1	Total Pressure Recovery $C_{p2-5}$ .....	114
5.3.2.2	Subdivided Pressure Recoveries .....	117
5.4	COMPARISON BETWEEN THE EXPERIMENTAL AND THEORETICAL RESULTS.....	121
5.5	UNSTEADY PERFORMANCE OF THE COMPRESSOR STAGE.....	125
5.5.1	<i>Unsteady Flow in the Inducer</i> .....	126
5.5.2	<i>Unsteady Flow in the Impeller</i> .....	129
5.5.3	<i>Unsteady Flow in the Diffuser</i> .....	134
<b>6.</b>	<b>CONCLUSIONS AND RECOMMENDATIONS .....</b>	<b>136</b>
	<b>BIBLIOGRAPHY.....</b>	<b>140</b>

## **LIST OF TABLES**

Table 4-1 Design parameter of the tested vaneless diffusers.....	77
Table 4-2 Measurement Locations And Measured Quantities.....	81
Table 4-3 Instrument specifications.....	93
Table 5-1 Surge Characteristics through the Compressor Stage with VNLD1 and VNLD2 at all Impeller speeds Using Transducer D.....	134



## LIST OF FIGURES

Figure 1.1 Turbomachines categorization according to flow path: .....	3
Figure 1.2 Turbomachines categorization according to function: .....	3
Figure 1.3 Typical centrifugal compressor .....	5
Figure 1.4 Separation on a blade .....	6
Figure 1.5 Pattern of Rotating Stall (Pampreen 1993).....	8
Figure 2.1 Types of vaned diffusers .....	15
Figure 2.2 Assembly of centrifugal impeller and radial vaneless diffuser .....	16
Figure 2.3 Pressure-recovery coefficient versus range for vaned and vaneless Radial Diffusers (Wilson 1991) .....	17
Figure 2.4 Flow through centrifugal compressor stage .....	18
Figure 2.5 Velocity diagrams at impeller inlet and impeller exit.....	19
Figure 2.6 Enthalpy-Entropy diagram for the complete centrifugal compressor stage....	20
Figure 2.7 Flow path in vaneless diffuser (Elder and Forster 1987) .....	25
Figure 2.8 Critical Inlet Flow Angle vs. Diffuser Width (Frigne 1980).....	29
Figure 2.9 Diffuser inlet shape .....	30
Figure 3.1 Diffusion mechanisms: (a) isolated airfoil; (b) duct diffuser .....	35
Figure 3.2 Diffuser types based on shape: a) conical, b) annular, c) square section, d) two-dimensional or rectangular (channel) .....	36
Figure 3.3 Diffusion in a constant-area bend .....	37
Figure 3.4 Simple schematic of the channel diffuser (Runstadler, et al. 1975) .....	39
Figure 3.5 Comparison of compressor maps (Stein and Rautenberg 1985) .....	40
Figure 3.6 Pressure rise through the vaned diffuser (Clements and Artt 1988).....	41
Figure 3.7 Representative locations of several optima of performance.....	43
Figure 3.8 Diffuser performance map, $AS=0.25$ , $M=0.6$ , $B=0.08$ .....	44
Figure 3.9 Compressor flow range and compressor efficiency versus $2\theta$ (Clements and Artt 1987).....	45
Figure 3.10 Leading edge shapes (Yoshinaga et. al. 1980) .....	46
Figure 3.11 Effect of leading edge shapes on the stage efficiency (Yoshinaga et. al. 1980) .....	46
Figure 3.12 Diffuser recovery (Bammert et. al. 1983) .....	48
Figure 3.13 Pressure recovery of vaneless and vaned diffusers versus area ratio.....	49
Figure 3.14 Circumferential static pressure distribution (Jiang and Yang 1982) .....	50
Figure 3.15 Effect of diffuser vane number (Rodgers 1982) .....	51
Figure 3.16 Blade number effects for $r_{1in}/r_2=1.106$ (Camatti et. al. 1995).....	52
Figure 3.17 Comparison of measured and boundary-layer predicted stall limit .....	54
Figure 3.18 Effect of diffuser leading edge Mach number and incidence on range (Reeves 1977).....	55
Figure 3.19 Aerodynamic blockage.....	57
Figure 3.20 Choke and surge.....	63
Figure 3.21 Different kinds of surge (Cumpsty 1989).....	65
Figure 3.22 Elementary View of Flow in Vaneless Diffuser.....	67

Figure 4.1 Centrifugal Compressor test rig.....	75
Figure 4.2 Impeller of the tested configuration.....	76
Figure 4.3 Measurement planes in inlet pipe .....	78
Figure 4.4 Measurement Planes in the Compressor Stage.....	79
Figure 4.5 Probe location in the diffuser.....	80
Figure 4.6 Unsteady pressure signal flow path .....	97
Figure 5.1 Performance characteristics of the compressor stage with VNLD1 .....	102
Figure 5.2 Performance characteristics of the compressor stage with VNLD2 .....	103
Figure 5.3 Total operating range of the compressor stage with VNLD1 and VNLD2 vs. impeller tip Mach number $M_t$ .....	104
Figure 5.4 Compressor stage at peak efficiency vs. impeller tip Mach number $M_t$ for VNLD1 and VNLD2 .....	105
Figure 5.5 Loss coefficient at peak efficiency vs. $M_t$ for VNLD1 and VNLD2.....	106
Figure 5.6 Influence of diffuser type on the compressor stage pressure history with VNLD1 .....	108
Figure 5.7 Influence of diffuser type on the compressor stage pressure history with VNLD2 .....	109
Figure 5.8 Vaneless diffuser performance characteristics: diffuser efficiency total-to- static for VNLD1 and VNLD2.....	111
Figure 5.9 Vaneless diffuser performance characteristics: diffuser efficiency static-to- static for VNLD1 and VNLD2.....	112
Figure 5.10 Variation of Total Diffuser Pressure Recovery $C_{p2-5}$ for VNLD1.....	115
Figure 5.11 Variation of Total Diffuser Pressure Recovery $C_{p2-5}$ for VNLD2.....	115
Figure 5.12 Pressure Recovery $C_{p2-3}$ for VNLD1 .....	116
Figure 5.13 Pressure Recovery $C_{p2-3}$ for VNLD2 .....	116
Figure 5.14 Pressure Recovery $C_{p3-4}$ for VNLD1 .....	118
Figure 5.15 Pressure Recovery $C_{p3-4}$ for VNLD2 .....	118
Figure 5.16 Pressure Recovery $C_{p4-5}$ for VNLD1 .....	119
Figure 5.17 Pressure Recovery $C_{p4-5}$ for VNLD2 .....	119
Figure 5.18 Variation in the Static Pressure Ratio with the Radius ratio for VNLD1 and VNLD2 .....	122
Figure 5.19 Variation in the squared of Local Flow Mach Number with the Radius ratio for VNLD1 and VNLD2.....	123
Figure 5.20 Power spectrum of the compressor stage with VNLD1 at 32000 rpm Transducer A.....	127
Figure 5.21 Power spectrum of the compressor stage with VNLD2 at 32000 rpm Transducer A.....	128
Figure 5.22 Power spectrum of the compressor stage with VNLD1 at 32000 rpm Transducer C .....	130
Figure 5.23 Power spectrum of the compressor stage with VNLD2 at 32000 rpm Transducer C .....	131
Figure 5.24 Power spectrum of the compressor stage with VNLD1 at 32000 rpm Transducer D.....	132
Figure 5.25 Power spectrum of the compressor stage with VNLD2 at 32000 rpm Transducer D.....	133

## NOMENCLATURE

$A$	area ( $\text{m}^2$ )
$\vec{A}$	area vector
$a$	speed of sound
$b$	diffuser width, width at the impeller exit (mm)
$C$	absolute velocity (m/s)
CVND	conventional vaned diffuser
$C_p$	pressure recovery coefficient
$c_p$	specific heat (J/kg K)
$d, D$	diameter (mm)
$F$	Force (N)
$g$	acceleration of gravity ( $\text{m/s}^2$ )
$h$	enthalpy per unit mass (J/kg)
$M$	local flow Mach number
$M_t$	impeller tip Mach number
$m$	mass (kg)
$\dot{m}$	mass flow rate (kg/s)
$N, \Omega$	rotational speed (rpm)
$P$	pressure ( $\text{N/m}^2$ )
$R$	gas constant (J/kg.K)
$r$	radial coordinate, radius (m)
$T$	temperature ( $^{\circ}\text{C}$ ), torque (N.m)

$U$	impeller or tip speed (m/s)
$\vec{V}$	velocity vector
$\Psi$	volume ( $\text{m}^3$ )
VNLD	vaneless diffuser
$W$	relative velocity (m/s)
$w$	work done by a unit mass of flowing fluid (J/kg)
$Z$	vane number
$z$	axial coordinate

### **Greek Symbols**

$\alpha$	flow angle with respect to tangent (deg)
$\beta$	vane angle with respect to tangent (deg)
$\phi$	flow coefficient
$\gamma$	ratio of specific heats
$\eta$	efficiency
$\eta_{\text{diff}}$	diffuser effectiveness
$\lambda$	radius ratio across the diffuser
$\mu$	dynamic viscosity ( $\text{kg}/(\text{ms}) = \text{N s}/\text{m}^2$ ), work coefficient
$\nu$	kinematic viscosity ( $\text{m}^2/\text{s}$ )
$\pi$	pressure ratio
$\rho$	density ( $\text{kg}/\text{m}^3$ )
$\tau$	temperature ratio

$\xi$	loss coefficient
$\psi$	head coefficient

### **Superscripts**

.	time rate of change
-	average or mean value
o	degree

### **Subscripts**

0	stagnation or total condition
1	stage inlet, diffuser number
2	impeller exit, diffuser number
2a	impeller exit - measurement station
3	diffuser inlet
4	diffuser middle - measurement station
5	diffuser exit
6	stage exit
c	compressor
r	radial component
s	isentropic, surface
u	circumferential or tangential component
z	axial component

# **1. INTRODUCTION**

## **1.1 Turbomachines: Definition and Categorization**

Turbomachines could be defined as all devices in which energy is transferred either to or from a continuously flowing fluid by dynamic action of one or more moving blade rows. The rotation of these blade rows (rotor) changes the stagnation enthalpy of the fluid moving through it by either doing positive work (producing power) or negative work (absorbing power), depending upon the effect required of the machine. These enthalpy changes are linked with the pressure changes occurring simultaneously in the fluid. Machines that could be classified as turbomachines are fans, pumps, compressors, and turbines. The term pump is used when referring to machines that increase the pressure of a flowing liquid. Fan is used for machines imparting only a small increase in pressure to a flowing gas. A compressor gives a substantial rise in pressure to a flowing gas. The boundary between fans and compressors is often taken as the area where the pressure ratio across the machine is 1.05-1.1. The subject matter usually included under turbomachines is restricted moreover to the energy exchange process between the rotor of a turbomachine and the fluid passing through it. Topics such as turbine blade vibrations are therefore excluded.

The categorization of turbomachines varies depending on the purpose of each. They could be categorized by flow path as indicated by the simple diagram in Figure 1.1. As indicated by this Figure, the machine could be termed an axial flow turbomachine when the path of the through-flow is parallel to the axis of rotation. On the other hand, the machine could be termed a radial (centrifugal) flow turbomachine when the path of the through-flow is in a plane perpendicular to the axis of rotation. The mixed flow term refers to the direction of the through-flow at rotor outlet when both radial and axial velocity components are present in significant amounts.

Turbomachines could be categorized also by function. Referring to Figure 1.2, they could be categorized as those absorbing power to increase the fluid pressure or head (fans, compressors, and pumps) and those that produce power by expanding fluid to a lower pressure or head (hydraulic, steam, and gas turbines). Analysis and discussion throughout this work are limited to the diffusion process in the centrifugal compressors.

## **1.2 The Centrifugal Compressor**

In the 1940s and early 1950s most of the gas turbine engines designed and/or built in the United States used centrifugal-flow compressors. Today, gas turbine engines are built with axial-flow compressors, centrifugal-flow compressors, and combinations of one or more axial-flow stages followed by a centrifugal-flow compressors. Interest in the centrifugal compressors rises because of the wide field of their applications, e.g., in small gas turbines for road vehicles and commercial and military helicopters as well as for diesel engine turbochargers, chemical plant processes, factory workshop air supplies, and large-scale air-conditioning plants, etc. The centrifugal compressor has more than one advantage over the axial unit. The construction of the centrifugal compressor is simple

and rugged, which results in a lower drop in performance with adherence of dust to blades. It has higher stage pressure ratio than the axial compressor. It has a shorter length for the same pressure ratio, wider range of stable operation between surging and choking limits at a given rotational speed, and a flow direction of discharge air that is convenient for the installation of an intercooler and/or heat exchanger.

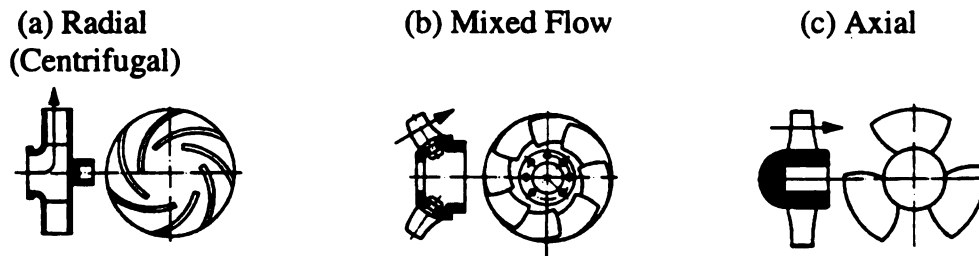


**Figure 1.1 Turbomachines categorization according to flow path:**

**(a) Radial (or centrifugal); (b) Mixed flow; (c) Axial**

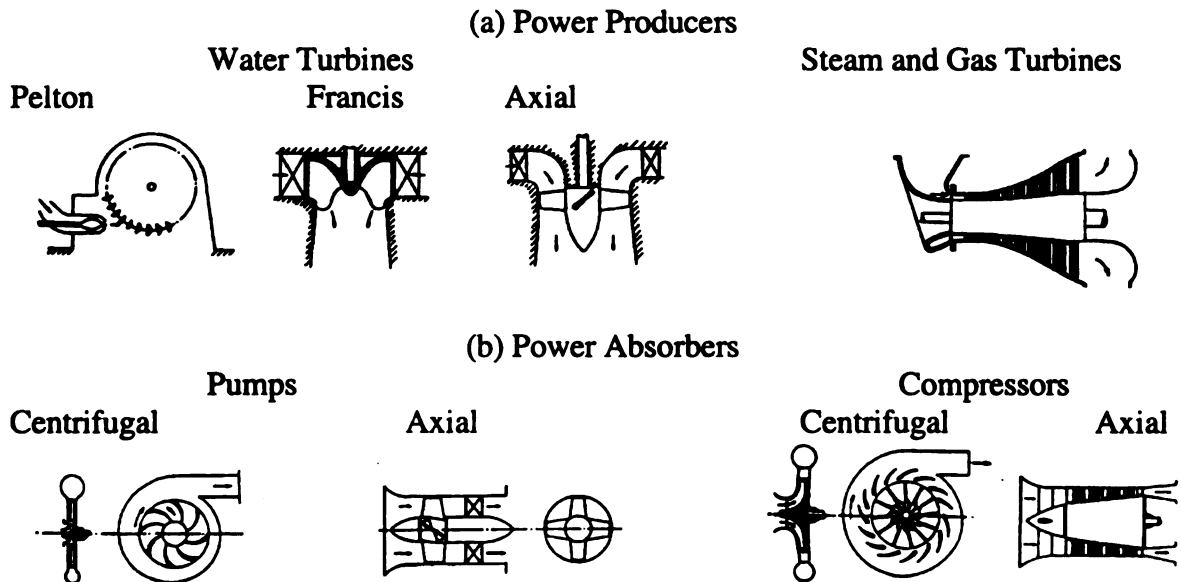


**Figure 1.2 Turbomachines categorization according to function:**

**(a) Power producers; (b) Power absorbers**



### **1.2.1 Steady flow in centrifugal compressor**

Figure 1.3 shows a common type of centrifugal compressor. It consists essentially of a rotating impeller followed by diffuser. Fluid enters the impeller through the eye or inducer, whose function is to turn the relative flow as it enters the impeller passages. If there are no prewhirl vanes in front of the impeller, the fluid flow into the impeller will be in the axial direction. For this case the impeller blades should be curved in the direction of rotation for smooth entry. The amount of curvature (twist) varying from hub to tip at the inlet and depending on the axial velocity and the impeller rotational speed.

The function of the impeller is to increase the energy level of the fluid by whirling it outwards, thereby increasing the angular momentum of the fluid. Both the static pressure and the velocity are increased within the impeller. At the impeller exit, the blades shown in Figure 1.3 are straight and in the radial direction. The velocity of the air leaving this impeller, in contrast to that of the air leaving the axial impeller or rotor, has no axial component. After leaving the impeller, the air passes through a radial diffuser, consisting of vaned or vaneless flow passages in which momentum is exchange for pressure. Radial diffusers may consist of a vaneless portion, as shown, followed by a series of stator vanes. The purpose of the diffuser is to convert the kinetic energy, which is as high as 50% of the total energy added by the impeller, of the fluid leaving the impeller into pressure energy. This shows the significance that a well-designed diffuser can have on the stage efficiency.

In the case of vaneless diffusers (VNLD), the flow is further decelerated downstream of the jet-wake mixing process. However, the radial component is reduced by the increase of the flow area, which is determined by the conservation of mass; while

the tangential component is reduced with increase in radius, which is determined by the conservation of angular momentum. The VNLD provides a wide operating range with a reasonable efficiency.

In the case of a conventional vaned diffuser (CVND), the vanes are separated from the impeller by a short vaneless space in which the jet and wake mix and the flow is decelerated to subsonic velocities. In the semivaneless space, the region between the leading edge and throat of the diffuser changes the pattern of the isobar from nearly parallel to perpendicular to the flow direction. In the divergent channel, a further decrease of the velocity is realized with a subsequent increase of static pressure, which leads to an excellent performance. The throat of the CVND limits the maximum massflow that can flow through the compressor stage. If the massflow is reduced, the boundary layers in the diffuser channel can be so weak that separation occurs.

The air leaving the diffuser is then directed either to a return channel (if the stage is followed by additional stages) or to the collector. The function of the collector, which is also called scroll or volute, is to collect the flow from the diffuser and deliver it to the outlet pipe.

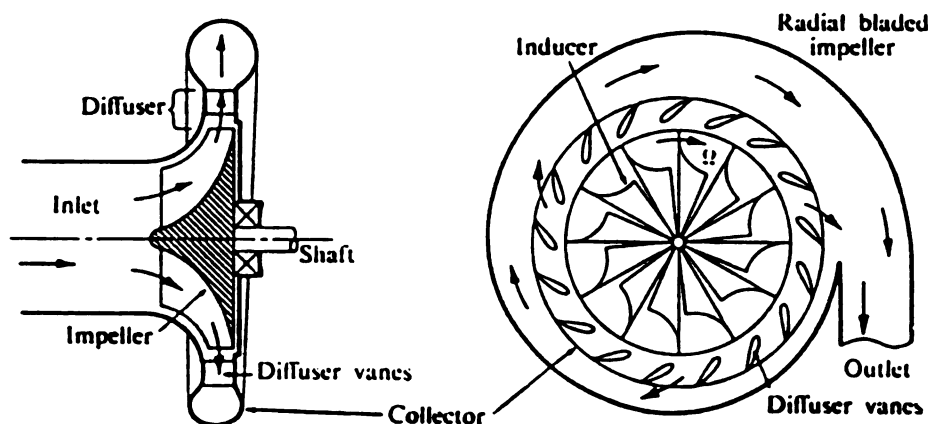


**Figure 1.3 Typical centrifugal compressor**

### 1.2.2 Centrifugal Compressor Stall

Stall can be regarded as the cessation of continued rise in lift on an airfoil to the former or in static pressure recovery in a diffuser or cascade to the latter. In the either case, stall is the result of boundary layer separation. In cascade aerodynamics, stall refers to a drop in the turning angle and lift ( $C_L$ ). The lift achieves a maximum just before the stall occurs as angle of attack increases from low values to high values. At a certain angle of incidence the flow separates on the suction side like shown in Figure 1.4. Similarly, stall can occur if the diffusion is too high. The flow will separate, if the kinetic energy in the flow is too low to sustain the flow against the forces caused by the adverse pressure gradient.

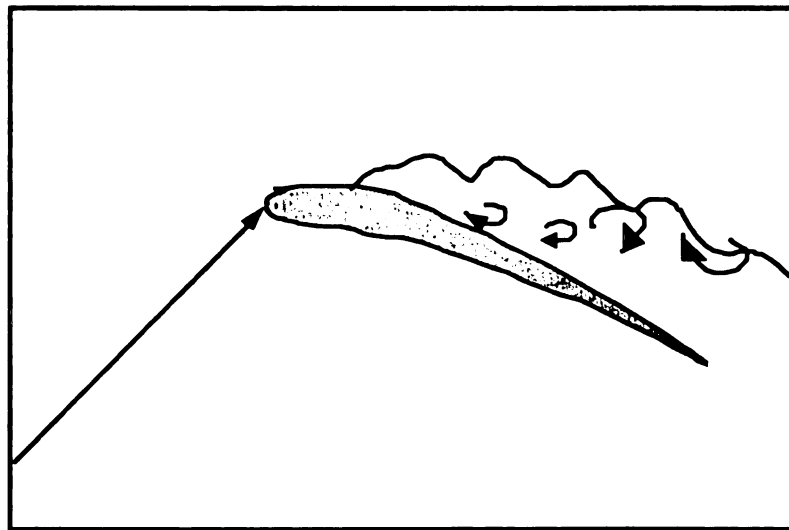


**Figure 1.4 Separation on a blade**

Stall can be defined as the response of a component on a local separation of the boundary layer. The corresponding perturbation can propagate upstream and downstream but is triggered by impeller or diffuser flow. It limits the pressure rise that can be achieved in one component of the compressor and can occur at positive and negative values of the pressure rise curve of the whole system. After Jansen (1964) investigated rotating pressure fluctuations in a vaneless radial diffuser both theoretically and

experimentally, it was necessary to extend the definition for stall. Jansen reported pressure fluctuations due to instability in the main flow. This is also called stall in the ongoing work. In contrast to stall, surge affects the whole system and not only certain components. The pressure fluctuations at a surged operating point are present in the compressor as well as in the inlet pipe and discharge pipe. Stall can appear in all components of the compressor stage, but this distortion disappears in the inlet and discharge pipe.

Rotating stall is a flow phenomenon characterized by rotating circumferential distortions in the flow field. Such distortions may be described by equidistant rotating zones of low flow surrounded by zones of relatively high flow, as shown in Figure 1.5. The zones of low flow are called stall cells and may rotate relative to the impeller. In rotating stall, impeller passages take turns stalling, then recovering. Rotating stall can occur as an intermittent series of local static pressure oscillations or as a continuous fluctuation of local static pressure. In both cases, large pressure oscillations indicate the presence of zones of retarded flow that rotate circumferentially either in the same or in the opposite sense as the rotor rotation.

Rodgers (1977a) showed that both impeller and diffuser can trigger rotating stall. The former is called impeller rotating stall; the latter is called diffuser rotating stall. Kaemmer (1984) reported that both impeller and diffuser influence the stall behavior of the other part. Despite this, most publications take only the impeller or diffuser in consideration by itself. This leads to non-comparable results in their stall investigations.

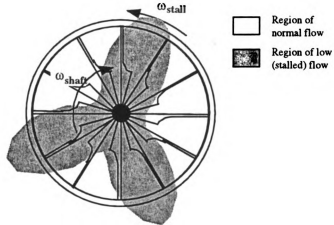


**Figure 1.5 Pattern of Rotating Stall (Pampreen 1993)**

Stall in the impeller can be due to unsteady phenomena in the inducer or in the radial part of the impeller. Both kinds of stall are of a different nature, so they will be treated here separately. Inducer stall can be observed only in compressors without inlet guide vanes. The flow separates if the incidence angle at the inducer is too high. Therefore, inducer stall is due to flow separation because of incidence.

For impeller rotating stall, pressure fluctuations occur throughout the entire meridional extent of blade channels. The boundary layer separates on the blade pressure side, and the subsequent backflow is supported strongly by the relative eddy effect. The fluid is first driven back along the blade pressure side and further upstream along the blade suction side towards the passage entry. Here fluid moves out of the passage into the inducer. If, due to the rotation, the passage flow conditions becomes more favorable, the passage flow can recover and the motion is repeated. However, in the case of stall the flow is separating at the pressure side, while the flow at a stable operation point separates at the suction side, due to the jet-wake pattern.

For diffuser stall, Jansen (1964) performed one of the first experimental and theoretical investigations in self-excited rotating pressure fluctuations. He showed in his calculations that even potential flow in a radial diffuser can become unstable. This instability causes rotating pressure perturbations. This has been called rotating stall based on patterns observed in axial cascades. Jansen suggested the separation of the three-dimensional wall boundary layer as a trigger for rotating stall. Diffuser stall resulted in a degradation of diffuser static pressure recovery. Overall stage efficiency and range are limited by this effect. Both amplitude and the rotational speed of the pressure pattern gradually increase as the mass flow rate in the machine is gradually decreased beyond the critically stable operating conditions.

### **1.3 Objective of the Current Work**

The demand for improved diffuser performance becomes increasingly insistent with refinement in impeller design and emphasis on high compressor efficiency. The energy size of a single stage centrifugal compressor can vary from few kilowatts to megawatts. The centrifugal compressor consists of three basic components: inducer, impeller, and diffuser. The heart of the compressor is the impeller, where all the energy transfer takes place; it would therefore be the likely suspect for any shortcomings that could occur. Surprisingly, the designer has had more success with the impeller than with the inducer or the diffusing system. In most centrifugal compressors both the rotor and the radial diffuser are limited by the diffusing capabilities of the flow channels.

At the inducer, the fluid comes from the pippins on board into the impeller, which could be rotating from 1000 to 100,000 rpm making it a challenging spot where the designer must apply all his knowledge and experience. The diffuser system is a

stationary part of the machine that accepts the fluid from the high speed impeller and slows it down; a high proportion of the fluid energy (50% sometimes) can be kinetic energy. The design of an appropriate diffusing system to slow down the fluid efficiently has been for a long time, and still is, one of the main difficulties in compressor design.

The diffuser system of a centrifugal compressor comes basically in two general categories either as a vaneless or vaned diffuser, each followed by a collector, a volute, or the next stage. Vaned diffusers can generally be further subdivided into two types depending on channel geometry as straight channel or curved channel, or depending on solidity as conventional or low solidity. In the vaneless diffuser, basically, diffusion occurs in a radial space bounded by two plane walls. The vaneless diffuser, the most common diffuser, employed for centrifugal compressors and pumps, is similar in flow physics to the channel, conical, and annular diffusers. It may be said to represent the most complex diffusion of these family of diffusers. Through the years a wide range of experimental research has been carried on conical, channel, and annular diffusers as discrete elements, as opposed to the vaneless diffuser, which has always been handled as part of a turbomachinery system.

Actual flow in the vaneless space is where the flow scrubs the side walls at high velocities, which results in a boundary layer growth from the initial conditions at the tip of the impeller. In order for boundary layer calculations to be made, these initial conditions must be known; but they are only vaguely understood today. Under the adverse pressure gradients in the vaneless space, the boundary layer grows. If it grows thick, significant secondary flows will develop.

The vaneless diffuser is the most popular diffuser because of its characteristics:

- simple and inexpensive construction
- wide operating range and
- the ability to reduce sonic absolute velocity to a subsonic one without the formation of shock waves

The flow in the vaneless diffuser is basically governed by the continuity, energy, and momentum equations. In practice, the compressor designer is often interested only in how certain aerodynamic parameters vary radially as the flow diffuses in the vaneless diffuser. The most important of these being:

- |                                  |                             |
|----------------------------------|-----------------------------|
| • $P$ , static pressure          | • $P_0$ , total pressure    |
| • $\alpha$ , flow angle          | • $\rho$ , density          |
| • $C$ , absolute velocity        | • $M$ , the Mach number.    |
| • $T$ , static temperature       | • $T_0$ , total temperature |
| • $rC_u$ , unit angular momentum |                             |

The fundamental part of any compressor, whether centrifugal or axial, is the impeller where the energy increase of the air passing through occurs. However, the impeller development is restricted by the mechanical limitations that permit very little variation in the blade or rotor design. However, no matter how good the impeller design from an aerodynamic point of view, the flow at the impeller exit needs to be modified for several reasons. For air delivery to a pipe system or to a second stage in a multistage machine, it is necessary to concentrate the flow in a given direction. Also, a considerable portion of the energy of the flow at the exit of the impeller is in the form of kinetic energy. This kinetic energy in the absence of guide vanes or a spiral casing is entirely lost, which results in lower stage efficiency. For these reasons, it is generally found



desirable to increase the static pressure at the expense of a reduced velocity of the air stream exiting from the impeller. This could be done in the stationary elements of the compressor. Therefore, diffuser design and development is the area that can provide further improvement in centrifugal compressor performance. Additionally, a diffuser is much less restricted by the mechanical limitations when compared to the impeller of a centrifugal compressor.

Due to the wide range of its operating conditions, vaneless diffusers have been used in SAUDI ARAMCO (Saudi ARAMCO Oil Company), SABIC (Saudi Basic Industries Corporation) and other companies in Saudi Arabia. Therefore, in Saudi Arabia research and development are needed on the vaneless diffuser.

This current work is based on a theoretical and experimental flow analysis of two vaneless diffusers. One of these vaneless diffusers is a typical industrial vaneless diffuser and the second one was designed by the MSU Turbomachinery Lab for high performance and good pressure recovery. The comparative theoretical and experimental study and analysis of these two vaneless diffusers is expected to give detailed information on:

- the actual flow mechanism in these diffusers
- the influence of geometrical parameters on the diffuser performance
- the influence of aerodynamic parameters on the diffuser performance
- the pressure recovery characteristics and
- performing unsteady performance analysis of the compressor

These two vaneless diffusers will be tested downstream of the same impeller at the MSU Turbomachinery Lab. The theoretical and experimental results will be compared.

## **2. FLOW IN VANELESS DIFFUSERS**

### **2.1 Types of Radial Diffusers**

Different types of radial diffusers have been used and developed. This is a result of the wide applications of the centrifugal compressors to increase the pressure ratio and efficiency. Radial diffusers could be divided into two types: vaned diffusers and vaneless diffusers.

#### **2.1.1 Vaned Diffuser**

The concept of the vaned diffuser is to shorten the flow path compared to the long flow path in the vaneless diffuser. Also, vanes can be used to direct the flow more in the radial direction, to increase the rate of diffusion, and to decrease the losses. The efficiency is related directly to the number of vanes in the diffuser. As the number of vanes increases, the angle of divergence is smaller; and the efficiency increases until friction and blockage overcome the advantage of more gradual diffusion. With this advantage of higher efficiency (higher pressure recovery), the flow range is limited at low flow rate due to vane stall and due to throat choke.

Vaned diffusers may be of many forms, some of which are illustrated as follows (Figure 2.1):

**Straight Channel/Wedge Diffuser:** It has a simple geometry; and due to this simplicity, it is easy to manufacture and very popular. The disadvantage is its large size.

**Straight Plate Diffuser:** It has a large number of vanes,  $Z > 30$ , but the pressure recovery is not good. Like the Straight Channel/Wedge diffuser, it has simple geometry and is easy and inexpensive to manufacture.

**Vaned Island Diffuser:** This is a refined straight channel, which is used for a high pressure ratio and transonic inlet Mach number  $M_3 > 1$ . Again, it is large in size, but the number of vanes is small.

**Circular Arc Diffuser:** It has a simple geometry, so it is easy to manufacture; but it doesn't have any outstanding aerodynamic characteristic.

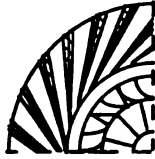
**Cambered/Aerofoil Diffuser:** This type of diffusers is used for transonic and subsonic flow applications. Small in size with a good pressure recovery, it has been designed based on axial cascade data.

**Twisted Diffuser:** It is a refined cambered vane, which has a 3-D twisted shape to produce good efficiency. It has a wide range and high pressure ratio.

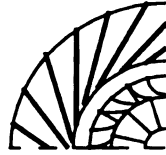
**Multiple Cascade Diffuser:** Again, it is a cambered vane in cascade to produce higher efficiency. Due to the high number of vanes at the increased radii, the risk of separation is reduced.

**Pipe/Conical Diffuser:** It is used for a higher pressure ratio and transonic flow applications. It is large in size but with good pressure recovery.

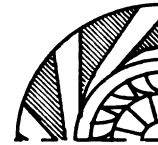
**Low Solidity Vaned Diffuser:** It is used for low flow angles or coefficients but with good pressure recovery and wide operating range. Nowadays, it is of great interest.



(a) Straight Channel Diffuser



(b) Straight Plate Diffuser



(c) Vaned Island Diffuser



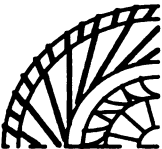
(d) Circular Arc Diffuser



(e) Cambered/Aerofoil Diffuser



(f) Twisted Diffuser



(g) Multiple Cascade Diffuser



(h) Pipe / Conical Diffuser



(i) Low Solidity Vane Diffuser

**Figure 2.1 Types of vaned diffusers**

### 2.1.2 Vaneless Diffuser

Diffusion in vaneless diffuser occurs in a radial space bounded by two plane walls as shown in Figure 2.2. Thus, a vaneless diffuser requires a considerable radial space, which results in the long path of the spiral flow that is the opposite of the vaned diffuser.

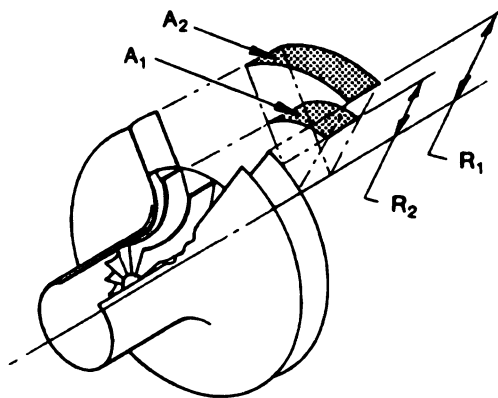


**Figure 2.2 Assembly of centrifugal impeller and radial vaneless diffuser**

The vaneless diffuser has certain inherent advantages over the vaned diffuser. The vaneless diffuser has a wide range of air flows and tip speeds over the vaned diffuser as shown in Figure 2.3. The distribution of velocities at the impeller outlet, both in magnitude and direction, precludes the possibility of introducing fixed vanes that will provide the optimum angle of attack for all incident air at any operating condition. Changes in this angle with volume flow and tip speed reduce still further the probability of satisfactory incidence. In addition to that, the presence of diffuser vanes near the impeller outlet may result in relative velocities equal to that of sound, with consequent shock losses. On the other hand, continuous diffusion of supersonic circumferential-velocity components apparently can be accomplished in the vaneless diffuser and changes in the flow angle, in the absence of vanes, apparently will produce no serious

increase in diffuser losses. Moreover, the vaneless diffuser is inexpensive to manufacture and more tolerant to erosion and fouling than vaned diffusers. However, the vaneless diffuser needs a large diameter because of its low diffusion ratio. The vaneless diffuser could be used widely in automotive turbochargers because of the wide range it offers.

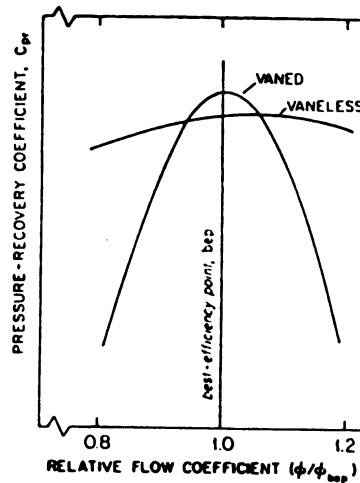


**Figure 2.3 Pressure-recovery coefficient versus range for vaned and vaneless Radial Diffusers (Wilson 1991)**

## **2.2 Vaneless Diffuser**

### **2.2.1 Mode of Operation**

The flow in a vaneless diffuser is similar in flow physics to the channel, conical, and annular diffusers. These types of diffusers will be discussed in the next chapter from the geometric point of view. It could be said that the flow in the vaneless diffuser represents the most complex diffusion of this family of diffusers. In the past, a wide range of experimental research has been conducted on conical, channel, and annular diffusers as discrete elements; while the vaneless diffuser has been handled as a turbomachine element.

To analyze the flow in vaneless diffuser, a brief description of the flow through the centrifugal compressor is needed. The flow through a centrifugal compressor stage is shown on Figure 2.4. As described earlier in Section 1.2, the fluid is drawn into the impeller (where the energy transfer occurs) through the inlet casing. Within the impeller, both the static pressure and velocity are increased. The curved surface of revolution of the impeller is called the hub, and the curved surface forming the outer boundary to the flow of fluid is called the shroud.

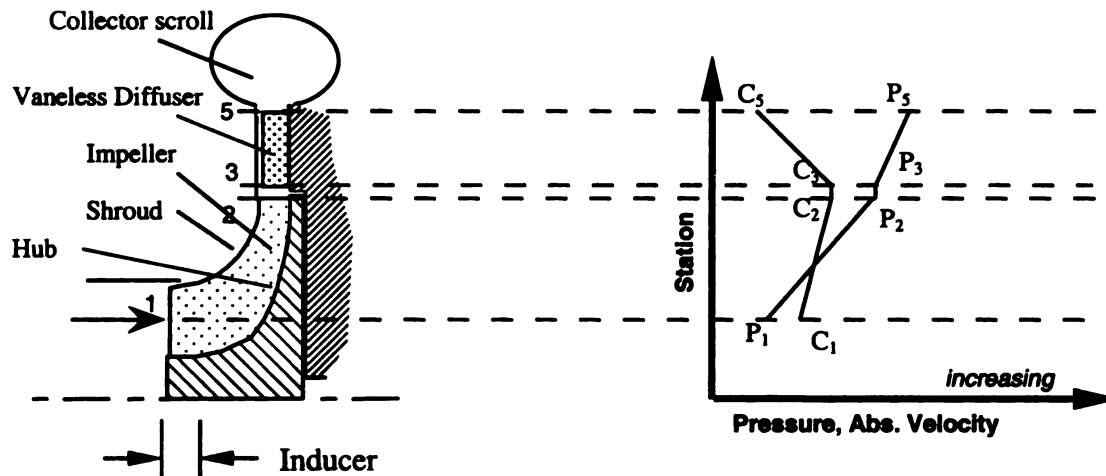


**Figure 2.4 Flow through centrifugal compressor stage**

At the entry to the impeller the flow has a relative velocity  $W_1$  at an angle  $\beta_1$  to the axis of rotation as shown in Figure 2.5. The inducer section or rotating guide vanes as they are sometimes called turns this relative flow into the axial direction. The inducer starts at the inlet casing and finishes in the region where the flow is beginning to turn into the radial direction.

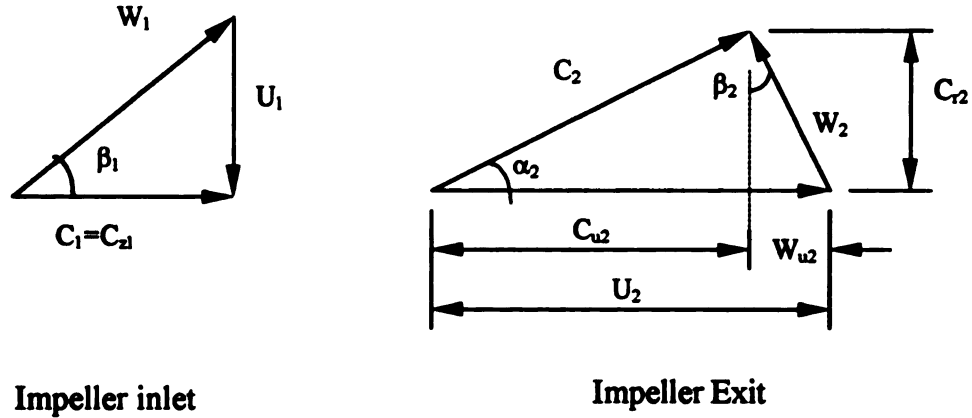


**Figure 2.5 Velocity diagrams at impeller inlet and impeller exit**

As mentioned before, the energy transfer takes place in the impeller, which results in work done on the fluid. This work is equal to the stagnation enthalpy rise (see Figure 2.6) in the impeller, which could be expressed by the Euler equation as

$$w = U_2 C_{u2} - U_1 C_{u1} = h_{02} - h_{01} \quad (2.1)$$

where the stagnation enthalpy is 
$$h_o = h + \frac{C^2}{2} \quad (2.2)$$

The energy transformation takes place in the vaneless diffuser, which is indicated by path 3-5 on Figure 2.6. The vaneless diffuser consists of two parallel planes that the air from the impeller flows between them (See Figure 2.2). So the diffusion occurs in a radial space bounded by the two parallel planes. According to this, actual flow in the vaneless space is where the flow rubs the sidewalls at high velocities, which results in a boundary layer growth from the initial conditions at the tip of the impeller. Since the flow at the impeller outlet is nonuniform, the conditions at the impeller tip have been assumed to be steady with a uniform velocity profile. With this assumption, the diffusion may be efficiently accomplished and could be controlled by the diffusion rate and the wall boundary layer.



### 2.2.2 Losses in Vaneless Diffuser

The losses in the vaneless diffuser could be divided into losses due to impact and losses due to friction. The impact losses arise when the impeller width is less than the diffuser width and/or if the active flow doesn't fill the impeller cross-sectional width at the exit. For such cases, the impact losses at the entrance to the diffuser must be added to the frictional losses. This is the general case, but it should be noted that the equality of the velocities at the impeller outlet and diffuser inlet is a result of the filling of the outlet width of the impeller and the equality of the widths of the impeller and diffuser for the given compressor, which is the condition always obtained. This condition causes a considerable deviation between the theoretical and experimental results.

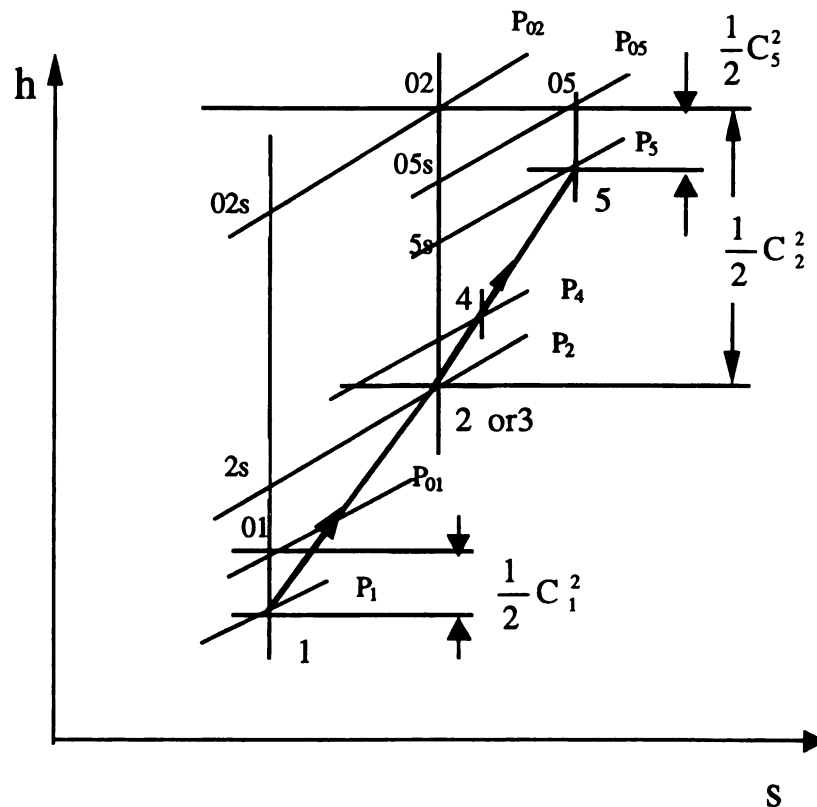


**Figure 2.6 Enthalpy-Entropy diagram for the complete centrifugal compressor stage**

The frictional losses occur at the diffuser wall during the passage of the gas through the vaneless diffuser where the conversion of kinetic energy into pressure rise takes place. These losses are usually expressed in terms of a friction coefficient that is a measure of the loss in total pressure through the diffuser. The available data on friction coefficients in vaneless diffusers are meager and show a rather wide scatter, partly because of the difficulties inherent in the determination of such coefficients and partly because of diversity in their definition. Accordingly, for certain applications (for example in design of diffusers) it is recommended that each designer check appropriate values of the friction coefficient based on similar machines when contemplating a new design.

### **2.3 Research Status on Vaneless Diffuser**

During the last years, the research in the vaneless diffuser area has been active. Part of the previous research work related to vaneless diffusers will be surveyed in this section as well as the next chapter.

One of the earliest efforts to predict the performance of the vaneless diffuser was done by Polikovsky. and Nevelson (1943). A theoretical and experimental investigation was initiated on the vaneless diffuser of a centrifugal fan. The method of computation is based on the principles developed by Pfleiderer. Polikovsky and Nevelson worked over and developed this principle so as to provide a practical method for the computation of vaneless diffusers. Their method was based on one-dimensional analysis. The comparison of the computations with experimental data shows sufficiently good agreement and permits the determination of the limits within which the friction

coefficient lies. They generalized their conclusion, which they were found applicable to the centrifugal fan, to that for axial fans.

Brown and Bradshaw (1947) presented a method of designing vaneless diffusers using data given for simple conical diffusers. They designed and studied experimentally a family of diffusers with different cone angles having the same throat height. They then studied them for different throat height with the same diffuser. This method was investigated with five vaneless diffusers in combination with a mixed-flow impeller in a variable component test rig. They found that this method resulted in compressor efficiencies equal to those shown by the vaned diffuser designed for the same impeller and retained the characteristically wide operating range of vaned diffuser.

Barina (1947) develops a paper similar to the previous one in which an experimental investigation has been conducted in a variable component rig of two vaneless diffusers. These two vaneless diffusers are of different passage curvature and are designed for similar mixed-flow impellers. The result of this paper showed that the large difference in passage curvature of these diffusers made no appreciable differences in diffuser performance at the peak compressor efficiency for the range of speeds investigated.

Brown (1947) investigated friction coefficients for three constant-area vaneless diffusers. These coefficients have been calculated from total- and static- pressure surveys in conjunction with a centrifugal impeller. These surveys have been taken at several radii and from the usual over-all measurements of temperature, pressure and air flow. Brown found that the average value of the friction coefficient through the entire diffuser was approximately 50 percent higher than that for fully developed turbulent flow in smooth

pipes while at the diffuser entrance was about three times the pipe values and in the middle of the diffuser agreed well with the smooth-pipe values. He also found that the friction coefficients computed from total pressures were significantly larger than smooth-pipe values only at the diffuser entrance. Average values of the static-pressure friction coefficient over the entire flow path in the diffuser were about 50 percent higher than those found from von Karman's equation for turbulent, smooth-pipe flow. Finally, he found that the over-all friction coefficient increased with decreasing diameter.

Bradshaw and Laskin (1948) did an experimental study in a variable-component rig of four vaneless diffusers of different diameters over a range of tip speeds from 500 to 1300 feet per second and air flows from open throat to surge. They found that the important losses in efficiency occurred in the vicinity of the diffuser entrance and diffuser exit regions, internal losses being comparatively negligible. Diffuser-entrance losses were approximately constant at about 6% for all diameters. Diffuser-exit losses increased from 3 to 15 points as diffuser diameter decreased, the losses being approximately inversely proportional to the square of the diffuser diameter. The overall efficiency of the compressor is therefore reduced as the diffuser diameter is reduced. Also, they found that the effect of diameter on diffuser-entrance losses, internal losses in the diffuser, and impeller efficiency was slight. In addition, variation in load coefficient and impeller tip speed produce comparatively small changes in diffuser efficiency and the changes are, in general, similar for diffusers of different diameters.

Stanitz (1952) introduced a comprehensive treatment of the vaneless diffuser and published a correct set of one-dimensional equations for the radial momentum, tangential momentum, conservation of mass, conservation of energy, and the equation of state. In

this paper, the analysis method and the design method have been developed for one-dimensional, compressible flow with friction, heat transfer, and arbitrary area change in vaneless diffusers with arbitrary profiles in the axial-radial plane. The effects of mixing losses due to nonuniform flow conditions at the impeller discharge were not included. He presented three groups of numerical examples in which the effects of friction, heat transfer, and diffuser wall spacing are investigated. As a result of these examples, he found that heat transfer from the fluid has the opposite effect of friction on pressure rise in vaneless diffusers and is therefore to be desired.

Stanitz (1952) showed that a typical static pressure rise coefficient for a vaneless diffuser is lower than for a vaned diffuser because the radial distance over which a sufficient reduction is achieved corresponds to a very long flow path especially at small flow angles  $\alpha_2$ . Referring to Elder and Forster (1987), the flow in a vaneless diffuser with a radius ratio of 2 and an inlet flow angle of  $5^\circ$  will rotate  $400^\circ$  before leaving the diffuser as shown in Figure 2.7. High friction losses result, and the real pressure rise is much lower than the ideal one. On the other hand the vaneless diffusers are well suited for off-design operation because they are compatible with a wide range of absolute flow angles  $\alpha_2$ , and they can only choke if the radial component of the Mach number exceeds unity (VKI 1965). Dean (1976) states that backflow into the impeller is less frequent with vaneless diffusers than with vaned diffusers caused by vane pressure loading.

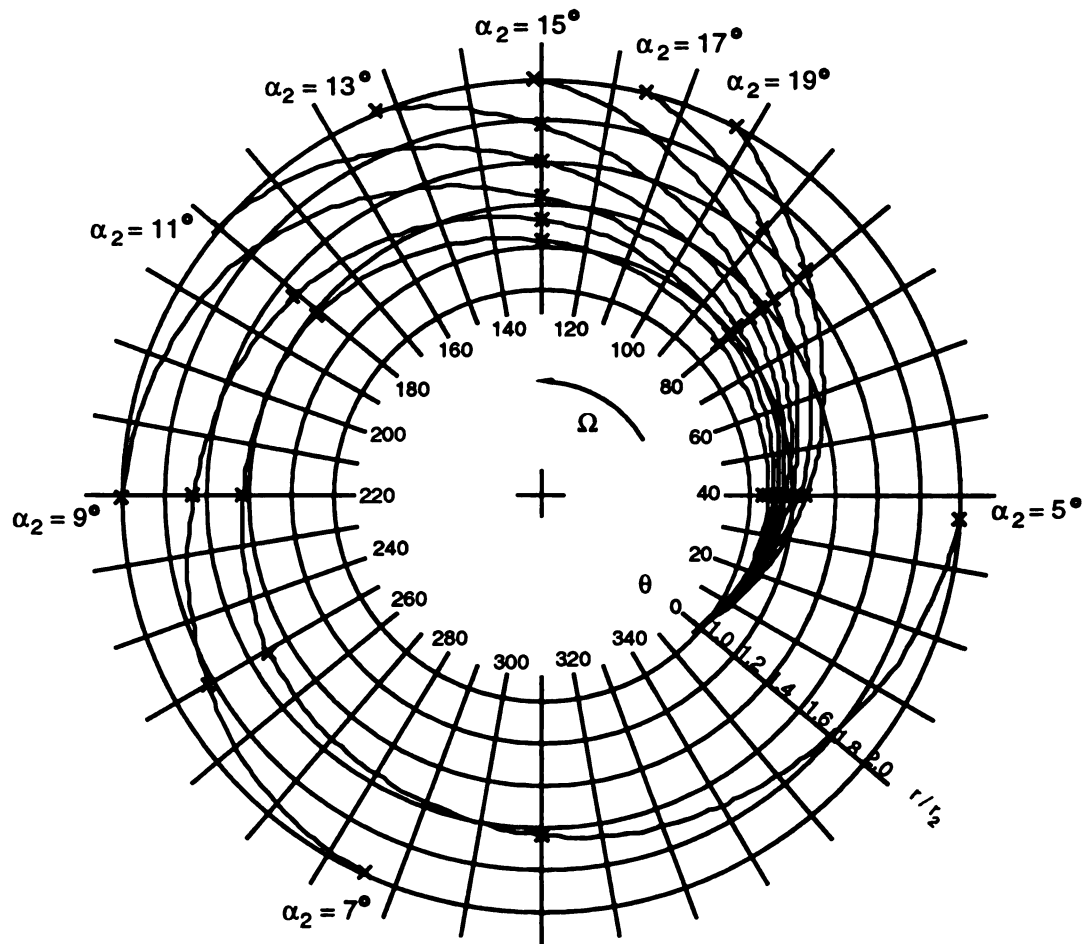


**Figure 2.7 Flow path in vaneless diffuser (Elder and Forster 1987)**

Stanitz (1952) found also that even with relatively low friction coefficients and a neglect mixing losses at the impeller tip, the friction losses in most vaneless diffuser designs are considerable, where the computed diffuser efficiencies in the low 80's; and these losses result from the usually large ratio of wetted surface to flow area in vaneless diffusers. Finally, Stanitz suggests that the diffuser efficiency can be improved as the compressor flow coefficient decreased so that the diffuser walls can be spaced farther

apart (thus, reducing the ratio of wetted surface to flow area) without increasing the length of the flow path in the diffuser.

Through their paper, Dean and Senoo, (1960) have developed a new and more realistic theory for approximating real flows in vaneless diffusers. The theory is not complete, since it doesn't include compressibility and the blockage effect of diffuser sidewall, boundary layer growth. However, it does introduce the important unsteady flow phenomena of re-distorted flow leaving a centrifugal impeller and entering a vaneless diffuser. The following particular results were obtained:

1. Inlet-flow distortions can have significant influences on vaneless-diffuser flow behavior. The magnitude of the influence depends upon the impeller discharge angle, the degree of distortion, the diffuser wall friction and geometry, and on other variables in the theory such as impeller flow and work coefficients.

2. It is impossible to predict the behavior of a diffuser receiving a distorted inlet flow from information on axisymmetric flow.

3. A rotating distorted flow in a vaneless diffuser leads to a significant pressure work transfer between high and low relative velocity regions.

4. The mixing shear stresses between jet and wake regions are shown to be less important than wall shear stresses in governing the flow behavior.

5. The total pressure loss in the diffuser as a fraction of inlet dynamic pressure may be less for distorted than for undistorted flow. However, with backward-leaning blades, the impeller work input is always larger for undistorted flow.

6. These results point out the need for a realistic prediction of the flow pattern discharged from a centrifugal impeller if the diffuser flow is to be predicted.

With Jansen (1964), the flow in radial diffusers in the absence of unsteady flow is isolated, and an extensive analytical and experimental study concerning this has been undertaken. In the absence of wakes from the impeller or other unsteady flow phenomena, the formation of a boundary layer on the sidewalls of the diffuser is the main cause of a loss in diffuser efficiency. The boundary layers, which are three dimensional in character, are investigated for several inlet conditions; and the theoretical results are compared with those of the experiments. Jansen (1964) eliminated the discrepancies between theory and experiment by adjusting the friction factor  $f$  so that it varied along the radius and so that its magnitude resulted in the experimentally found pressure loss. He pointed that when the fluid passes a stationary section prior to entering the diffuser the flow may enter the diffuser with a fully developed boundary layer. On the other hand, the boundary-layer growth in a diffuser could develop so rapidly that at a certain point the boundary layers of the two sidewalls would meet at the center. Accordingly, he said that some of the relations stated in his paper concerning the free-stream flow are no longer applicable. Jansen (1964) also pointed that the Mach number associated with the total velocity is often close to 1.3. At these Mach numbers compressibility effects influence the behavior of the boundary layer to a large extent, and this in turn affects the pressure rise in the diffuser. In his study, Jansen (1964) extended the compressible turbulent boundary-layer transformation to the axisymmetric case. This transformation changes the physical geometry of the diffuser in such a fashion that one obtains an equivalent shape for which the incompressible flow equations are valid. He found that the present transformation is applicable to the fully developed boundary layer without modification if one takes the diverging wall into account.



Johnston and Dean (1966) developed two simple analyses to predict losses in centrifugal compressor (or pump) vaneless diffusers. These two simple analyses are one-dimensional, axisymmetric friction loss and sudden-expansion mixing to account for losses in the diffuser caused by wakes of separated impeller blades. They restricted their analyses to incompressible flow so that no shocks will exist and one can obtain a good approximation for the actual losses. In their analyses, they determined total pressure losses (and hence the diffuser efficiency) by the use of an apparent friction factor or wall friction coefficient. It was account for the actual wall shear stress and for changes of momentum flux due to alteration in velocity-profile shape along the diffuser flow path. They showed that these theories of friction loss and sudden-expansion might be used to replace the more exact, but more difficult, method of Dean and Senoo (1960) over a very wide range of compressor parameters. Johnston and Dean (1966) also found that their analyses are consistent with available experimental data.

Senoo (1978) pursued a different route and calculated the incompressible, circumferentially symmetrical, stationary flow in VNLD including boundary layer effects. This calculation showed that the streamlines at the wall flow inward at certain radial positions. Senoo (1979) verified his theoretical results experimentally. In his model, he states that rotating stall occurs if the boundary layer of the diffuser hub and shroud wall grow together. Senoo (1979) investigated flow parameters at the diffuser inlet affecting rotating stall by using his model. He showed that the axial inhomogeneity in the flow has large influence on the rotating stall. Furthermore, he showed that rotating stall occurs in diffuser with smaller diffuser width ratio can be operated stable at lower massflows as a diffuser with a larger diffuser width ratio. The radius ratio only has

influence on the critical diffuser inlet angle on diffuser with a large diffuser width ratio. Additionally, he showed that the critical flow angle at diffuser inlet is higher at higher Mach numbers.

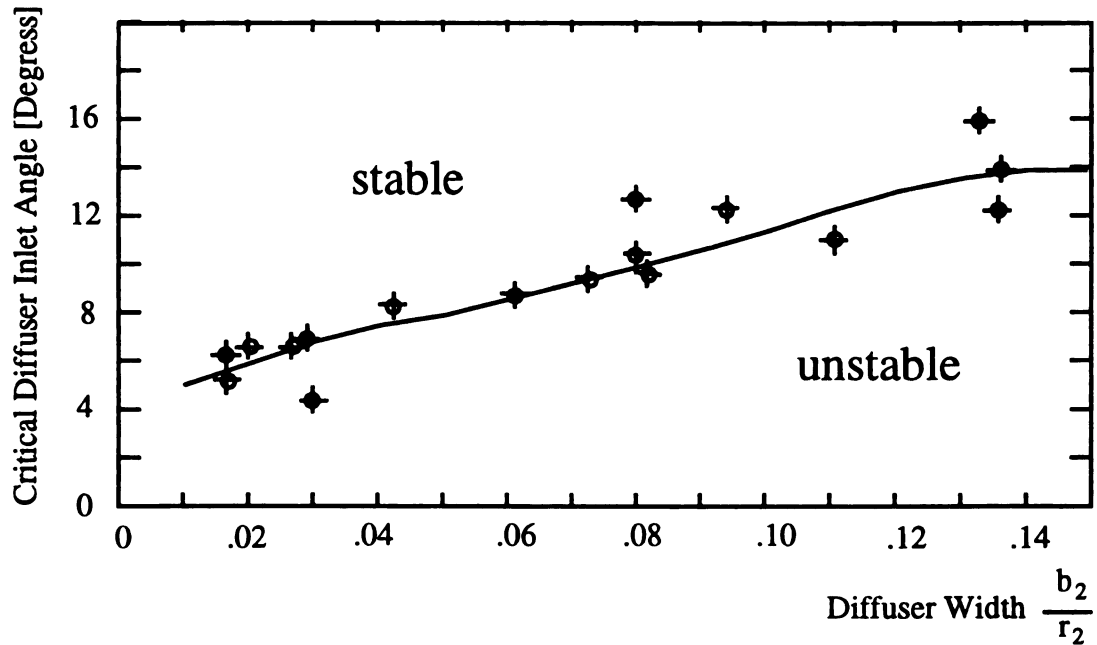


**Figure 2.8 Critical Inlet Flow Angle vs. Diffuser Width (Frigne 1980)**

Ligrani (1982) shows that the Reynolds number has an influence on rotating stall in the VNLD. The model of Senoo showed a good agreement with the experiments if the critical impeller exit angle is corrected with the Reynolds number. The corrected flow angle at the diffuser inlet, diffuser width, and stable operation range is shown in Figure 2.8.

Nishida (1995) observed in a two-process compressor that the critical flowangle also depends on contraction ratio  $b_3/b_2$  and inlet curvature radius  $r_1$  as shown on Figure 2.9. He developed a correlation for the critical flow angle at the impeller inlet, which is based on the correlation of Senoo. On the other hand, he showed again that the stall

pattern depended on the diffuser and the impeller. The same diffuser with different impellers had different stall pattern just as the same impeller with different diffusers.

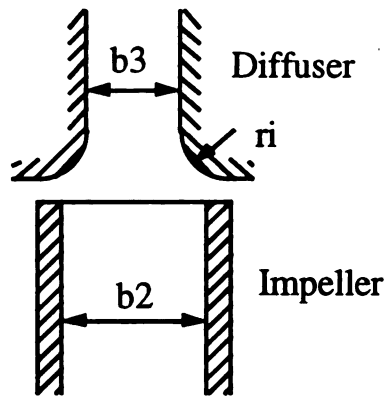


**Figure 2.9 Diffuser inlet shape**

Through their paper, the Whitfield and Roberts (1983) compared the performance of a turbocharger compressor with two prototype diffuser-volute systems to the performance with the standard turbocharger volute system. The two prototype volutes are substantial modifications to the standard design with a significant reduction in vaneless diffuser radius ratio. Although no improvements in performance in terms of pressure ratio and surge margin are shown, the comparison is encouraging in terms of the changes in volute design. Also, the prototype volutes were designed with tongues, which prevented any recirculating flows in the volute passage. They found that the effect of the tongues upon the pressure variation with azimuth angle has been demonstrated, and it is intended to further test these volutes with the tongues cut back.

Inoue and Cumpsty (1984) investigated the discharged flow from centrifugal impellers, which is highly distorted. Its behavior in the diffuser could be expected to have a determining effect on the performance of the compressor. A limited number of experiments were carried out, and extensive measurements were made in building a

vaneless diffuser. Also, a number of experiments were carried out on vaned diffusers. The performance of the vaneless diffuser can be predicted with reasonable accuracy at the design point, provided the flow profile entering the diffuser is either known or can be estimated. Inoue and Cumpsty (1984) found that although the unsteady part of the pattern at inlet to the vaned diffuser was generally similar to the vaneless diffuser, it was affected to some extent by the diffuser vanes. Also, they found that the circumferential mean radial velocity profile in the axial direction at the vaned diffuser inlet was almost identical with that for vaneless diffuser. Reversed flow, on the other hand, appeared in the low radial velocity region near the diffuser vane leading edge when the flow rate was small, and this led to an increase of loss near the sidewalls.

Yingkang and Sjolander (1987) in this paper present measurements of the steady aerodynamic characteristics of a series of five vaneless diffusers with walls varying from mildly divergent to strongly convergent. They determined that the static pressure recovery and the flow were traversed at the inlet and the outlet of the diffuser for a broad range of flow rates in each case. They also found that the wall convergence results in a negative (stabilizing) slope in the pressure rise curve for the diffuser. In the middle of the flow range the highest pressure recovery was obtained with the 5.5 degree diffuser (maximum convergent). They also found that at a high flow rate, convergence was observed to reduce the pressure recovery far less than one would expect and at intermediate flow rates convergence actually improved the pressure recovery. They also found that when convergent walls are used, the flow uniformity at the diffuser outlet was improved. They found also that the convergent diffusers had the useful characteristic of suppressing flow reversal towards the outlet of the diffuser. This could delay the

appearance of rotating stall in wide diffusers where the stall appears to be triggered by the onset of flow reversal near the outlet. Finally, they suggested a useful rule of thumb for choosing the convergence angle for different values of inlet height to radius.

Through his paper, Aungier (1988) presented a fast and accurate analysis to predict the overall performance of stationary vaneless diffuser passages in turbomachines. This method employs a three-dimensional boundary layer analysis, supplemented by simple but effective models to account for flow separation and merged boundary layers. He presented a practical engineering method to predict the overall aerodynamic performance of vaneless annular passages, specifically aimed at the vaneless diffuser and return bend of centrifugal compressors. His method employs a simple inviscid flow analysis based on the assumptions that the flow is axisymmetric and time steady. Also, he assumed that the total pressure, total enthalpy, and angular momentum vary linearly with mass-flow function. He found that this method is computationally very fast and convergence problems are extremely rare. He compares the predicted and experimental overall vaneless diffuser performance, which are the total pressure loss coefficient and the static pressure recovery coefficient. He found that the agreement between predictions and experiment is very satisfactory. He suggested that this method should be applicable to other vaneless, annular passage flows such as inlets and exhaust diffusers. Engeda (1995-1) discusses and develops simple analytical procedures to account for the diffusion process. In his method, he applies the conservation laws on the fluid as it leaves the impeller. He restricted his analysis to two-dimensional, inviscid and incompressible flow. He compared the experimental and the predicted values to show the variation of the mean pressure, flow angle, and tangential

velocity radially in the diffuser. He found that the general trends are similar, but more similarity can be obtained by accounting for compressibility and viscous effects. He pointed out that this comparison is a comparison of the mean values at design point, so any deviation from design point becomes difficult to predict even for the advanced theoretical analysis.

Through this paper, Engeda (1995-2) analyzes the flow in a vaneless radial diffuser using a viscous code. This code is VANDUCT (Viscous Annular Duct), which was modified for this work. With this code, Engeda examines the validity of using 2D or 3D viscous and inviscid solution methods on the basis of flow prediction in a radial vaneless diffuser. He applied this code to predict both the pinched and unpinched diffuser configuration; which are the tangential velocity, pressure ratio, and flow angle in this work. He obtained fair, general trends for both pinched and unpinched versions. However, the pinching effect on flow angle was accurately predicted. He suggested that numerical codes have come a great way and should be classified as design tools in turbomachinery.

### **3. THEORY OF DIFFUSION**

Through this work, a diffuser is defined as any passage in which the flow decelerates between the inlet and outlet. A nozzle is then the functional inverse - any passage in which the flow accelerates between the inlet the outlet. It is common experience that nozzles tend to work and that diffusers tend to give trouble. Any reasonable approach to nozzle design will suffice to give a low fluctuation level at the outlet.

#### **3.1 Diffusion Phenomenon**

The design of a turbomachine is dominated by diffusion, the conversion of velocity into static pressure rise. In most centrifugal compressors both the impeller and the radial diffuser are limited by the diffusion capabilities of the flow channel. A large proportion of the aerodynamic losses (apart from kinetic energy leaving losses) in turbomachines is due to local or general areas of boundary layer separation resulting from a local or general degree of diffusion that is too large for the boundary layer to overcome. Accordingly, the understanding of diffusion will result in an efficient compressors and pumps.

Diffusion can occur on an isolated surface or in a duct as shown in Figure 3.1. It can occur because of area change or of flow curvature. In both cases, the boundary layer

must remain attached in order to reduce the velocity from  $W_1$  to  $W_2$ . When separation occurs, the main flow forms a jet that dissipates into turbulence.

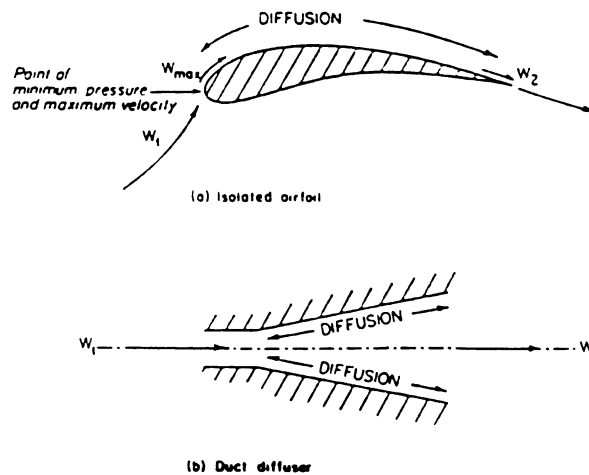


**Figure 3.1 Diffusion mechanisms: (a) isolated airfoil; (b) duct diffuser**

Some symmetrical, straight-axis diffusers of area change type are shown in Figure 3.2. These diffusers are of increasing area type (diverging), which is good for subsonic inlet conditions. For supersonic inlet conditions, a converging supersonic diffuser should be used. Diffusion in a constant area bend is also shown in Figure 3.3. In this Figure, diffusion occurs locally when flow approaches a bend in a constant-area duct. Therefore, diffusion occurs when approaching the outside of a bend and leaving the inside of a bend. These are locations where boundary layers are less stable and where separation is possible.



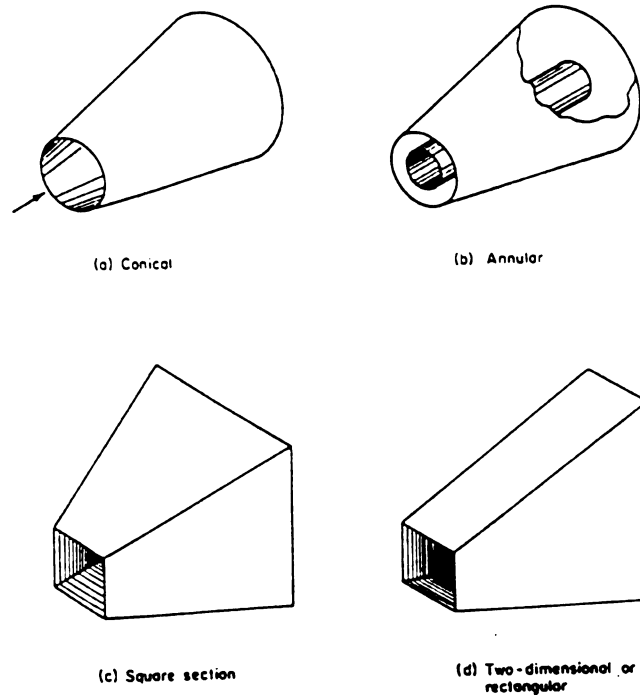


**Figure 3.2 Diffuser types based on shape: a) conical, b) annular, c) square section, d) two-dimensional or rectangular (channel)**

The inlet boundary-layer condition has a very significant influence on the performance of any diffuser. In laminar boundary layers the drag forces between layers is small, and this is why laminar flows cannot diffuse for without separation. In turbulent flows, the inner strata of the boundary-layers are given energy by exchange of “packets” of fluid from the higher energy regions. Accordingly, flows with laminar boundary layers at inlet will not withstand as much diffusion without separation as will turbulent layers.

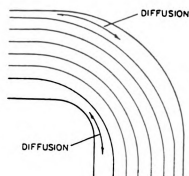


**Figure 3.3 Diffusion in a constant-area bend**

The term separation is short for separation of the flow from the guiding surface, which occurs when the main flow is encountering a pressure rise (or rate of diffusion) severe enough to bring the boundary layer to rest. Separation is a steady-flow phenomenon. However, frequently it is unsteady. The type of unsteadiness is where a jet oscillates from one wall of a rectangular diffusing passage to another. This will give high losses in the diffuser. Such a flow can also produce losses in downstream blade row designed to accept a fully attached flow. Radial flow compressors of high pressure ratio generally experience a region of separation near the impeller circumference on the suction side of the blades. In the cases where a diffuser is used downstream of the impeller it is appear desirable to allow a relatively short distance, of about 5 percent of the impeller radius, for the jets and wakes to mix out sufficiently for the diffuser to be capable efficiently.

Accordingly, diffusion could be done by one, or both, of two principal conversion techniques:

1- The conservation of mass principle  $\rho C_r A = \text{const.}$  (3.1)

2- The conservation of angular momentum principle  $r C_u = \text{const.}$  (3.2)

The radial velocity in the law of conservation of mass (3.1) determines the dimensions of the downstream cross-sections, but since its amount is low compared to the tangential component, the main part of the pressure rise is gained by reducing the circumferential velocity with increasing radius. This context is explained by the conservation of angular momentum in equation (3.2).

### **3.2 Performance Parameters of Diffusion**

As indicated in the previous chapter, large gains in efficiency and pressure ratio could be made in a centrifugal compressor design by increasing the diffusion of kinetic energy to pressure energy. The specification of a wide variety of geometric and aerodynamic parameters is essential before the performance of a diffuser is uniquely given. In this section, the geometric, aerodynamic, and overall performance parameters of diffusion will be discussed.

#### **3.2.1 Geometric Performance Parameters**

For all classes of diffusers, various geometric parameters are used. In the following sections the most important geometric parameters and their influence on the performance parameters are described briefly. As these investigations are very time and cost extensive, several papers of different investigators are consulted. For illustration purposes, a simple schematic of the channel diffuser is shown in Figure 3.4.

Aspect ratio  $AS=b/w_1$ , Area ratio  $AR=A_2/A_1$

Non-dimensional length  $L/W_1$

$W$  = throat width,  $b$  = throat depth

$L$  = centerline length,  $2\theta$  = divergence angle

$A_t$  = throat area =  $bW_1$ ,  $A_e$  = exit area =  $bW_2$

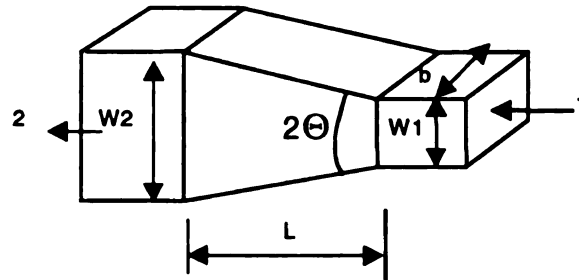


**Figure 3.4 Simple schematic of the channel diffuser (Runstadler, et al. 1975)**

### 3.2.1.1 Passage Width/Radius

The efficiency of the compressor stage can be improved by reducing the passage width of the vaned diffuser. Stein and Rautenberg (1985) achieved an increase in overall pressure rise and efficiency by reducing the passage width of a vaned diffuser by 10%. Strictly speaking for the narrow diffuser ( $b_3/r_2 = 0.108$ ), the maximum efficiency is 2% higher and the efficiency near surge exceeds the wide version ( $b_3/r_2 = 0.12$ ) by 4%. This effect loses importance at lower speeds. Figure 3.5 shows that reducing the passage width/radius causes the shift in the choke lines to the left (lower mass flow rate) in a higher extent than the surge lines. Thus, the overall flow range of the compressor is decreased. The passage width reduction equalizes the difference in the flow angles at hub and shroud from  $30^\circ$  to  $10^\circ$ , which has a positive influence on the flow conditions at the diffuser inlet; and thereby it provides a good component matching. By reducing the passage width/radius, one can push the surge point of a compressor with vaned diffuser to be same as that with a vaneless diffuser.

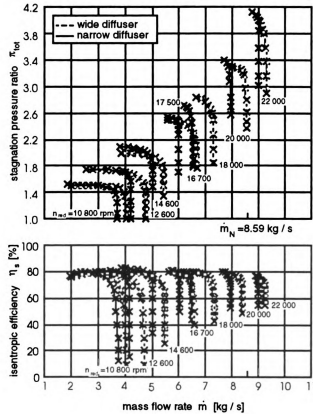


**Figure 3.5 Comparison of compressor maps (Stein and Rautenberg 1985)**

### 3.2.1.2 Length to Width Ratio

In order to find the optimum length to width ratio, the opening angle always has to be taken into consideration. One can thus obtain maximum diffusion in a straight channel diffuser either with a high length to width ratio in combination with a small opening angle or a small length to width ratio in combination with a high opening angle. Clements and Arrt (1988) tested different channel length to width ratios of straight wedge diffusers in a turbocharger compressor, and they found an optimum value of 3.7. The

existence of an optimum value can be explained by several effects. The first half of the channel has the highest influence concerning the pressure rise whereas the latter part contributes only a small amount of pressure recovery. This is caused by the boundary layer growth over the channel length. Reaching a certain thickness, the boundary layers may become unstable and the resulting increase of blockage causes the point of separation to move towards the diffuser throat. Therefore, the optimum length to width ratio will decrease. This hypothesis is proved by Figure 3.6 where the pressure gradient in the latter half of the diffuser channel is significantly lower at the higher throat blockage condition.

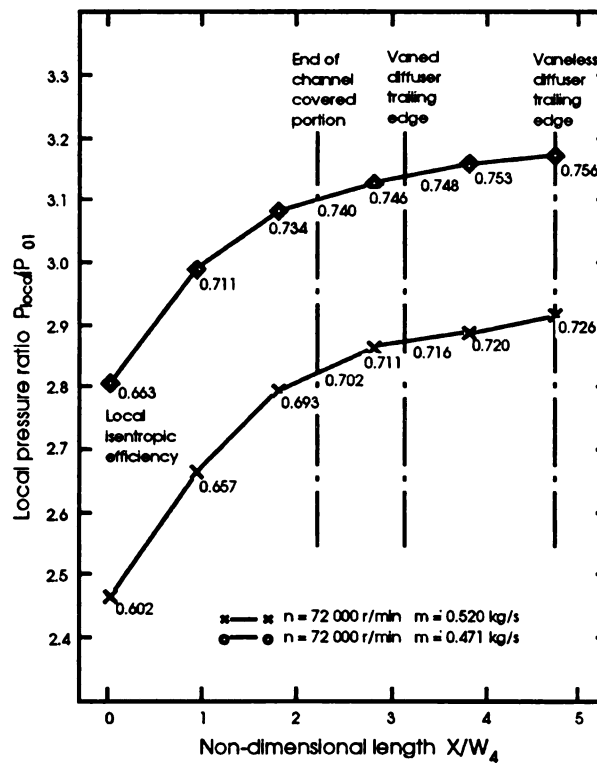


**Figure 3.6 Pressure rise through the vaned diffuser (Clements and Artt 1988)**

Moreover, Clements and Arrt found that a reduction of the diffuser diameter does not necessarily lead into a loss of stage performance. Furthermore, the minor loss in the channel pressure recovery can be compensated in the downstream vaneless part and in the volute, which can be explained by a higher exit dynamic head and a less distorted exit velocity profile in the shorter channel. Falling short of a minimum diffuser diameter, stage efficiency losses occur because the downstream vaneless part and the volute cannot compensate for the loss of the high pressure gradients anymore, which are typical for the vaned part.

### 3.2.1.3 Divergence Angle

Taking a simple pipe with  $2\theta = 0^\circ$ , the static pressure decreases due to losses. This results in  $C_{PR} < 0$  and  $\eta_p = -\infty$ . On the other hand, a raising divergence angle up to about  $2^\circ$  will lead to an equilibrium between momentum conversion and frictional static pressure loss leading into zero values both for  $C_{PR}$  and  $\eta_p$ . With a further lifting of the divergence angle the additional losses increase resulting into optimum values for the pressure recovery and efficiency.

Kline et al. (1959) have shown that for 2-dimensional diffusers that the maximum  $C_{PR}$  cannot occur at the same angle as the maximum  $\eta_p$ , but it will be reached later at a divergence angle of about  $8^\circ$ . This is qualitatively illustrated in Figure 3.7.

A value of  $6^\circ < 2\theta < 8^\circ$  was determined by Reneau et al. (1967) for the maximum effectiveness, maximum pressure recovery and minimum head loss, but the optimum pressure recovery exists over a wide range of geometries.

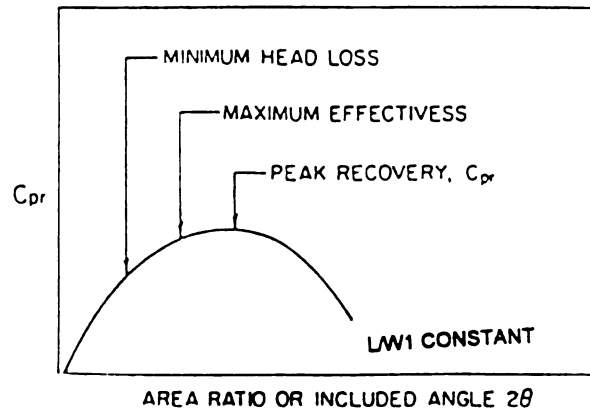


**Figure 3.7 Representative locations of several optima of performance  
at constant  $L / W_1$  (Reneau et. al. 1967)**

In order to find the best suited divergence angle, Runstadler and Dean (1969) show in various performance maps like Figure 3.8 the interaction with the length to width ratio and the area ratio. A long diffuser should have a relatively small divergence angle because the boundary layers grow over the length and result into separation, but they still provide a high pressure recovery. Contrary to this, a short diffuser allows a higher divergence angle; but as separation takes place near the diffuser channel inlet, at small area ratio, only a lower pressure recovery can be obtained.



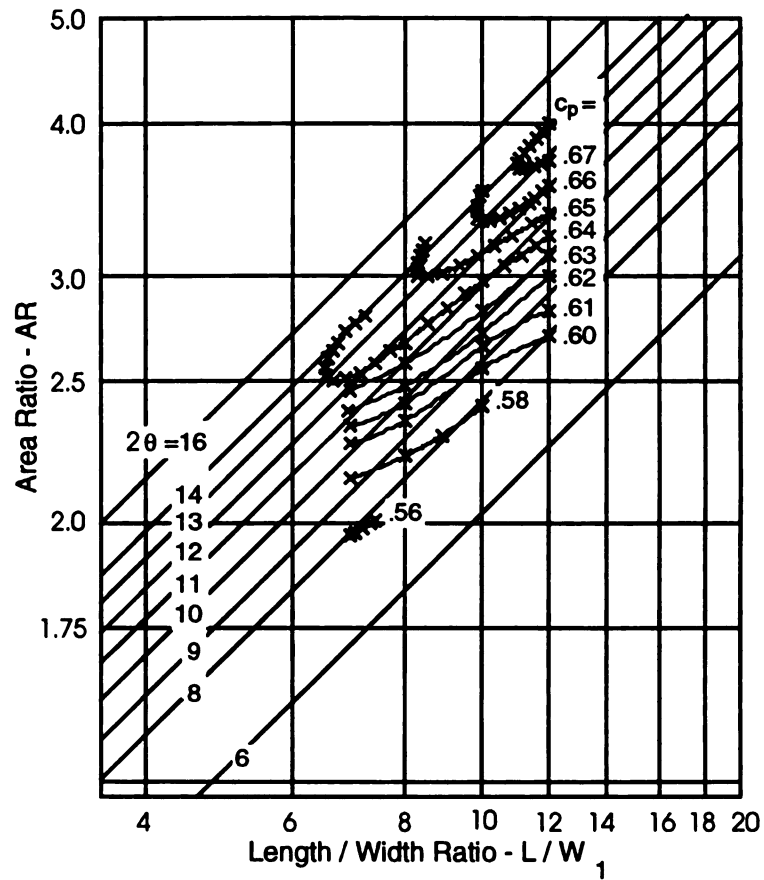


**Figure 3.8 Diffuser performance map,  $AS=0.25$ ,  $M=0.6$ ,  $B=0.08$**

**(Runstadler and Dean 1969)**

In Figure 3.9 Clements and Artt (1987) prove for a straight wedge diffuser a stagnating peak efficiency for  $2\theta > 12^\circ$  associated with a loss in flow range due to a decrease of the throat blockage.

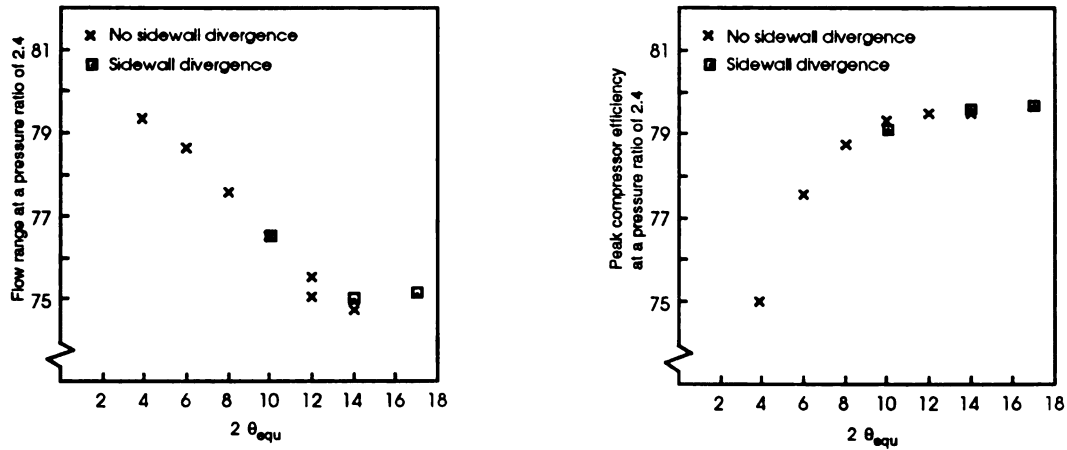


**Figure 3.9 Compressor flow range and compressor efficiency versus  $2\theta$  (Clements and Artt 1987)**

#### 3.2.1.4 Vane Leading Edge Shape

While trying to improve the stage efficiency of a centrifugal compressor, Yoshinaga et. al. (1980) concluded from their experimental investigations with sixteen camber vaned diffusers that the leading edge shape of vanes have considerable influence on the performance of the diffuser and the attendant centrifugal compressor. The validity of this statement becomes obvious if one considers that the impeller exit flow is extremely distorted across the vane height. To analyze this problem the leading edges were cut out to the configurations shown in Figure 3.10.

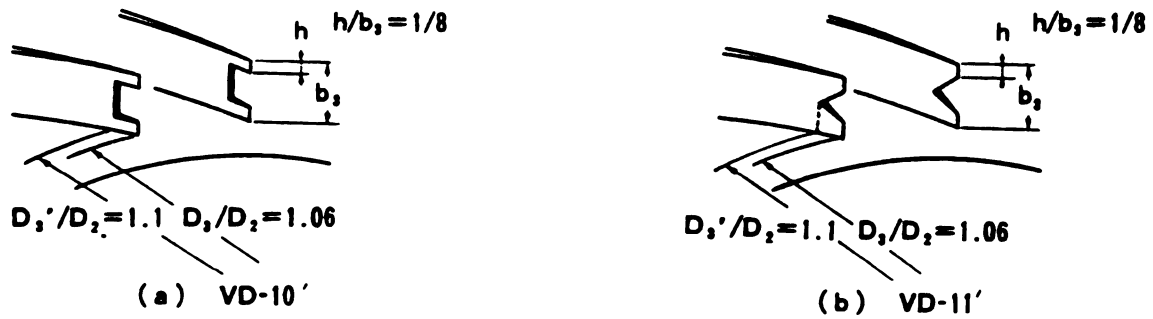


**Figure 3.10 Leading edge shapes (Yoshinaga et. al. 1980)**

Whereas the rectangular cutting resulted into a loss of efficiency the triangular cutting provided a rise in efficiency of more than 0.5% compared with its original stage at the design point as shown in Figure 3.11.

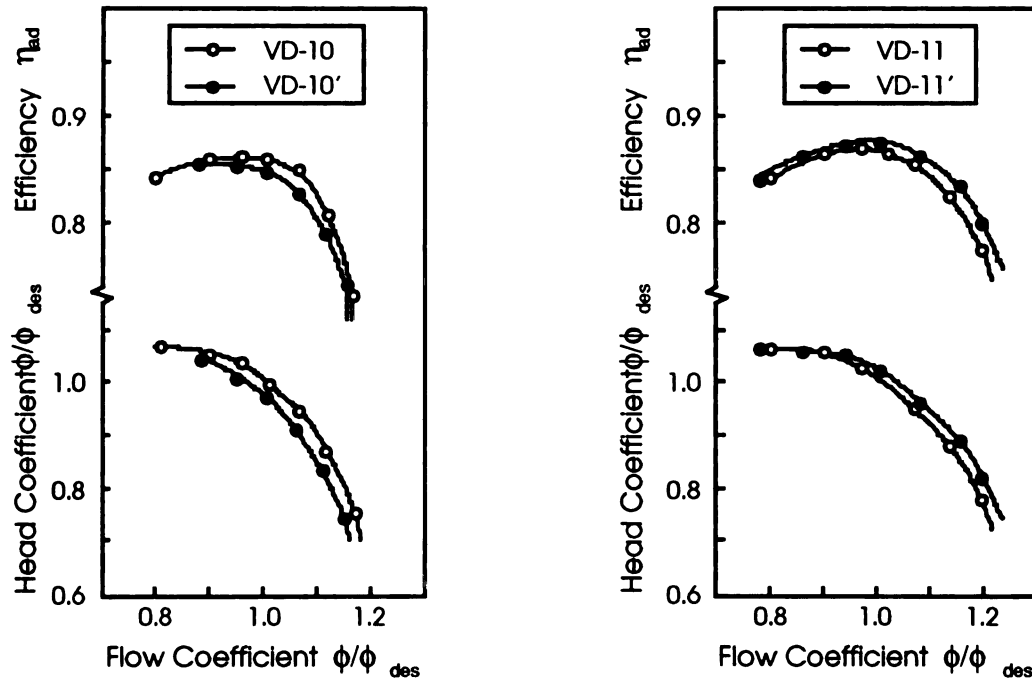


**Figure 3.11 Effect of leading edge shapes on the stage efficiency (Yoshinaga et. al. 1980)**

### **3.2.1.5 Vane Shape**

Bammert et al. (1983) used three different kinds of diffusers to investigate the influence of the vane shape on the performance of a centrifugal compressor stage. The tested vane shapes are cambered vanes, straight channel vanes, and twisted vanes.

By analyzing the essential compressor components they found out that the diffuser has only a weak effect on the impeller but a high influence on the collecting chamber. The diffuser blades do not affect the flow in the impeller very much because a possible retroaction of the heavy flow disturbances in the diffuser channel on the impeller flow is blocked upstream by the simultaneous supersonic phenomena taking place in the diffuser throat.

In the low speed range the performance map of the twisted diffuser was especially shifted towards higher mass flow in comparison to the cambered vane and the straight channel diffuser. Besides, the twisted diffuser shows its best efficiency at lower flow range. In detail its efficiency is 4% higher than for the compressor with the cambered vane diffuser and 3% higher than for the configuration with the straight channel diffuser. Another point of interest is the operation range, which is up to twice as high for the compressor with the twisted diffuser compared with the two other variants. Figure 3.12 shows the superiority of the twisted diffuser, which has a vane shape that matches with the incoming flow distribution.

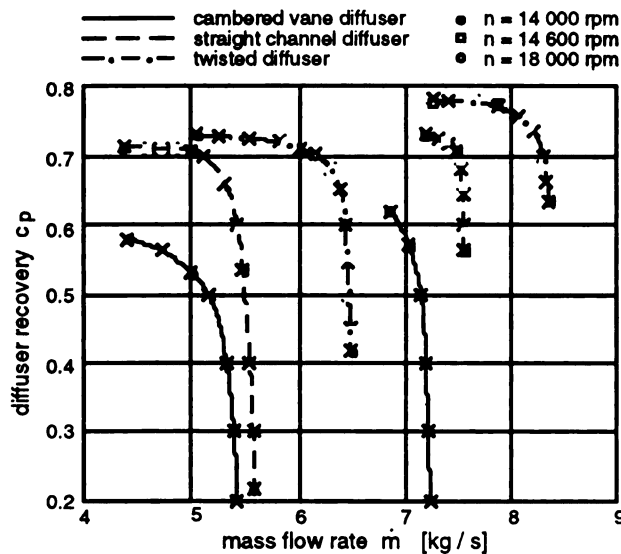


**Figure 3.12 Diffuser recovery (Bammert et. al. 1983)**

### 3.2.1.6 Area Ratio

Yoshinaga et al. (1980) investigated 16 different vaned diffusers on a model compressor rig in order to improve the efficiency of a centrifugal compressor stage. The pressure recoveries were compared with those of two-dimensional channel diffusers. This comparison showed that the vaned diffusers reach their peak pressure recovery at smaller area ratios and smaller length to width ratios. This peak pressure recovery was attained for a combination of the length to width ratio around 5.5 and an area ratio around 2, which is illustrated in Figure 3.13. The value for the given vaneless diffuser is lower because of its smaller area ratio. The obvious existence of an optimum area ratio is coupled with the values for the divergence angle and the length to width ratio because a change of the area ratio can be obtained by varying these parameters. If the divergence

angle exceeds a certain limit, separation may occur due to a high vane loading. In the case of increasing the length to width ratio the boundary layers grow and reduce the effective area ratio. Both effects lead to a drop in pressure recovery and show the usefulness of a well adjusted area ratio.

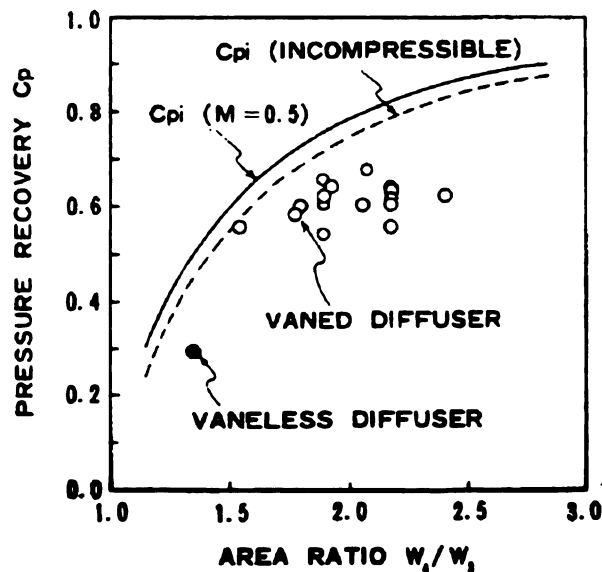


**Figure 3.13 Pressure recovery of vaneless and vaned diffusers versus area ratio**  
(Yoshinaga et. al. 1980)

### 3.2.1.7 Radius Ratio

The radius ratio is a very important geometric parameter since it determines the extent of mixing the jet and wake flow leaving the impeller. Eckardt (1976), who investigated the flow in a high speed centrifugal compressor impeller in detail, pointed out that "the flow equalization process takes place mainly across the channel width due to decreasing meridional curvature turbulence stabilization, whereas the Coriolis forces

maintain a remarkable circumferential flow distortion along the shroud wall up to  $r/r_i \approx 1.2$  ". The same value for the radius ratio was found by Jiang and Yang (1982) who tried to improve the pressure recovery of a vane island diffuser. Applying the vane island tip at four different radius ratios, they found that the pressure variation over the circumferential locations was about 20% at  $r/r_i \approx 1.05$  and 1.10. In order to provide a satisfactory mixing in the vaneless space the authors suggest a radius ratio from 1.15 to 1.20. This range provides a minimum of losses in combination with an optimum pressure recovery as it can be seen in Figure 3.14. Besides a rise in efficiency of 4% was obtained by lifting the radius ratio from 1.10 to 1.20.

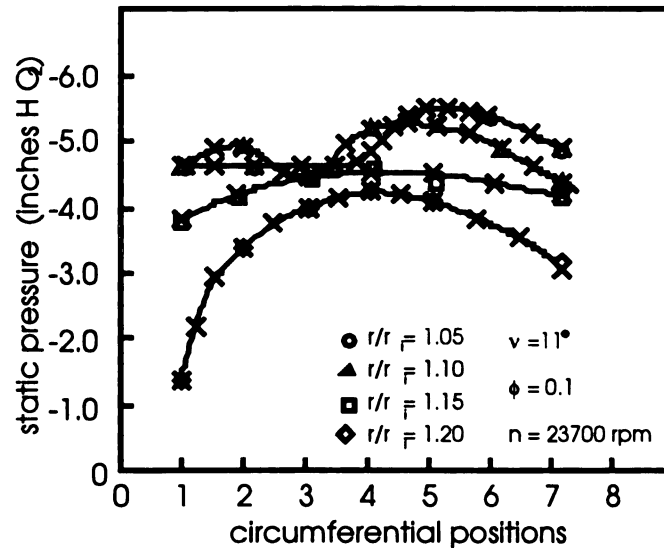


**Figure 3.14 Circumferential static pressure distribution (Jiang and Yang 1982)**

### 3.2.1.8 Vane Number

As a comparison of different investigations show, the number of vanes seems to be strongly dependent on the diffuser type.

Dean (1974) indicates that the number of vanes employed in vane island diffusers may vary in a range of 8 to 60. Came and Herbert (1980) could not find any significant difference in the compressor flow range with a vane number variation. Rodgers (1982) achieved similar results by comparing the stage performance of a high efficiency, low pressure ratio stage with both a 13 and a 21 vane channel diffuser at the same throat area. Figure 3.15 shows the obtained minor changes in flow ranges and pressure recovery.

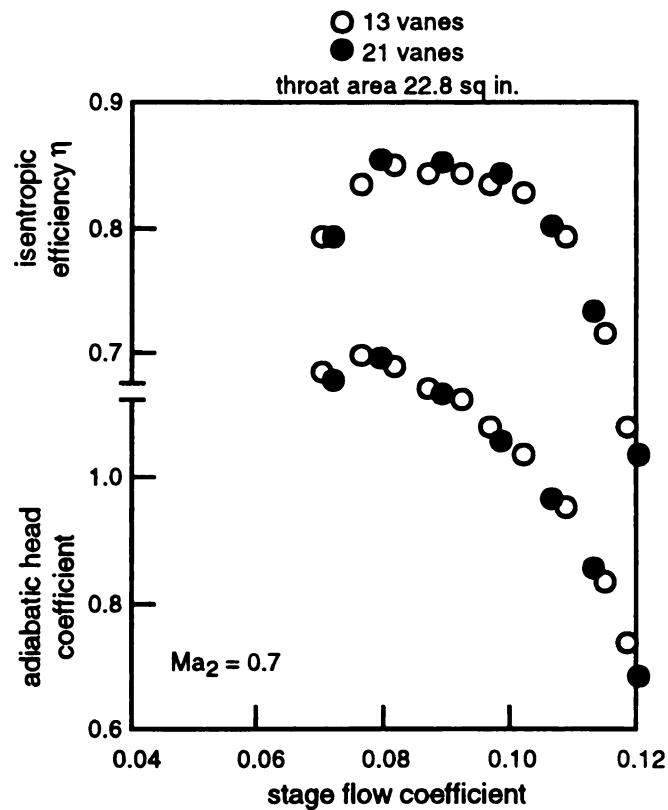


Figure 3.15 Effect of diffuser vane number (Rodgers 1982)



Yoshinaga et. al. (1980) expect an increasing number of vanes to move the surge limit of a centrifugal compressor to a higher flow rate. Therefore, they limit the vane number to 27 for their experimental investigations with radial airfoil cascades.

In this context Elder and Forster (1987) mention that a reduction of the number of diffuser vanes permits the mixing of jets and wakes in the vaneless space, which prevents the region being blocked by low momentum flow.

This argument is unimportant for low solidity vaned diffuser since the throat is missing. Nevertheless Camatti et. al. (1995) found an influence of the blade number on the performance of Low solidity vaned diffuser's. Figure 3.16 shows that an increase from  $Z=6$  to  $Z=12$  leads to higher efficiency but in a narrower range of volume flow coefficients.

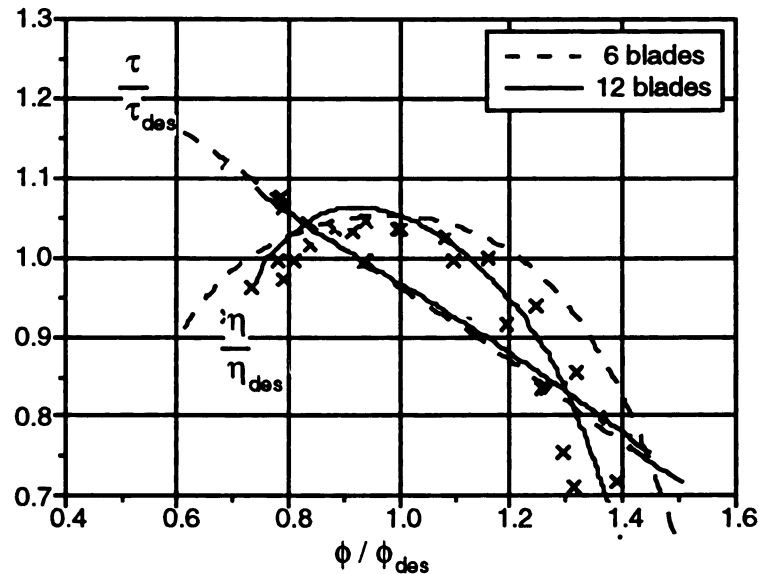


**Figure 3.16 Blade number effects for  $r_{in}/r_2=1.106$  (Camatti et. al. 1995)**

Another point of view is to determine the number of vanes with view to the optimum incidence angle that leads to the best flow range. Moreover, the rotor dynamics might be important for a stable operation, i.e. the number of the impeller and diffuser vanes have to be harmonized.

#### **3.2.1.9 Throat Blockage**

The blockage in the throat area is to be mentioned since it might amount up to one third of the physical throat area as stated by Rodgers (1982). The general aerodynamic blockage will be introduced in section 3.2.2.1.

Stall and choke occurring in the vaned diffuser limit the flow range of a centrifugal compressor. The conditions for choking are not only the mass flow itself but also the stagnating pressure and temperature and the effective cross sectional throat, for which even the blockage factor has to be taken into consideration.

Kenny (1970) concludes from his experiments with cambered and pipe diffusers a strong influence of the end wall boundary layer development on the static pressure rise ineffectiveness and total pressure loss. Later Kenny (1972) presented a method to predict the blockage by the use of a boundary layer analysis, which reflects the experimental data very well. Despite the analytical curve is 12% above the test curve, Figure 3.17 shows a good agreement for the measured and boundary-layer predicted stall limit. He further shows that the level of blockage is a function of the diffuser blade angle and/or the vane number whereas the influence of speed is negligible.

Conrad et. al. (1980) points out that a decrease of the stagger angle increases the blockage factor. This is due to the lengthening of the flow path, which produces thick boundary layers despite the reduction in pressure gradient.

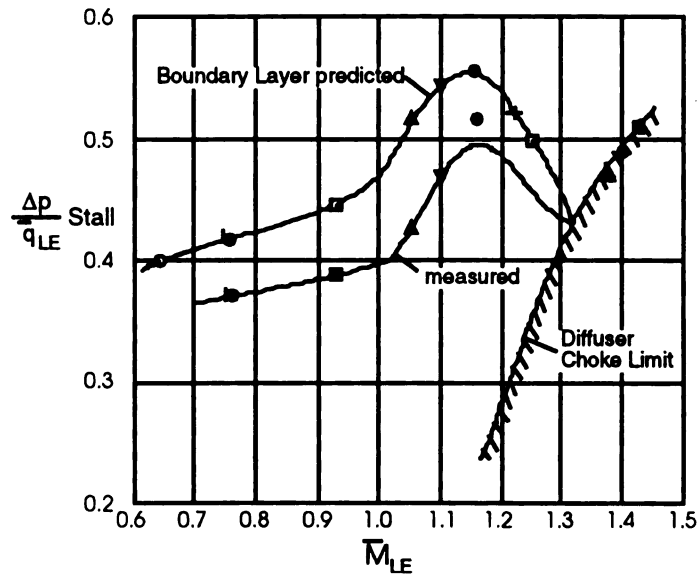


**Figure 3.17 Comparison of measured and boundary-layer predicted stall limit  
for pipe diffuser of a 6:1 pressure ratio (Kenny 1972)**

### 3.2.1.10 Incidence

The incidence angle in a radial diffuser has an important influence on the flow range with regard to the stall and choke behaviour. If the mass flow is reduced from the design value, the radial velocity decreases in contrast to the increasing tangential velocity. Hence, the angle of the mean absolute flow into the diffuser is inclined towards the tangential direction, which leads to a positive increase in incidence. In the case of transgressing a certain value for  $i$ , the pressure losses rise rapidly and stall phenomena occur. Conversely, a higher mass flow than that chosen for the design point causes the flow to enter more radially and therefore with a lower incidence angle. At very small incidences, the flow range is limited by choke effects.

Reeves (1976) carried out experiments with pipe diffusers and found a correlation between the flow range and both the Mach number and the incidence angle. At any leading edge incidence a lower leading edge Mach number corresponds to a greater range, and the range at a constant Mach number changes with the incidence. Reeves found an incidence angle for optimum matching that was somewhat negative, and located near the middle of the flow range as shown in Figure 3.18.

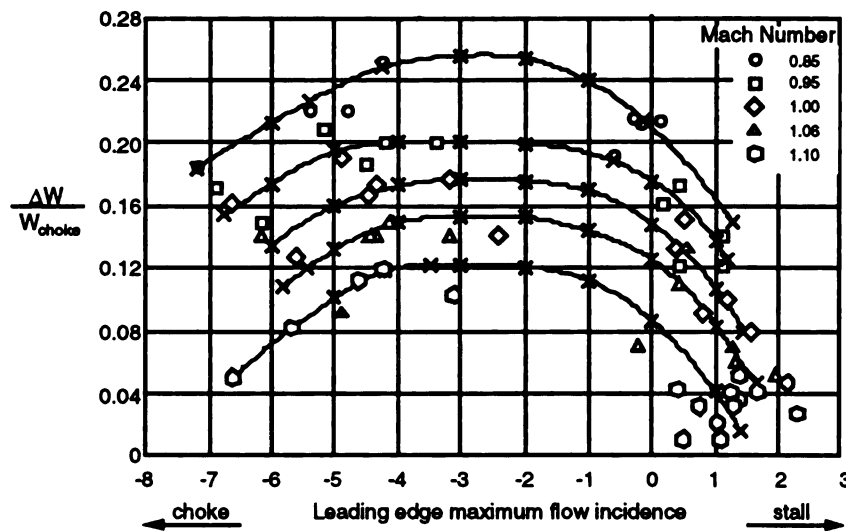


**Figure 3.18 Effect of diffuser leading edge Mach number and incidence on range (Reeves 1977)**

### 3.2.2 Aerodynamic Performance Parameters

The Aerodynamic parameters are found at the inlet to the diffuser. It was found that the aerodynamic parameters became important in order to specify the performance of the diffuser.

### 3.2.2.1 Aerodynamic Blockage

The blockage is the fraction, or percentage, of the inlet passage area that is occluded by the boundary layer displacement thickness on all walls.

Japikse (1984) mentions that the displacement thickness is frequently taken as equal on all surfaces, which show the following relationships for the blockage factor with regard to Figure 3.2:

for channel diffusers with high aspect ratio, i.e. neglecting the end walls

$$B = \frac{2\delta^*}{w_1} \quad (3.3)$$

for conical diffusers with uniform inlet boundary layers

$$B = \frac{4\delta^*}{d_1} \quad (3.4)$$

for annular diffuser with inlet passage height of  $h_1$

$$B = \frac{2\delta^*}{h_1} \quad (3.5)$$

As the velocity in the boundary layer is decreased, the total volume flow is obviously smaller than in the frictionless case. Therefore, the main stream is pushed away from the wall. The same displacement thickness would be caused by an imaginary layer of the thickness  $\delta^*$  where the velocity would be zero. Traupel defines  $\delta^*$  in the following way (Figure 3.19):

$$\delta^* \cdot U = \int_0^{\infty} (U - u) \cdot dy \quad (3.6)$$

Schlichting (1987) concludes from this formula the displacement thickness of any flow without pressure gradient as

$$\delta^* = 0.01738 \cdot Re^{0.861} \cdot \frac{v}{c} \quad (3.7)$$

The displacement thickness along the vanes can be calculated like the semivaneless space in a regular channel diffuser done for example by Hintelmann (1994).

$$B = \frac{\delta_{hub} + \delta_{shroud}}{h} + \frac{\delta_{vane}}{w} \quad (3.8)$$

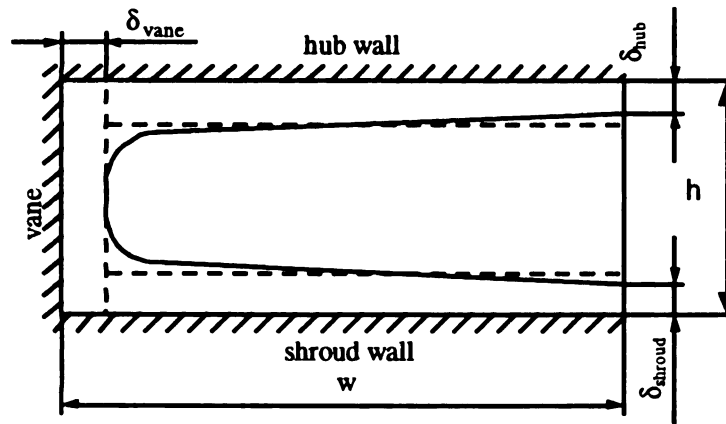


**Figure 3.19 Aerodynamic blockage**

### 3.2.2.2 Reynolds Number

This dimensionless number describes the relation of inertia forces to viscous forces and it is defined as

$$Re = \frac{\rho \cdot C \cdot D}{\mu} \quad (3.9)$$

where for any kind of diffuser a hydraulic diameter is typically introduced that is related to the special geometry. In other applications D is replaced by another characteristic length.

The Reynolds number is also used to distinguish laminar from turbulent flow, which depends on other factors like the hydraulic diameter or the surface roughness. If its value converges against infinity, the viscous forces can be neglected and the equations of conversation are called Euler-equations. In this case the flow is highly turbulent. If Re is very small, the inertia forces play a minor role; and the flow is called creeping flow, which is of the laminar type.

Rhoden (1956) and Stuart (1955) investigated the influence of the Reynolds number on the pressure distribution for 2-dimensional cascades. From these results it can be concluded that the pressure distributions on the suction side are about equal for Re-numbers larger than  $1.5 \cdot 10^5$  referred to the inlet velocity and the blade chord. According to Vavra (1960) slight deviations occur if the Reynolds number is decreased to  $10^5$  and entirely changed pressure patterns exist for values below  $10^5$ .

### 3.2.2.3 Mach Number

The Mach number, named after the Austrian physicist Ernst Mach, is defined as the flow speed to the speed of sound at a point in a fluid.

$$M = \frac{C}{a} = \frac{C}{\sqrt{\gamma \cdot R \cdot T}} \quad (3.10)$$

For smaller values than 0.3 the fluid can be assumed as incompressible, but for numbers larger than 0.3 compressibility effects have to be considered. If the Mach number of the inlet velocity exceeds certain values, the losses increase radically because of shock patterns that occur in the flow, which influence the behaviour of the boundary layers. Compressibility effects may also change the pressure distributions along the

blades, so that the blade loading may increase rapidly. Because shock patterns can be produced only if the velocities at stations on the profile become supersonic, it is frequently stated that the local speed of sound must not be exceeded at any point (Vavra 1960). Though the Mach number in the subsonic range does not have any overwhelming influence on diffuser performance, its variation is important for achieving higher performance.

#### **3.2.2.4 Inlet Velocity Profile**

At the impeller exit, the flow is often being considered as being made of two jets: one with a high velocity relative to the impeller, the other with a small or even zero velocity which is often referred as wake flow. Depending on the size of the vaneless space the two jets are mixed, and a smoother profile can be achieved so that the blockage of the region by low momentum flow can be prevented.



### 3.2.3 Overall Performance Parameters

#### 3.2.3.1 Pressure Recovery Coefficient

The fundamental purpose of a diffuser is to convert dynamic pressure at inlet to static pressure rise at outlet. The pressure recovery coefficient is defined as the ratio of these two parameters; in other words

$$C_p \equiv \frac{P_2 - P_1}{P_{01} - P_1} \quad (3.11)$$

Ideally, the value of  $C_p$  could reach unity. In practice, only in very favorable circumstances can a pressure recovery coefficient of over 0.8 be obtained.

An ideal or theoretical pressure recovery can be set if the flow is assumed to be compressible and isentropic. From the isentropic relations

$$\frac{P}{P_o} = \left[ \frac{T}{T_o} \right]^{\frac{c_p}{R}} \quad (3.12)$$

where the total and static values are related as

$$T_o = T + \frac{C^2}{2c_p} \quad (3.13)$$

Substitute into (3.12), then

$$\frac{P}{P_o} = \left[ \frac{T_o - \frac{C^2}{2c_p}}{T_o} \right]^{\frac{c_p}{R}} = \left[ 1 - \frac{C^2}{2c_p T_o} \right]^{\frac{c_p}{R}} \quad (3.14)$$

By using the first two terms of the binomial expansion, an approximate solution could be obtained as

$$\frac{P}{P_o} \approx 1 - \frac{C^2}{2RT_o} = 1 - \frac{\rho_o C^2}{2P_o} \quad (3.15)$$

or

$$P = P_o - \frac{\rho_o C^2}{2} \quad (3.16)$$

Substitute from (3.16) into (3.11) then

$$Cp \approx \frac{P_{o2} - P_{o1}}{\left(\frac{\rho_{o1} C_1^2}{2}\right)} + \left[1 - \frac{\rho_{o2}}{\rho_{o1}} \left(\frac{C_2}{C_1}\right)^2\right] \quad (3.17)$$

In an adiabatic diffuser, the total temperature does not change, which implies for perfect-gas that

$$\frac{\rho_{o2}}{\rho_{o1}} = \frac{P_{o2}}{P_{o1}} \quad (3.18)$$

And for frictionless flow,  $P_{o2} = P_{o1}$

Then

$$Cpi = 1 - \left(\frac{C_2}{C_1}\right)^2 \quad (3.19)$$

This is the ideal pressure recovery coefficient. It is simply a design guide and could be used to deduce some very important functional relationships.

### 3.2.3.2 Effectiveness

The ratio between the actual and the ideal pressure recovery coefficients is known as the diffuser effectiveness

$$\eta_{diff} = \frac{C_p}{C_{pi}} \quad (3.20)$$

It is an excellent parameter to use to judge the probable level of performance when it is required to estimate expected performance under unknown conditions, relative to the available data.

### 3.2.3.3 Total Pressure Loss

The losses of total pressure are expressed in the total pressure loss coefficient

$$\xi = \frac{\Delta P_0}{\frac{1}{2} \rho U^2} \quad (3.21)$$

This parameter must refer to the entire flow field; and, therefore, one must consider integrated total pressure loss values including all stream tubes through the diffuser. In the most common definition of loss coefficient that is given above, integrated mass average parameters are used across the diffuser inlet and outlet. At these points a detailed measurement with suitable numerical averaging across the entire flow field is required.

### 3.2.3.4 Flow Range

An important variable for determining the overall performance of a compressor is the mass flow rate. Its upper and lower limit define the flow range, which is illustrated in Figure 3.20.

The highest achievable mass flow rate appears at choke conditions when the velocity through the cross-sectional area at any of the compressor components appears to be sonic. At this state the density has to be evaluated at the sonic conditions, which leads to equation (3.22).

$$\dot{m}_{Choke} = A \cdot \rho^* \cdot a^* \quad (3.22)$$

Typically, a convenient nondimensional group is formed as the ratio of the actual mass flow rate  $\dot{m}$  to the choking mass flow rate  $\dot{m}_{Choke}$ .

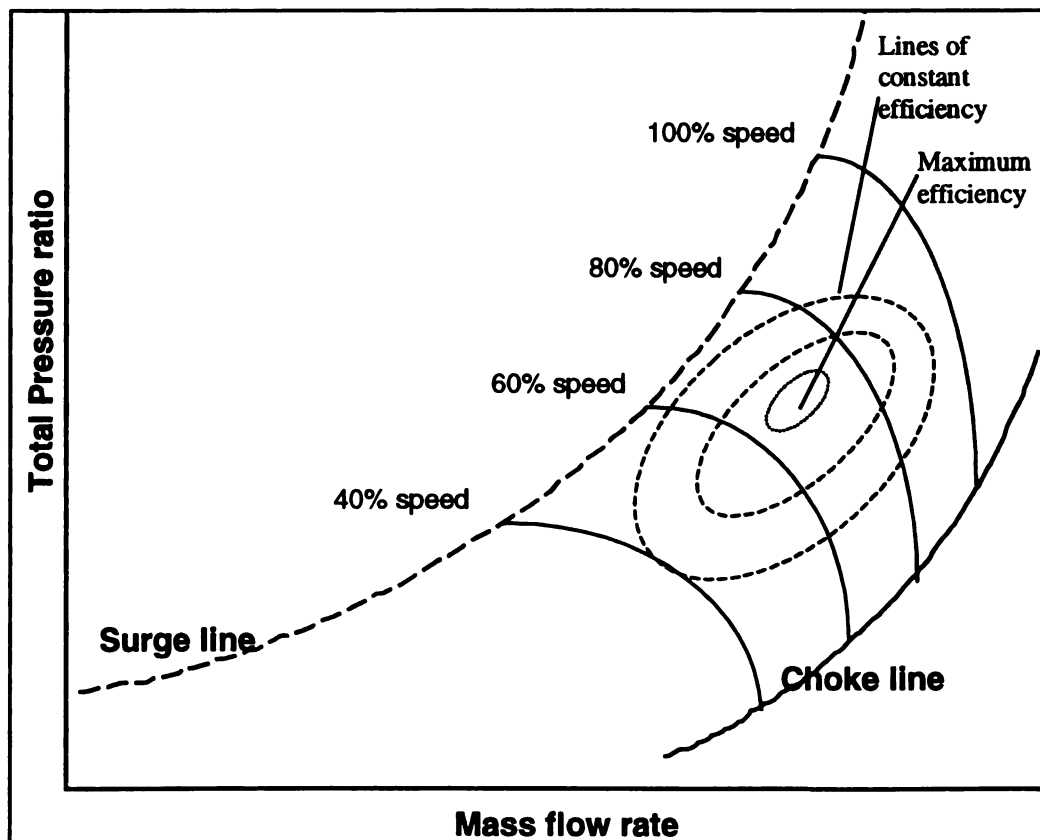
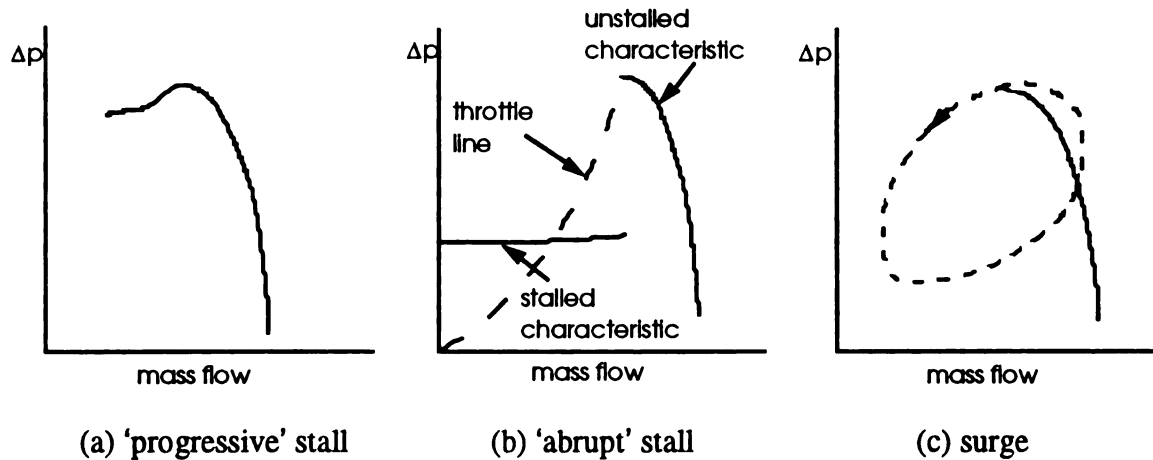


Figure 3.20 Choke and surge

On the other side, the minimum mass flow rate is limited by the effects called stall and surge. A brief description of the surge and stall phenomena will be given here in addition to the previous discussion of the in the previous chapters. These phenomena are very complex and regardless of the type of change occurring in the flow pattern, the conventional terminology for the point of instability is 'surge point' and the line marking the locus of these points for different rotational speeds is known as the 'surge line'.

Cumpsty (1989) distinguishes three different types of flow change shown in Figure 3.21. The first case (a) is called progressive stall characterized by a small drop in overall performance and it is indicated only by a change of noise or by high frequency instrumentation. Figure 3.21 (b) shows an abrupt stall leading into a large drop in pressure rise and flow rate. In both cases, a and b, the flow loses its axisymmetric characteristics, turning into a circumferential nonuniform pattern that rotates around the annulus. This phenomenon is often referred as a rotating stall and goes along with a constant time-mean mass flow despite a variable local mass flow. In the third case depicted in Figure 3.21 (c) the annulus averaged mass flow varies with the time, which causes the entire compressor to change from being stalled to unstalled and back again. In deep surge the flow distortion can even be reversed.



**Figure 3.21 Different kinds of surge (Cumpsty 1989)**

### 3.2.3.5 Distortion

The distortion level leaving a diffuser is an additional performance parameter that gains importance if the flow into a combustor is to be well understood or the flow into other critical elements such as a heat exchanger core or regenerator are points of interest. Unfortunately, the industry has not established a common standard and some techniques used have not even been documented as mentioned by Japikse (1983). The usual way to define the distortion is to show how the velocity field or the total pressure distribution departs from some type of norm at the diffuser exit.

### 3.3 Flow Analysis in Vaneless Diffuser

The flow in a vaneless diffuser could be analyzed by defining first the application area as indicated in Figure 3.22. As shown on this Figure, path o-t is the path of the flow leaving the impeller to a straight channel vaned diffuser. This means ideally that diffusion occurs by increasing the area. This path represents the upper limit of possible

paths. Path o-q is the path of the flow leaving the impeller to a cambered/curved vaned diffuser.

This means ideally that diffusion occurs by increasing area and flow around a curve. Path o-s is the path of the flow leaving the impeller to a vaneless diffuser. Ideally, it is a logarithmic spiral path, and it is the lower limit in these paths. According to this path, the flow in a vaneless diffuser with a radius ratio of 2 and an inlet angle of  $6^\circ$  rotates one round before leaving the diffuser. This will result in high friction losses due to viscous drag on the walls; and accordingly, its pressure recovery is significantly lower than that with vaned diffuser.

As illustrated earlier, the function of the diffuser is to convert the dynamic energy of the advancing flow into pressure as rapidly as possible without incurring flow separation at the most adverse operating condition. Because diffusion of the tangential component is essentially a function of radial distance only, any acceleration of the diffusion process must be affected by increasing the rate of diffusion of the radial and axial components of velocity, that is, by increasing the rate of expansion of the flow area. In other words, the radial component of the flow diffuses due to the area increase (conservation of mass), and the tangential component diffuses as it is inversely proportional to the radius (conservation of angular momentum).

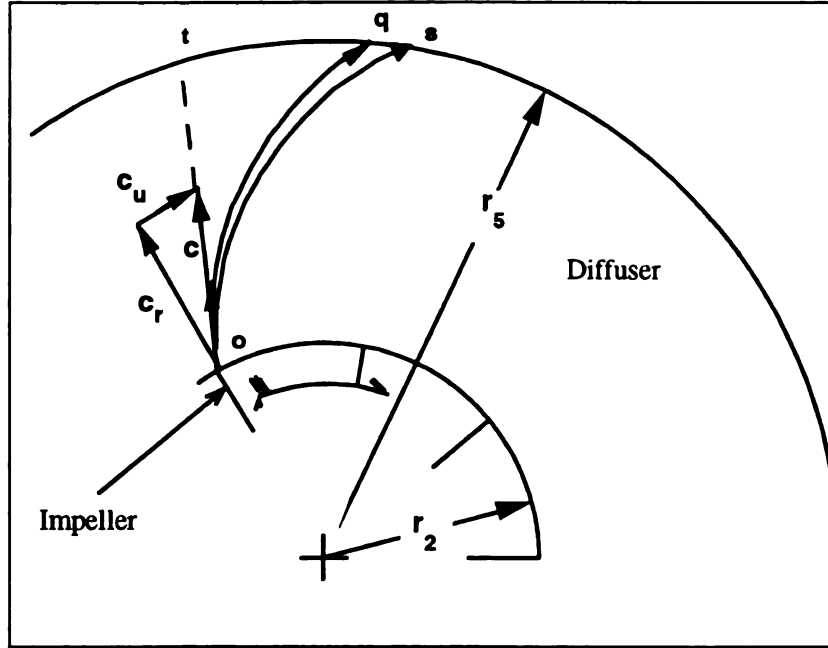


**Figure 3.22 Elementary View of Flow in Vaneless Diffuser**

The flow in the vaneless diffuser could be analyzed by estimating the radial change in the different parameters involved, which are:

Static Pressure,  $P$ ; Total Pressure,  $P_0$ ; Flow Angle,  $\alpha$ ; Absolute Velocity,  $c$ ; Density,  $\rho$ ; Static Temperature,  $T$ ; Total Temperature,  $T_0$ ; and Mach Number,  $M$ .

Analysis in this section will be applied on a two-dimensional model in cylindrical coordinates. This analysis could be achieved by applying the conservation equations on this two-dimensional simple case from the diffuser inlet to the diffuser outlet. Begin with Navier-Stokes (N-S) equations in the  $r$ - $\theta$ - $z$  coordinate system. The conservation equations in general forms are as follows:

( $C_r$ ,  $C_u$ , and  $C_z$  are the velocities in the  $r$ ,  $\theta$ , and  $z$  directions respectively)

Conservation of **mass (continuity)**:

$$\frac{\partial \rho}{\partial t} + \frac{1}{r} \frac{\partial}{\partial r} (\rho r C_r) + \frac{1}{r} \frac{\partial}{\partial \theta} (\rho C_u) + \frac{\partial}{\partial z} (\rho C_z) = 0 \quad (3.23)$$



### Conservation of linear momentum in r-direction

$$\begin{aligned} & \rho \left( \frac{\partial C_r}{\partial t} + C_r \frac{\partial C_r}{\partial r} + \frac{C_u}{r} \frac{\partial C_r}{\partial \theta} + C_z \frac{\partial C_r}{\partial z} - \frac{C_u^2}{r} \right) \\ &= F_r - \frac{\partial p}{\partial r} + \mu \left( \frac{\partial^2 C_r}{\partial r^2} + \frac{1}{r} \frac{\partial C_r}{\partial r} + \frac{1}{r^2} \frac{\partial^2 C_r}{\partial \theta^2} + \frac{\partial^2 C_r}{\partial z^2} - \frac{C_r}{r^2} - \frac{2}{r^2} \frac{\partial C_u}{\partial \theta} \right) \end{aligned} \quad (3.24)$$

### Conservation of linear momentum in $\theta$ -direction

$$\begin{aligned} & \rho \left( \frac{\partial C_u}{\partial t} + C_r \frac{\partial C_u}{\partial r} + \frac{C_u}{r} \frac{\partial C_u}{\partial \theta} + C_z \frac{\partial C_u}{\partial z} + \frac{C_r C_u}{r} \right) \\ &= F_u - \frac{1}{r} \frac{\partial p}{\partial \theta} + \mu \left( \frac{\partial^2 C_u}{\partial r^2} + \frac{1}{r} \frac{\partial C_u}{\partial r} + \frac{1}{r^2} \frac{\partial^2 C_u}{\partial \theta^2} + \frac{\partial^2 C_u}{\partial z^2} - \frac{C_u}{r^2} + \frac{2}{r^2} \frac{\partial C_r}{\partial \theta} \right) \end{aligned} \quad (3.25)$$

### Conservation of angular momentum

$$\vec{r} \times \vec{F}_s + \int_{cv} \vec{r} \times \vec{g} \rho dV + \vec{T}_{shaft} = \frac{\partial}{\partial t} \int_{cv} \vec{r} \times \vec{V} \rho dV + \int_{cs} \vec{r} \times \vec{V} \rho \vec{V} \cdot d\vec{A} \quad (3.26)$$

This analysis is restricted to a radial vaneless diffuser with constant width downstream of a centrifugal impeller. This analysis will be applied to two cases: 1) Incompressible and Inviscid flow and 2) Compressible and Inviscid flow.

#### 3.3.1 Incompressible and Inviscid Flow

##### Assumptions:

Steady state  $\left( \frac{\partial}{\partial t} = 0 \right)$ ;      Two-Dimension  $(r - \theta)$ ;      Neglect body forces;

Neglect surface forces;      Inviscid flow  $(\mu = 0)$ ;      Incompressible  $(\rho = \text{const.})$

Axi-symmetric  $\left(\frac{\partial}{\partial \theta} = 0\right)$ ; Adiabatic flow ( $q=0$ ); The z-axis aligned with the axes of rotation of the impeller

**Governing equations:** The governing equations after simplification will be:

Continuity equation

$$\frac{1}{r} \frac{\partial}{\partial r}(rC_r) = 0 \quad (3.27)$$

$$\text{or} \quad rC_r = \text{const.} \quad (3.28)$$

Momentum in the r-direction

$$C_r \frac{\partial C_r}{\partial r} - \frac{C_u^2}{r} = -\frac{1}{\rho} \frac{\partial P}{\partial r} \quad (3.29)$$

Momentum in the  $\Theta$ -direction

$$C_r \frac{\partial C_u}{\partial r} + C_r \frac{C_u}{r} = 0 \quad (3.30)$$

reduces to

$$\frac{C_u}{r} = -\frac{\partial C_u}{\partial r} \quad (3.31)$$

Substitute (3.31) into (3.29)

$$C_r \frac{\partial C_r}{\partial r} + C_u \frac{\partial C_u}{\partial r} = -\frac{1}{\rho} \frac{\partial P}{\partial r} \quad (3.32)$$

which becomes

$$\frac{\partial P}{\rho} + C_r \partial C_r + C_u \partial C_u = 0 \quad (3.33)$$

the flow is assumed to be adiabatic and frictionless (isentropic) then

$$\frac{\rho}{\rho_2} = \left( \frac{P}{P_2} \right)^{\frac{1}{\gamma}} \quad (3.34)$$

From the equation of state

$$\rho_2 = \frac{1}{RT_2} P_2 \quad (3.35)$$

From (3.35) into (3.34)

$$\frac{1}{\rho} = \frac{RT_2}{P_2} \left( \frac{P_2}{P} \right)^{\frac{1}{\gamma}} \quad (3.36)$$

Substitute into (3.33) to obtain

$$\left( \frac{P}{P_2} \right)^{-\frac{1}{\gamma}} \frac{\partial P}{P_2} + \frac{C_r \partial C_r + C_u \partial C_u}{RT_2} = 0 \quad (3.37)$$

From the velocity triangle

$$C^2 = C_r^2 + C_u^2 \Rightarrow C_2^2 = C_{r2}^2 + C_{u2}^2 \quad (3.38)$$

then

$$C_r \partial C_r + C_u \partial C_u = \frac{1}{2} d(C_r^2 + C_u^2) = \frac{1}{2} d(C^2) = C dC \quad (3.39)$$

Substitute (3.39) into (3.37) and integrate from  $P/P_2=1$  to  $P/P_2$ , and from  $C_2$  to  $C$

$$\int_{\frac{P}{P_2}=1}^{\frac{P}{P_2}} \left( \frac{P}{P_2} \right)^{-\frac{1}{\gamma}} d \left( \frac{P}{P_2} \right) = - \int_{C_2}^C \frac{C dC}{RT_2} \quad (3.40)$$

evaluate at the end points

$$\frac{\gamma}{\gamma-1} \left[ \left( \frac{P}{P_2} \right)^{\frac{\gamma-1}{\gamma}} - 1 \right] = -\frac{1}{2RT_2} (C^2 - C_2^2) \quad (3.41)$$

Further reduced

$$\left( \frac{P}{P_2} \right)^{\frac{\gamma-1}{\gamma}} = \frac{\gamma-1}{\gamma} \frac{C_2^2 - C^2}{2RT_2} + 1 \quad (3.42)$$

with

$$M = \frac{C}{\sqrt{\gamma RT}} \quad (3.43)$$

finally becomes

$$\left( \frac{P}{P_2} \right) = \left[ 1 + \frac{\gamma-1}{2} M_2^2 \left( 1 - \frac{C^2}{C_2^2} \right) \right]^{\frac{\gamma}{\gamma-1}} \quad (3.44)$$

Recall from velocity triangle at the impeller exit or diffuser inlet, equation (3.38) and

$$C_{r2} = C_2 \sin \alpha_2 \quad \text{and} \quad C_{u2} = C_2 \cos \alpha_2 \quad (3.45)$$

For analysis of turbomachines, and the rotating machines in general, the conservation of angular momentum equation (3.26), is often used in scalar form by considering only the component directed along the axis of rotation which is the z-axis as assumed before. Accordingly, equation (3.26) will be

$$T_z = \int_{CS} (\vec{r} \times \vec{V})_z (\rho \vec{V} \cdot d\vec{A}) \quad (3.46)$$

$$\text{where} \quad (\vec{r} \times \vec{V})_z = rC_{u2} - rC_{u1} \quad (3.47)$$

$$\rho \vec{V} \cdot d\vec{A} = \rho C_r A \quad (3.48)$$

then

$$T_z = \int_{A_2} r_2 C_{u2} \rho_2 C_{r2} dA_2 - \int_{A_1} r_1 C_{u1} \rho_1 C_{r1} dA_1 \quad (3.49)$$

Since the flow enter the impeller in the axial direction, then  $C_{u1}=0$ . Also, from continuity

$$\dot{m} = \rho_1 A_1 C_{r1} = \rho_2 A_2 C_{r2} = \text{const.} \quad (3.50)$$

$$\text{then} \quad T_z = \dot{m}(r_2 C_{u2} - r_1 C_{u1}^0) = \dot{m} r_2 C_{u2} = \text{const.} \quad (3.51)$$

$$\text{or} \quad r C_u = \text{const.} \quad (3.52)$$

which indicates that the tangential velocity component diffuses. It is unaffected by area change. This is because in axisymmetric flow, and in the absence of turning vanes and wall friction, the tangential velocity is inversely proportional to the radius.

Accordingly

$$\frac{C_u}{C_{u2}} = \frac{r_2}{r} = \frac{1}{\lambda} \quad (3.53)$$

where the radius ratio is defined as

$$\lambda = \frac{r}{r_2} \quad (3.54)$$

Again from the continuity equation (3.50) it is known that across the diffuser and for compressible flow

$$\rho_1 2\pi b r C_r = \rho_2 2\pi b r_2 C_{r2} \quad (3.55)$$

then

$$\frac{C_r}{C_{r2}} = \frac{\rho_2}{\rho} \frac{r_2}{r} = \frac{\rho_2}{\rho} \frac{l}{\lambda} \quad (3.56)$$

Substituting from (3.53), (3.56), and the velocity triangle relations, (3.38) and (3.45) into equation (3.44) we get, considering the vaneless space between  $r_2$  and  $r$  with constant width  $b$

$$\frac{P}{P_2} = \left\{ 1 + \frac{\gamma-1}{2} M_2^2 \left[ 1 - \frac{l}{\lambda^2} \left( \frac{\rho_2}{\rho} \right)^2 \sin^2 \alpha_2 - \frac{l}{\lambda^2} \cos^2 \alpha_2 \right] \right\}^{\frac{\gamma}{\gamma-1}} \quad (3.57)$$

This is for the general case, i.e. compressible and incompressible cases and both for inviscid flow. For incompressible flow  $\rho = \text{constant}$ , then from (3.57) we will have

$$\frac{P}{P_2} = \left\{ 1 + \frac{\gamma-1}{2} M_2^2 \left[ 1 - \frac{2}{\lambda^2} \right] \right\}^{\frac{\gamma}{\gamma-1}} \quad (3.58)$$

From the velocity triangle, the flow angle for incompressible case could be expressed as

$$\alpha = \tan^{-1} \left( \frac{C_r}{C_{u2}} \lambda \right) \quad (3.59)$$

for variable angle across the diffuser. The local formula is defined as

$$\alpha = \tan^{-1} \left( \frac{C_r}{C_u} \right) = \tan^{-1} \left( \frac{C_{r2}}{C_{u2}} \right) \quad (3.60)$$

### 3.3.2 Compressible and Inviscid Flow

For Inviscid and Compressible case, substitute from (3.34) into (3.57) for isentropic flow

$$\frac{P}{P_2} = \left\{ 1 + \frac{\gamma-1}{2} M_2^2 \left[ 1 - \frac{1}{\lambda^2} \left( \frac{P}{P_2} \right)^{-\frac{2}{\gamma}} \sin^2 \alpha_2 - \frac{1}{\lambda^2} \cos^2 \alpha_2 \right] \right\}^{\frac{\gamma}{\gamma-1}} \quad (3.61)$$

Or solve for Mach number

$$M_2 = \left[ \frac{\left( \frac{P}{P_2} \right)^{\frac{\gamma-1}{\gamma}} - 1}{\frac{\gamma-1}{2} \left( 1 - \frac{1}{\lambda^2} \left( \frac{P}{P_2} \right)^{-\frac{2}{\gamma}} \sin^2 \alpha_2 - \frac{1}{\lambda^2} \cos^2 \alpha_2 \right)} \right]^{\frac{1}{2}} \quad (3.62)$$

The flow angle for compressible flow could be expressed as

$$\alpha = \tan^{-1} \left( \frac{C_r}{C_{u2}} \frac{\rho}{\rho_2} \lambda \right) \quad (3.63)$$

for variable angle across the diffuser. The local formula is defined as

$$\alpha = \tan^{-1} \left( \frac{C_r}{C_u} \right) = \tan^{-1} \left( \frac{C_{r2}}{C_{u2}} \right)$$

which the same as that for incompressible flow equation (3.60).

## 4. EXPERIMENTAL SETUP

### 4.1 The Centrifugal Compressor Test Stand

The present investigations of performance of different diffusion systems for a centrifugal compressor were carried out on the first stage of a plant air-package compressor. The schematic outline of the test rig is shown in Figure 4.1. A variable speed motor with a maximum power input of 225 kW drove the centrifugal compressor. The impeller and the motor were coupled through a gearbox of 9.06 gear ratio. The speed of the motor was accurately controlled by a frequency controller capable of adjusting the power supplied to motor in accordance to the load on compressor.

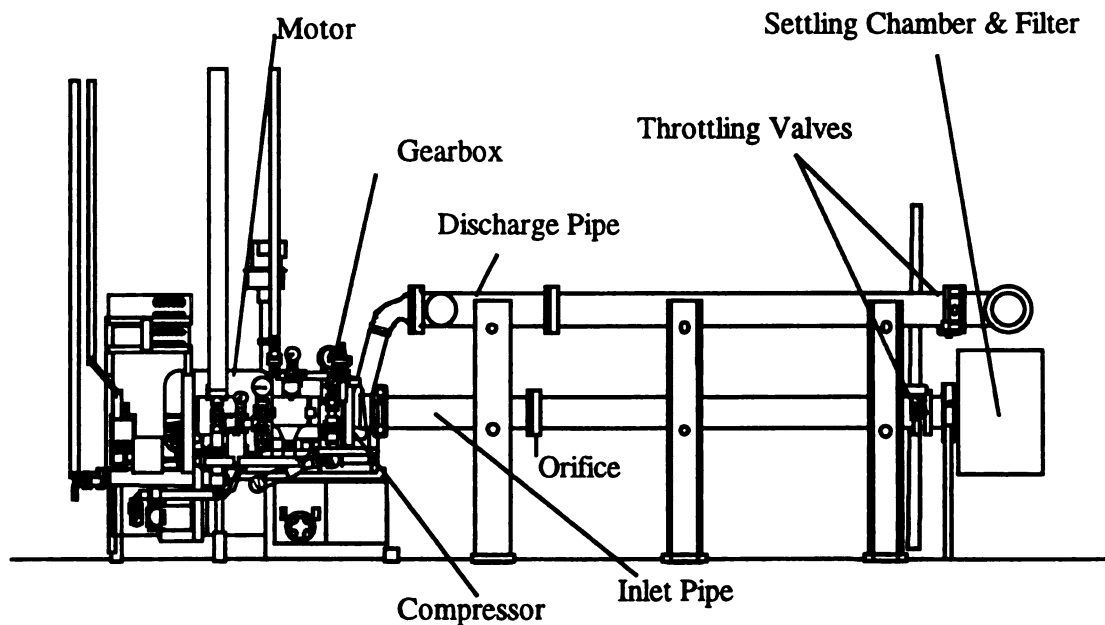


**Figure 4.1 Centrifugal Compressor test rig**

The unshrouded cast impeller has 19 blades with  $19.3^\circ$  backsweep. The blade camberlines have ellipsoidal shapes in cylindrical sections. The inlet hub and shroud



diameters were  $r_{1i}/r_2 = 0.193$  and  $r_{1s}/r_2 = 0.605$  respectively. The exit blade width at the tip was  $b_2/r_2 = 0.0546$ . The compressor was tested in an open air loop. The air entered the compressor through an air filter, settling chamber, and inlet pipe. The settling chamber provided the compressor with an air supply free of the temperature stratification and thus enabled the compressor inlet temperature to be measured accurately. After being compressed in the impeller, the air is discharged to the outlet pipe after passing through the diffuser and the volute of the compressor. The air in the outlet pipe is muffled before it is discharged. The mass flow rate through the compressor could be controlled by throttle valves located in the inlet and the outlet pipes. However, for the results presented here, the mass flow rate was controlled by the throttle valve located in the outlet pipe.



**Figure 4.2 Impeller of the tested configuration**

## 4.2 Investigated Vaneless Diffusers

Two vaneless diffusers were tested in this work. Both diffusers were tested downstream of the same impeller and were fixed to the casing of the compressor with three flat head screws. They had the same diffuser inlet radius to impeller tip radius ratio ( $r_3/r_2$ ) of 1.09 and the same diffuser exit radius to impeller tip radius ratio ( $r_5/r_2$ ) of 1.53. In order to investigate and understand the effect of diffuser width on the centrifugal compressor performance and the matching of the diffuser with the upstream impeller and the downstream volute, the two vaneless diffusers had different  $b_3/r_2$  ratio. The  $b_3/r_2$  ratio for VNLD1 and VNLD2 were 0.077 and 0.092, respectively. Both VNLD1 and VNLD2 were pinched from  $b_2/r_2$  (0.109) to  $b_3/r_2$  in a radial distance of 0.44 mm. The major geometric parameters of the two diffusers are given below in Table 4-1.

**Table 4-1 Design parameter of the tested vaneless diffusers**

	$r_2(\text{mm})$	$r_{1H}/r_2$	$r_{1S}/r_2$	$b_2/r_2$	$b_3/r_2$	$r_3/r_2$	$r_5/r_2$
Impeller	122	0.193	0.605	0.109	-	-	-
VNLD1	-	-	-	-	0.077	1.09	1.53
VNLD2	-	-	-	-	0.092	1.09	1.53

## 4.3 Measurement Positions and Measurements

The contents of this work involve both steady and unsteady experimental results taken from a centrifugal compressor having different vaneless diffuser configurations described in the previous section. Several static and total temperatures, static and total pressures, and unsteady pressure fluctuations were measured at different planes of the compressor stage in order to determine the mass flow rate through the stage, the overall performance, and the performance and interaction of various components of the

compressor stage. This section presents the details of all the measurement locations and the measured quantities at these locations. The mass flow rate was measured with an ASME standard orifice plate. Two total and two static temperatures were measured at different circumferential positions located opposite to each other at the same plane of the inlet pipe, upstream of the orifice. The differential pressure across the orifice plate was measured by two sets of static taps located down and upstream of the plate. The total pressure at the orifice was also measured at two locations in the same plane, upstream of the plate. The stage inlet static and total pressures were measured at two 90° apart circumferential positions each. Similarly, the inlet static and total temperatures are also measured at two different circumferential positions. The pressures are measured at a plane mid-way between the orifice plate and the inducer, while the temperatures are measured at a plane located at 330.2 mm from the inducer. Figure 4.2 shows all the measurement planes in the inlet pipe.

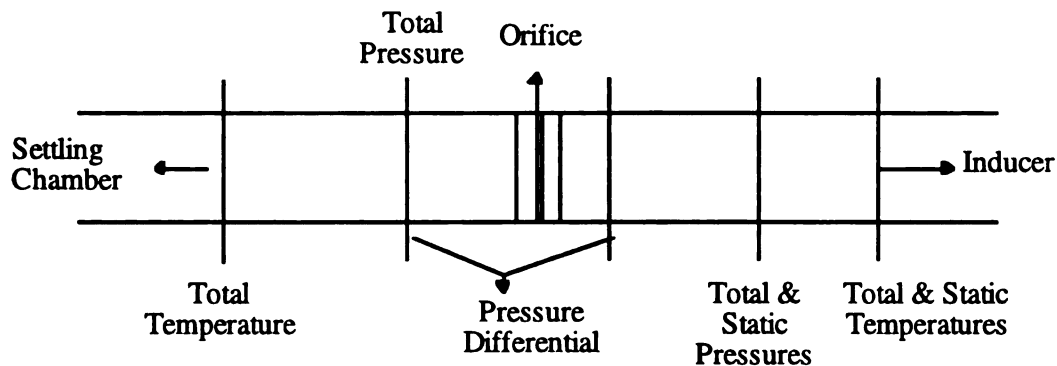


**Figure 4.3 Measurement planes in inlet pipe**

The inducer behavior is studied by measuring the static temperature just upstream of the inducer and the static pressures at two different axial positions in the inducer. Moreover, the pressure fluctuations at the inlet of the inducer are also measured. Figure 4.3 shows the location of the different planes, where measurement probes are installed.

The pressure fluctuations and the static pressure in the impeller are measured at  $r_{imp}/r_2$  ratio of 0.77. All measurements in the impeller are done at the same circumferential plane, and both the dynamic transducers measuring pressure fluctuations and the static pressure taps were located at an angle of  $42.5^\circ$  with respect to each other. All the static taps and the dynamic transducers in the inducer and the impeller were located on the casing of the compressor. The pressures at the exit of the impeller and at various locations in the diffuser were measured by the taps drilled on the backplate of the compressor. All these taps were located  $150^\circ$  -  $210^\circ$  away from the volute tongue in order to avoid any flow asymmetry caused by the presence of volute. Figure 4.4 shows the location of the different probes on the backplate of the compressor. In all, eight static taps were used to measure the pressure recovery from the impeller exit to the diffuser exit. A set of static taps was located at a radius ratio of  $(r_{2a}/r_2)$  1.04 to measure the static pressure at the impeller exit.

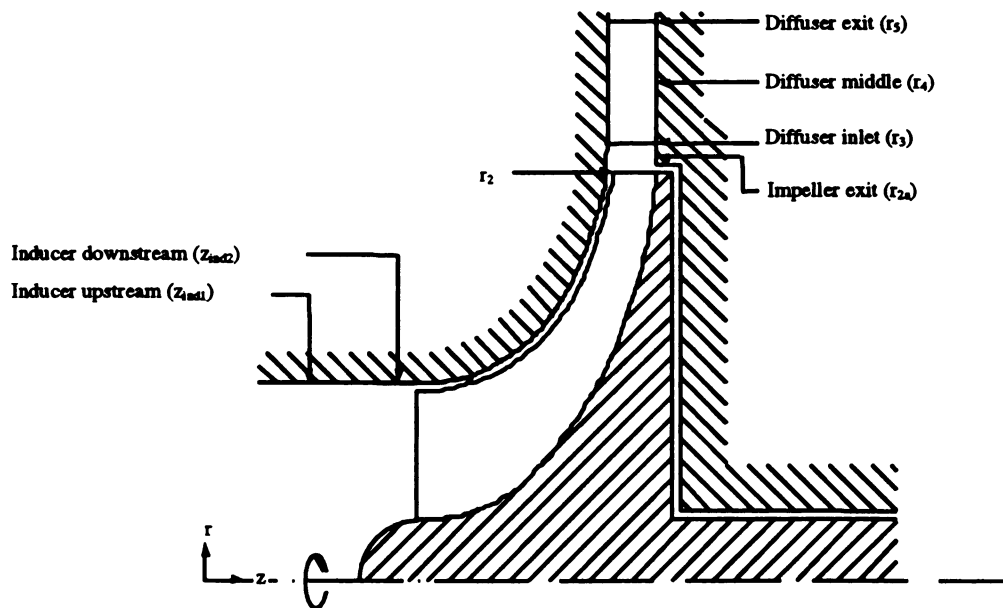


**Figure 4.4 Measurement Planes in the Compressor Stage**

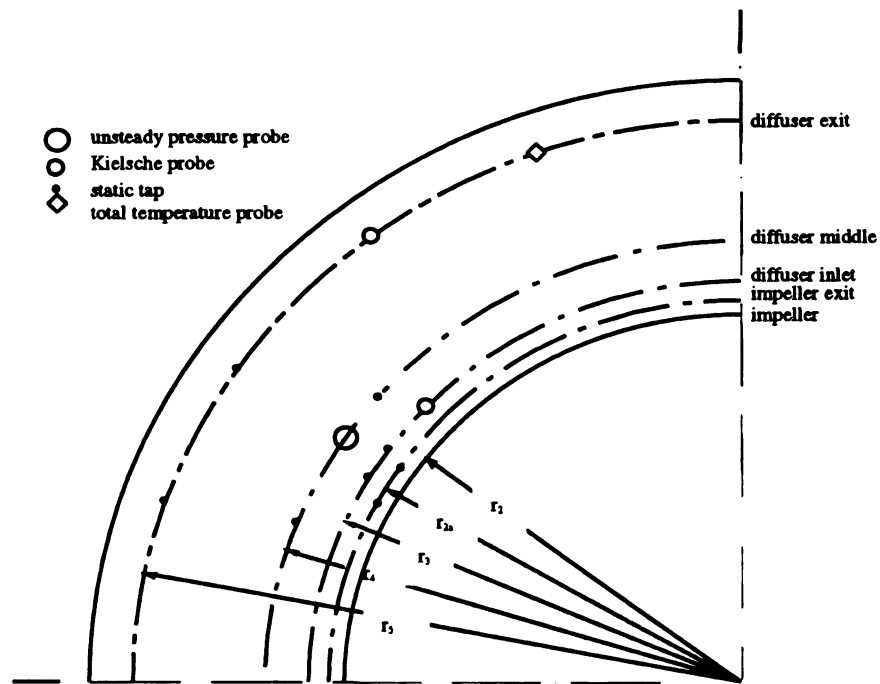


**Figure 4.5 Probe location in the diffuser**

The stage exit pressures and temperatures are measured in the pipe connected to the volute. The exit total and static pressures as well as the exit total and static temperatures are measured at four circumferential locations  $90^\circ$  apart in the pipe. The exit total and static temperatures are measured at a 76.2 mm downstream of the plane where pressures measured. In order to avoid the heat transfer effects on the temperature measurements, the casing of the compressor was covered with the insulating material. Table 4-2 summarizes all measurement locations and the quantities measured.

**Table 4-2 Measurement Locations And Measured Quantities**

Location	Position	Static pressure taps	Name	Other probes	Unsteady pressure transducers
Orifice	as described in ASME regulations	2	$p_{orf}$		
Inlet Pipe	$\frac{z_1}{r_{1s}} = 5$	2	$p_1$	2 total pressure 2 total temperature	
Inducer Upstream	$\frac{z_{ind1}}{r_{1s}} = 0.74$	1	$p_{ind1}$		
Inducer Downstream	$\frac{z_{ind2}}{r_{1s}} = 0.396$	1	$p_{ind2}$	1 temperature	Transducer A
Impeller	$\frac{r_{imp}}{r_2} = 0.77$	2	$p_{imp}$		Transducer B & C $\Delta\phi = 42.5^\circ$
Impeller Exit	$\frac{r_{2a}}{r_2} = 1.04$	2	$p_2$		
Diffuser Inlet	$\frac{r_3}{r_2} = 1.1$	2	$p_3$	1 total pressure	
Diffuser Middle	$\frac{r_4}{r_2} = 1.21$	2	$p_4$		Transducer D
Diffuser Exit	$\frac{r_5}{r_2} = 1.53$	2	$p_5$	1 total pressure 1 total temperature	
Discharge pipe		2	$p_6$	2 total pressure 2 total temperature	

## **4.4 Steady Performance Measurement**

This section enumerates the details of the instrumentation used to obtain the steady data, along with the data reduction procedure and the uncertainties in the performance parameters. Amineni (1996) and Kim (1998) designed and performed tests on the low solidity vaned diffusers with the same configuration.

### **4.4.1 Instrumentation**

The steady static and total pressures were measured with three different types of pressure measuring devices:

- 1) Validyne - variable reluctance pressure transducers
- 2) Omega - hand held manometers
- 3) water/mercury manometers

The water and mercury manometers had 1/10 of an inch resolution. One of the water manometers was used to measure the differential pressure across the orifice plate and the other was used for measuring the stage inlet static pressure; while the only mercury manometer was used to measure the stage exit static pressure. The usage of the water and mercury manometers at these locations was considered necessary to validate the proper functioning of the Validyne and Omega pressure transducers.

The static pressures were measured with 1/8-inch (3.18 mm) taps and the total pressures were measured with Kielsche type pressure probes. Flexible tubing was routed from the static pressure taps and the Kiel probes to the Validyne and Omega transducers. The Validyne transducers were connected to the Validyne digital transducer indicators with Belden type 8434 cable, while the Omega transducers had digital display integrated

to the transducer. The Validyne transducers were calibrated with an Omega pressure calibrator in conjunction with the water and mercury manometers. The water and mercury manometers used during the calibration process provided an additional check. On the other hand, the Omega pressure transducers were factory calibrated, and they were checked for proper function with the water and mercury manometers before use. All pressures were read to the second decimal digit, either in inches of water or mercury.

The total temperatures were measured by half shielded with bleed-slot, total temperature probes. All temperature measurements were done by copper-constantan (T-type) thermocouples connected to the Omega digital temperature indicators. The digital displays were calibrated by switching the display to a built in calibration setting and applying 0.00 mV at the thermocouple input to adjust zero reading and similarly applying 39.00 mV for full scale display reading of 560.0. Once calibrated, the digital displays were capable of indicating temperatures in either  $^{\circ}\text{F}$  or  $^{\circ}\text{C}$ . For the present study  $^{\circ}\text{C}$  display was chosen with 0.1  $^{\circ}\text{C}$  resolution.

#### **4.4.2 Data Collection and Reduction**

The compressor was tested at four different impeller speeds of 18800 rpm, 24000 rpm, 28000 rpm, and 32000 rpm for each vaneless diffuser configuration. The corresponding impeller tip Mach numbers are  $M_t = 0.7, 0.89, 1.04, \text{ and } 1.19$ . At each speed the temperature and pressure measurements were collected from all probe locations for approximately 9 to 11 different mass flow rates, ranging from compressor choke to surge in order to obtain a complete speed line. As mentioned earlier, the mass flow rate through the compressor was controlled with the throttle valve located at the stage exit.



At each flow point, the data were collected when the compressor stage reached stability in terms of the temperatures. Stability was reached if the temperatures at the stage inlet and exit stayed steady within  $\pm 0.1^{\circ}\text{C}$ . Thus, the stage inlet and exit temperatures were continuously monitored and recorded every 2 minutes until stability was attained. When the stage was considered stable, all the pressures and temperatures were recorded and transferred to a PowerPC for further data reduction and processing.

An Excel program was used for the data reduction and processing. The program first converts the recorded pressures and temperatures into  $\text{N/m}^2$  and  $^{\circ}\text{K}$  from either inches of mercury or inches of water and  $^{\circ}\text{C}$  respectively. At this stage the temperatures and pressures at each measurement plane are compared with each other and with downstream and upstream measurement planes. In this way any faulty or malfunctioning transducers are detected, and the data from them are eliminated before obtaining average pressures and temperatures at each measurement plane. The overall performance of the stage is calculated by using the averaged pressures and temperatures at various planes. The program is also capable of plotting these performance parameters with the mass flow rate or the impeller exit flow angles. This on-line plotting capability of the program acts as a good tool to monitor the behavior of the stage and the whole system; moreover, it also provides greater flexibility in control and operation.

There are too many parameters for the whole field to have been more than spotted with experiment. These parameters which will be calculated are the stage static and total pressure ratios, the total temperature ratio, the total-to-total isentropic efficiency of the stage, the head coefficient, the work coefficient, and the stage pressure recovery. In addition to the above mentioned overall performance parameters, individual component

performance was determined by calculating the impeller pressure ratio; the impeller total-to-total efficiency; and the pressure recovery of the impeller, the diffuser, and the volute.

The stage and impeller total pressure ratio compares the total pressures at the stage exit and rotor exit with the stage inlet total pressure. Because of the existence of a jet and wake system at the impeller exit, it was not possible to measure the total pressure at this location. Therefore, the closest available pressure probe placed downstream was used to obtain the necessary information. In other words, state three in equation (4.1) replaced state two. As such, they are

$$\pi_{0,rotor} = \frac{P_{03}}{P_{01}} \quad (4.1)$$

and

$$\pi_{0,stage} = \frac{P_{06}}{P_{01}} \quad (4.2)$$

Similarly, the rotor and stage static pressure ratios are given as

$$\pi_{rotor} = \frac{P_2}{P_1} \quad (4.3)$$

$$\pi_{stage} = \frac{P_6}{P_1} \quad (4.4)$$

The isentropic efficiency can likewise be calculated for both the rotor and the stage. Efficiency is the ratio of work done in an ideal process to the actual work in a real process. For compression process between two states 1 and 2, this can be expressed as a ratio of the isentropic work (representing the ideal process) and the real work. In terms of enthalpy, this becomes (Figure 2.6)

$$\eta_s = \frac{w_s}{w} = \frac{h_{02s} - h_{01}}{h_{02} - h_{01}} \quad (4.5)$$

For an ideal gas with constant  $c_p$ , the relation  $dh = c_p dT$  can be used to rewrite equation (4.5) in terms of temperatures

$$\eta_s = \frac{w_s}{w} = \frac{T_{02s} - T_{01}}{T_{02} - T_{01}} \quad (4.6)$$

In an isentropic process with constant properties, the pressures and temperatures are related according to

$$\frac{P_{02}}{P_{01}} = \left( \frac{T_{02s}}{T_{01}} \right)^{\left( \frac{\gamma}{\gamma-1} \right)} \quad (4.7)$$

Thus, substituting into equation (4.6), the isentropic efficiency for a compression process between state 1 and 2 can be written as

$$\eta_s = \frac{\left( \frac{P_{02}}{P_{01}} \right)^{\left( \frac{\gamma-1}{\gamma} \right)} - 1}{\frac{T_{02}}{T_{01}} - 1} \quad (4.8)$$

It is also known as total-to-total isentropic efficiency as the total conditions at states 1 and 2 are used to for calculation.

In the present investigation, equation (4.8) was used to find the isentropic total to total efficiency of the rotor and the stage. However, the heat transfer through the casing is assumed to be negligible; and, therefore, the stage exit total temperature is used for calculating the rotor efficiency too, i.e.  $T_{06} = T_{03}$ . The ratio of stage exit to inlet total temperature is also given as

$$\tau_0 = \frac{T_{06}}{T_{01}} = \frac{T_{03}}{T_{01}} \quad (4.9)$$

Thus, the appropriate expressions for rotor and stage efficiency are

$$\eta_{i-i, rotor} = \frac{\left(\pi_{0, rotor}\right)^{\left(\frac{\gamma-1}{\gamma}\right)} - 1}{\tau_0 - 1} \quad (4.10)$$

and

$$\eta_{i-i, stage} = \frac{\left(\pi_{0, stage}\right)^{\left(\frac{\gamma-1}{\gamma}\right)} - 1}{\tau_0 - 1} \quad (4.11)$$

The energy transferred by the rotating blades to the gas passing through the impeller per unit mass is defined as the compressor “head”. Although the compressor produces head, it cannot be measured directly. However, it can be calculated from the measured pressure ratio, inlet and exit temperatures and gas properties. The circumferential speed at state 2 is used to obtain a nondimensional form of the head coefficient according to equation (4.12)

$$\psi = \frac{\Delta h_{0s}}{\frac{1}{2}U_2^2} \quad (4.12)$$

and is known as isentropic head coefficient. Using equation (4.7) the head coefficient can be written in terms of measured quantities and gas properties as

$$\psi = \frac{c_p T_{01} \left[ \left(\pi_{0, stage}\right)^{\left(\frac{\gamma-1}{\gamma}\right)} - 1 \right]}{\frac{1}{2}U_2^2} \quad (4.13)$$

The work coefficient relates the isentropic head coefficient and the isentropic efficiency. It is a nondimensional value of the actual head produced by the compressor and is given as

$$\mu = \frac{c_p (T_{0s} - T_{01})}{\frac{1}{2}U_2^2} \quad (4.14)$$

The relation between the head coefficient, work coefficient and the efficiency is

$$\mu = \frac{\psi}{\eta} \quad (4.15)$$

The static pressure recovery between any two stations 1 and 2 was calculated as the percentage of impeller peripheral dynamic (or velocity) pressure.

$$Cp = \frac{P_2 - P_1}{\frac{1}{2} \rho_0 U_2^2} \quad (4.16)$$

Thus the pressure recovery of all the compressor components and the static pressure rise between various stations in the diffuser were calculated using equation (4.16). In addition to the static pressure recovery of the diffuser calculated as mentioned above, the static pressure rise from the diffuser inlet to the diffuser exit was also calculated as percentage of the dynamic pressure at the diffuser inlet.

$$Cp' = \frac{P_5 - P_3}{P_{03} - P_3} \quad (4.17)$$

The total pressure loss from the diffuser inlet to the volute exit was determined in terms of total pressure loss coefficient, which is expressed as

$$\xi = \frac{P_{03} - P_{06}}{\frac{1}{2} \rho_0 U_2^2} \quad (4.18)$$

The mass flow rate through the compressor was calculated from the differential pressure measured across the orifice as per the ASME standards. The equations used for the calculation are given in Miller (1992). In this report the mass flow rate is presented in nondimensional form known as flow coefficient that is given by

$$\phi = \frac{\dot{m}}{\rho_0 U_2 \frac{\pi d_2^2}{4}} \quad (4.19)$$

The flow angles at the impeller exit were calculated at the diffuser inlet as the static and total pressures at this station were measured. From the measured total and static pressures, the Mach number was determined

$$M_3 = \sqrt{\frac{2}{\gamma-1} \left[ \left( \frac{P_{03}}{P_3} \right)^{\left( \frac{\gamma-1}{\gamma} \right)} - 1 \right]} \quad (4.20)$$

Assuming that there was negligible heat transfer through the casing, i.e.  $T_{03}=T_{06}$  and the Mach number obtained above, the static temperature at the diffuser inlet was calculated

$$T_3 = \frac{T_{06}}{1 + \frac{\gamma-1}{2} M_3^2} \quad (4.21)$$

Now the absolute flow velocity was calculated from the basic relation that relates the total and static temperature at any point

$$C_3 = \sqrt{2 c_p T_{06} \left[ 1 - \left( \frac{T_3}{T_{06}} \right) \right]} \quad (4.22)$$

On the other hand, the radial component of the velocity at diffuser inlet was calculated from the continuity

$$C_{r3} = \frac{\dot{m}}{2\pi r_3 b_3 \rho_3} \quad (4.23)$$

The flow angle then was obtained from equations (4.22) and (4.23), with referring to Figure 2.5

$$\alpha_3 = \sin^{-1} \left( \frac{C_{r3}}{C_3} \right) \quad (4.24)$$

However, in this calculation of flow angle, no blockage caused by the boundary layer growth was considered. Thus, the flow angles calculated were invariably higher than the actual flow angles.

The diffuser efficiency,  $\eta_D$ , measures the diffuser performance between the diffuser inlet at  $r_3$  and the diffuser outlet at  $r_5$ . Referring to Figure 2.6, it is defined as the ratio of the ideal to the actual enthalpy rise required to accomplish the actual pressure rise between the radii  $r_3$  and  $r_5$ . It dose not involve any work transfer because  $h_{02}=h_{05}$ . Depending on the outlet point, the diffuser efficiency could be defined either as diffuser static-to-static efficiency if the enthalpy rise taken from inlet static to outlet static. On the other hand, it could be defined as diffuser total-to-static efficiency if the enthalpy rise taken from inlet static to outlet total.

$$\eta_{D,s-s} = \frac{h_{5s} - h_2}{h_5 - h_2} \quad (4.25)$$

$$\eta_{D,t-s} = \frac{h_{05s} - h_2}{h_{05} - h_2} \quad (4.26)$$

Assume that the fluid behaves as a perfect gas and using equation (4.7), then

$$\eta_{D,s-s} = \frac{\frac{T_{5s}}{T_2} - 1}{\frac{T_5}{T_2} - 1} = \frac{\left(\frac{P_5}{P_2}\right)^{\frac{\gamma-1}{\gamma}} - 1}{\frac{T_5}{T_2} - 1} \quad (4.27)$$

$$\eta_{D,t-s} = \frac{\frac{T_{05s}}{T_2} - 1}{\frac{T_{05}}{T_2} - 1} = \frac{\left(\frac{P_{05}}{P_2}\right)^{\frac{\gamma-1}{\gamma}} - 1}{\frac{T_{05}}{T_2} - 1} \quad (4.28)$$

All the quantities are measured except  $T_2$ , so the ratios  $T_5/T_2$  and  $T_{05}/T_2$  should be replaced using equation (4.21) and that  $T_{02}=T_{05}$ , then

$$\eta_{D,s-s} = \frac{\left[ \left( \frac{P_5}{P_2} \right)^{\frac{\gamma-1}{\gamma}} - 1 \right] \left[ 1 + \frac{\gamma-1}{2} M_5^2 \right]}{\frac{\gamma-1}{2} (M_2^2 - M_5^2)} \quad (4.29)$$

$$\eta_{D,s-s} = \frac{\left( \frac{P_{05}}{P_2} \right)^{\frac{\gamma-1}{\gamma}} - 1}{\frac{\gamma-1}{2} M_2^2} \quad (4.30)$$

Equations (4.29) and (4.30) give the diffuser efficiencies in terms of measured and computed values of total and static pressures and mach numbers at the diffuser inlet and diffuser outlet.

#### 4.4.3 Instrument Accuracy and Result Uncertainty

Errors could present when experimental measurements are made. These errors could be due to instrument accuracy, competence of the people using the instruments, etc. The interest is in knowing the uncertainty in the final result due to the uncertainties in the primary measurements. Experimental error may be of two types. Fixed or systematic error causes repeated measurements to be in error by the same amount for each trial. Fixed error is the same for each reading and can be removed by proper calibration or correction. Random error or nonrepeatability is different for every reading and hence cannot be removed. The factors that introduce random error are uncertain by their nature. To eliminate the effects of fixed errors, it is assume that the equipment has been constructed correctly and calibrated properly. It is assume also that instrumentation has



adequate resolution and that fluctuations in readings are not excessive. Also, it is assume that care is used in making and recording observations so that only random errors remain. The estimation in the probable random errors in experimental results could be taken care of by performing uncertainty analysis. Through this section, the accuracy of the instrument used and the stage efficiency uncertainty will be presented.

The Validyne pressure transducers were able to measure with an accuracy of  $\pm 0.25\%$  of full scale; which includes the effects of linearity, hysteresis, and repeatability at an operating temperature range of  $0^\circ\text{F}$  ( $-17.78^\circ\text{C}$ ) to  $160^\circ\text{F}$  ( $71.1^\circ\text{C}$ ). The accuracy of the Omega digital temperature indicators was  $\pm 0.5^\circ\text{C}$  at  $0.1^\circ\text{C}$  resolution setting under the operating temperatures of  $5$  to  $45^\circ\text{C}$  for T-type thermocouples. Equation (4.11) indicates that the stage efficiency is a function of  $P_{01}$ ,  $P_{06}$ ,  $T_{01}$ , and  $T_{06}$ .

$$\eta_{1-2, \text{stage}} = \frac{(\tau_{0, \text{stage}})^{\left(\frac{\gamma-1}{\gamma}\right)} - 1}{\tau_0 - 1} = \eta(P_{01}, P_{06}, T_{01}, T_{06})$$

Let  $u_\eta$  be the uncertainty in the stage efficiency and  $u_{P_{01}}$ ,  $u_{P_{06}}$ ,  $u_{T_{01}}$ , and  $u_{T_{06}}$  be the uncertainties in the independent variables or the primary measurements. Holman (1994) showed that the uncertainty in the result is

$$u_\eta = \left[ \left( \frac{\partial \eta}{\partial P_{01}} u_{P_{01}} \right)^2 + \left( \frac{\partial \eta}{\partial P_{06}} u_{P_{06}} \right)^2 + \left( \frac{\partial \eta}{\partial T_{01}} u_{T_{01}} \right)^2 + \left( \frac{\partial \eta}{\partial T_{06}} u_{T_{06}} \right)^2 \right]^{0.5} \quad (4.31)$$

In this work, data reduction is performed which results in rather complicated affairs. Accordingly, a small adaptation is provided for direct calculation of uncertainties without resorting to analytical determination of the partial derivatives in equation (4.31). For enough changes in the independent values which assigned as  $x$  here, the partial derivatives can be determined by

$$\frac{\partial \eta}{\partial x} \approx \frac{\eta(x + \Delta x) - \eta(x)}{\Delta x} \quad (4.32)$$

These values could be inserted in equation (4.31) to calculate the uncertainty in the compressor stage efficiency as shown in Table 4-3.

**Table 4-3 Instrument specifications**

	<b>P01</b>	<b>P06</b>	<b>T01</b>	<b>T06</b>	<b><math>\eta_{\text{stage}}</math></b>
<b>Company</b>	Validyne + u. sensor	Validyne+ u. sensor	Omega + u. sensor	Omega + u. sensor	-
<b>Range</b>	20 psi	50 psi	-99.9-401.4°C	-99.9-401.4°C	-
<b>Accuracy</b>	±1.25%	±1.25%	±1.1%	±1.1%	±2.35%

## **4.5 Unsteady Performance Measurement**

### **4.5.1 Obtaining and Storing the Pressure Signal**

The pressure fluctuations were measured by PCB pressure transducers. The transducers in the inducer and in the impeller were mounted on the shroud wall, as where the transducer in the diffuser was mounted on the compressor back plate. All pressure transducers were flush mounted because this eliminated any gap between the transducer diaphragm and the measurement location. Thus, no usable frequency range of the transducer was lost.

The PCB transducer uses a stack of thin piezoelectric quartz crystal wafers used to convert the applied pressure on the transducer diaphragm into electric charge. The charge produced is proportional to the applied pressure. The transducer has a built-in accelerometer that compensates for any acceleration and reduces distortion and resonance in high vibration environments. The transducer also has a built in temperature

compensation that allows it to operate in a temperature range of  $\pm 205^{\circ} C (\pm 401^{\circ} F)$ . The transducer can measure pressure fluctuations in a range of  $0-6.89 \times 10^5 \text{ N/m}^2$  with  $13.8 \text{ N/m}^2$  resolution. It has a natural frequency of 250 kHz with a usable frequency of 80 kHz. When a constant pressure is applied to the PCB transducers for a long time ( $> 100$  sec), the output charge does not remain constant and decreases with time. For the transducers used for experiments described in this report, the output charge would be constant for about 30-60 seconds. This makes it impossible to measure the steady absolute pressure with these transducers, and they can only measure pressure fluctuations. Thus, the averaged static pressure was measured through the static taps and Validyne transducers at every plane where unsteady transducers were mounted.

The signal from the PCB pressure transducer was conducted to an inline amplifier through 10 feet of low-noise coaxial cable. The inline amplifier conditions the transducer output signal. This amplifier has high input impedance ( $10^{11}$  ohms ) and a range capacitor in order to avoid any distortions in the signal through input capacitance shunting. The signal was then passed on to the signal conditioner through a 50 foot low-noise coaxial cable. Even though one inline amplifier was used for each transducer, one signal conditioner was used for all four signals. The signal conditioner powered both the inline amplifier and the PCB transducer and could also amplify the signal with fixed gain of 1, 10, or 100. During the system evaluation tests, it was found that the gain had no effect on the signal to noise ratio, indicating that the noise was being added to the signal before it reached the signal conditioner. Since the signal to noise ratio was unchanged with signal gain and the amplitude of the signal was small, a gain of 100 was used to obtain better resolution of the signal.

The amplified signals from the signal conditioner were transferred to a two-channel HP signal analyzer. The signals were stored and transferred to a PC for further processing and analysis through the signal analyzer and the signal processing software. The HP signal analyzer also provided the capability for on-line signal analysis through the various features available with it. It was possible to obtain the power spectrum, phase and cross-correlation between two signals for on-line monitoring of the compressor. The complete signal flow path is shown in Figure 4.5.

#### **4.5.2 Signal Processing**

Since the signal analyzer had only two channels, the signal capture through the signal analyzer was done in pairs of two transducers. Transducer B located in impeller was used as reference for all captures, i.e. signal from transducer B was captured through channel 1 and the signal from transducers A, C, and D was captured through channel 2 of the signal analyzer alternately at each flow point. Thus, at each flow point for a given capture frequency, three captures were made with BA, BC, and BD transducer combinations at the two channels of the signal analyzer.

Even though the captures could be made at any sampling frequency of up to 261.12 kHz per channel, most captures were made at 12 kHz and 4096 Hz sampling frequency. The high frequency was used to observe the blade to blade pressure fluctuations, and small captures of 5 to 10 records were taken. Each record had 1024 sample points. The captures at 2048 Hz were taken to study the unsteady flow patterns in different components of the compressors. The record lengths at this frequency ranged anywhere between 8 to 64 records. The choice of either 2048 Hz or 4096 Hz was based on the available memory of the signal analyzer and the required resolution of the capture.

Moreover, literature survey has shown that in most cases the rotating stall frequency was lower than the impeller rotational frequency. The maximum rotational frequency in the present experiments was 540 Hz, and with a 2048 Hz sampling frequency the usable frequency range was 800 Hz and with 4096 Hz sampling frequency the usable frequency range was 1600 Hz.

Once the capture was taken and stored on the PC, the signal data are processed using in-house signal processing software (UDACS). The software has various data preparation tools such as windowing, filtering, removal of mean, removal of linear trend, etc. It also provides options to choose different kinds of filters and windowing methods.

From the prepared data power spectrum, cross spectrum, amplitude spectrum, phase, and coherence are calculated. In addition to these features, the software was also capable of graphical display of the raw data and the results or processed data in time or frequency domain. The following parameters were used for the computation of the spectral functions:

- 64 records from each transducer were captured
- the sampling frequency was 4096 Hz
- each record contained 1024 discrete points, which corresponds to 0.5 seconds
- all records were detrended
- a Hanning window was applied
- 50% overlapping was used
- the power spectrum, the cross spectrum, and the phase shift were calculated
- the output is represented in terms of decibels, the reference being 1 kPa.

The details of the software and the procedures used to accomplish the results can be found in Wilmsen (1996).

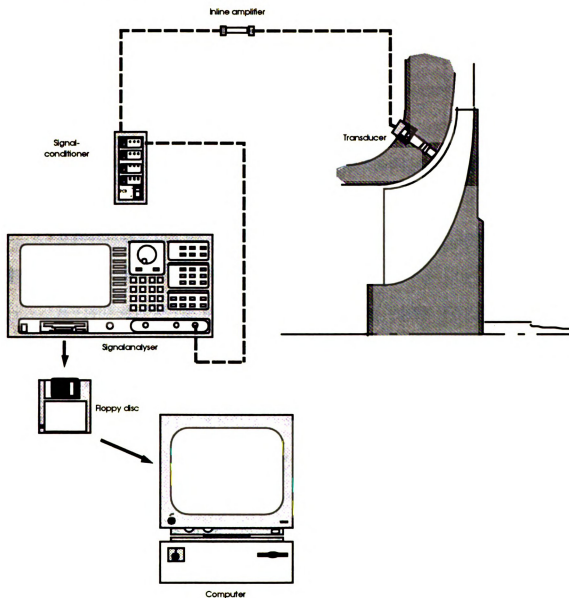


**Figure 4.6 Unsteady pressure signal flow path**

#### **4.5.3 Analysis of the Data**

After performing all the spectral analysis, one should determine whether any peaks could be found in the power spectra. If no single peaks are present, a periodic signal can be excluded; and consequently no rotating stall can be expected. If the power

spectrum increases for one operating point at all frequencies, this is a sign for a general increase of unsteadiness. But if one peak is detected, one should look at the cross spectrum of B and C, as well as at the coherence of B and C. If all graphs show the existence of a peak, the analysis described below should be followed:

- If a peak is not present at all transducer - locations, a surge can be excluded. If a surge occurs, the peak should be visible in all transducers.

- A peak that is present at all operating points is not due to flow phenomena. This may have its causes in vibrations or electrical distortions.

- If peaks occur that are not common in transducer B and C, a rotating stall in the impeller can be with good uncertainty excluded.

- If a peak appears that is common in all transducer and the phase shift between B and C is close to zero, this could be a surge. Ideally, the phase shift between B and C should be zero, but the setup with a volute could possibly make the flow uneven up to the impeller and cause a small phase shift between B and C.

- If a peak occurs only in the diffuser or in the inducer, a local periodic instability would be detected. It could be rotating or intermittent. This can be examined by examining the time domain. If the stall is rotating, no information about rotational speed and number of cells can be achieved; therefore, a second transducer at the same radial position is necessary. But if the signal is strong enough it might be also visible in the signals from the two transducers in the impeller. A peak that is common in B and C and where the phase shift is not close to zero could be a rotating stall.

## 5. RESULTS AND DISCUSSIONS

Two vaneless diffusers (VNLD1 and VNLD2) were tested experimentally downstream of the same impeller. Each vaneless diffuser was tested at four different impeller speeds, 18800 rpm, 24000 rpm, 28000 rpm, and 32000 rpm. These speeds correspond to impeller tip Mach numbers of  $M_t = 0.7, 0.89, 1.04, \text{ and } 1.19$ . At each speed, the compressor with each VNLD was investigated in terms of overall steady stage performance, component-wise detailed steady local performance, and unsteady performance. These investigations of each diffuser are compared in order to understand the advantages and disadvantages of both vaneless diffusers used in centrifugal compressor stage. That includes the operating range, the performance parameters at peak efficiency, the influence of diffuser type on pressure history, pressure recovery in both the vaneless diffusers, and the centrifugal compressor stage in addition to other performance parameters.

The effect of the vaneless diffuser type on the unsteady flow regimes in the inducer, the impeller, and the vaneless diffuser through the compressor stage is also investigated. Investigations also include a comparison between the experimental and theoretical results through the diffuser in terms of the pressure ratio.

Through this work, all the presented performance curves are normalized with respect to the design point flow and the performance parameters of VNLD1 at impeller speed of 28000 rpm ( $M_t = 1.04$ ). A typical test at any speed consisted of nine to eleven operating points and ranging from choke (maximum flow) to stall/surge.



## **5.1 Overall Compressor Stage Performance Characteristics**

### **5.1.1 Stage Efficiency and Head Coefficient**

As mentioned before, two vaneless diffusers (VNLD1 and VNLD2) were tested experimentally downstream of the same impeller at four different impeller speeds: 18800 rpm, 24000 rpm, 28000 rpm, and 32000 rpm. It is noted that VNLD2 is wider than VNLD1 by nearly 17%. Through this section, the overall performance characteristics of each of these two vaneless diffusers are compared with each other in order to investigate the effect of both vaneless diffusers on the centrifugal compressor stage. Also, the results obtained from both vaneless diffusers will be compared in terms of operating range, the performance parameters at peak efficiency, and the influence of diffuser type on the pressure history.

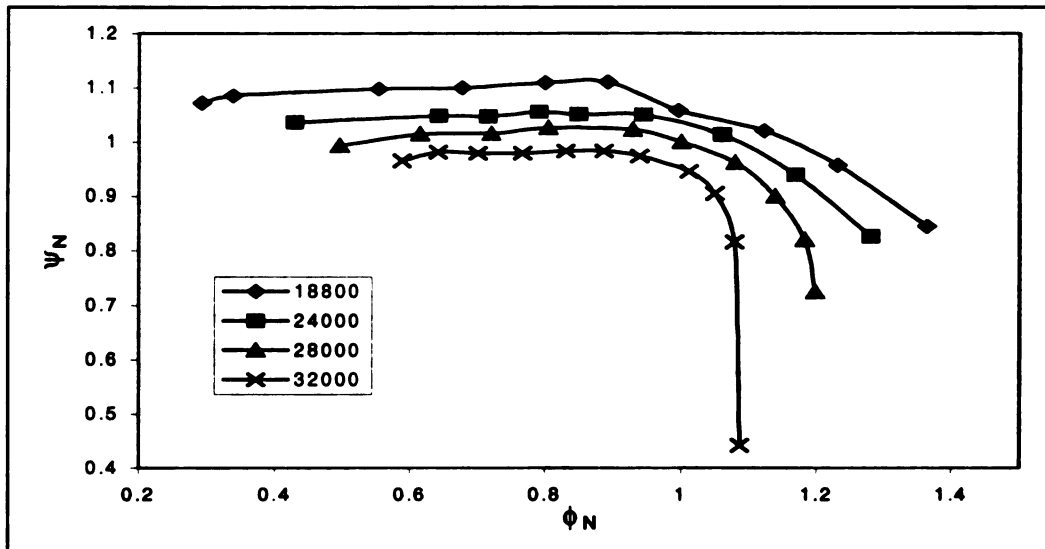
The performance characteristics of the centrifugal compressor stage with VNLD1 and VNLD2 at four different impeller speeds are shown in Figure 5.1 and Figure 5.2. These performance characteristics consisting of the normalized head coefficient ( $\psi_N$ ) and the normalized stage efficiency ( $\eta_N$ ) both versus the normalized flow coefficient ( $\phi_N$ ). All curves in Figure 5.1 and Figure 5.2 have the same characteristic shape. Starting with a high mass flow at the choke condition, the values of  $\psi_N$  and  $\eta_N$  rise rapidly to a certain extent and decrease much slower until the diffuser stalls and gives rise to compressor surge. That condition is clearer as the impeller speed increased.

It should be noted in the beginning that the normalized head coefficient, which is a measure of the energy transferred by the compressor to the fluid passing through it, is decreased as the impeller speed increased. By comparing the head coefficients plots for both vaneless diffusers and at all speeds, it could be seen that generally VNLD2 showed a

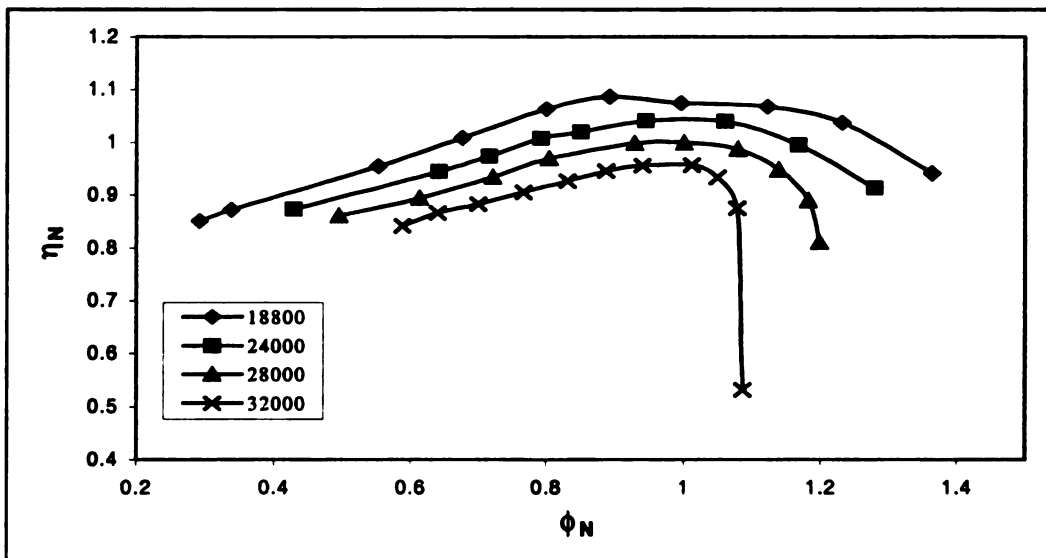
better head coefficient than VNLD1 at low to medium impeller speeds (18800 rpm, 24000 rpm, and 28000 rpm). At 32000 rpm, VNLD1 has a better head coefficient over the whole flow range. Note that as the impeller speed increased, the difference in the head coefficient between VNLD1 and VNLD2 decreased.

The normalized stage efficiency curves showed a similar manner in which they decrease as the impeller speed increases. The centrifugal compressor with VNLD2 showed a better efficiency than with VNLD1 at impeller speed of 18800 rpm, 24000 rpm, and 28000 rpm. At 32000 rpm, VNLD1 has a better efficiency than VNLD2 over the whole flow range.

In addition to having better head coefficient and stage efficiency, the centrifugal compressor with VNLD2 had a wider flow range than with VNLD1 at each impeller speed. This could be noted from the performance curves on Figure 5.1 and Figure 5.2, which show that the choke and surge flow conditions for both vaneless diffusers are different. VNLD2 choked at a higher mass flow rate at all impeller speeds. Also VNLD2 has the lowest surge mass flow rate, indicating more stability than VNLD1.

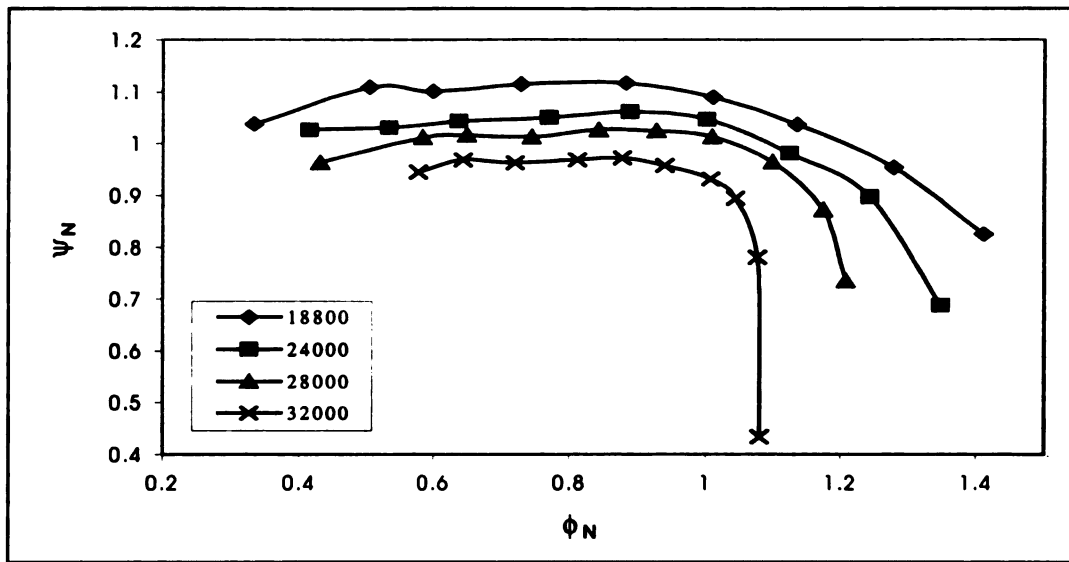


(a) Head coefficient  $\psi_N$  vs. flow coefficient  $\phi_N$

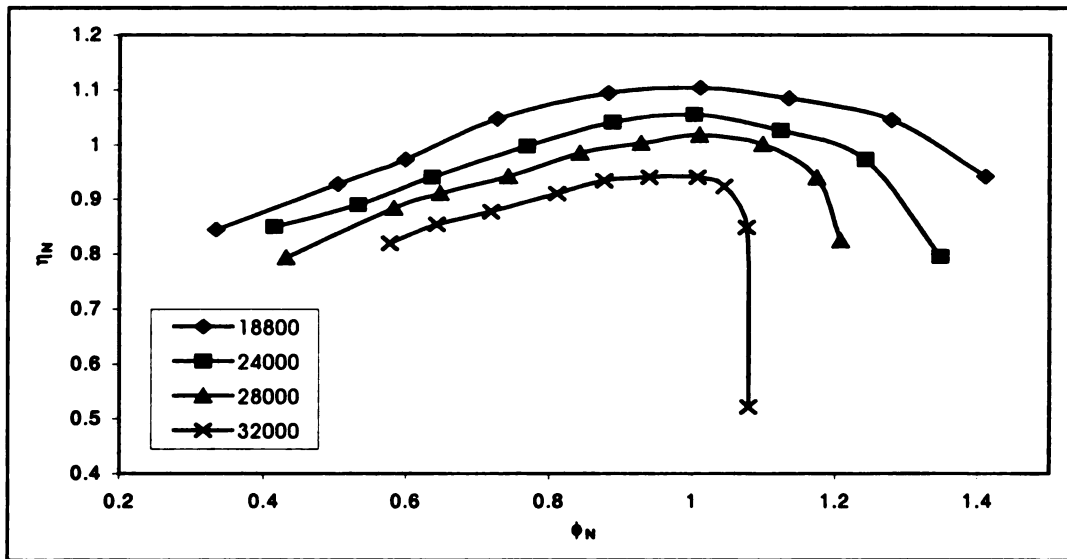


(b) Stage efficiency  $\eta_N$  vs. flow coefficient  $\phi_N$

**Figure 5.1 Performance characteristics of the compressor stage with VNLD1**



(a) Head coefficient  $\psi_N$  vs. flow coefficient  $\phi_N$



(b) Stage efficiency  $\eta_N$  vs. flow coefficient  $\phi_N$

**Figure 5.2 Performance characteristics of the compressor stage with VNLD2**

### 5.1.2 Flow Range

The total operating range of the centrifugal compressor stage (choke to surge) is shown in Figure 5.3 as a function of the impeller tip Mach number. As expected, VNLD2 has the higher operating range at impeller tip Mach number of 0.89, 1.04, and 1.19 by an average of 3%. At  $M_t=0.7$ , VNLD1 has slightly a higher operating range than VNLD2 due to the compressor stall at low flow rate. It could be noted that at each speed, the total operating range attained by each vaneless diffuser was limited by their surge mass flow rates. An interesting observation from Figure 5.3 is that VNLD1 and VNLD2 have a similar trend in decrease of operating range as the impeller speed increases. Their behavior is similar in that they show a linear decrease in the operating range.

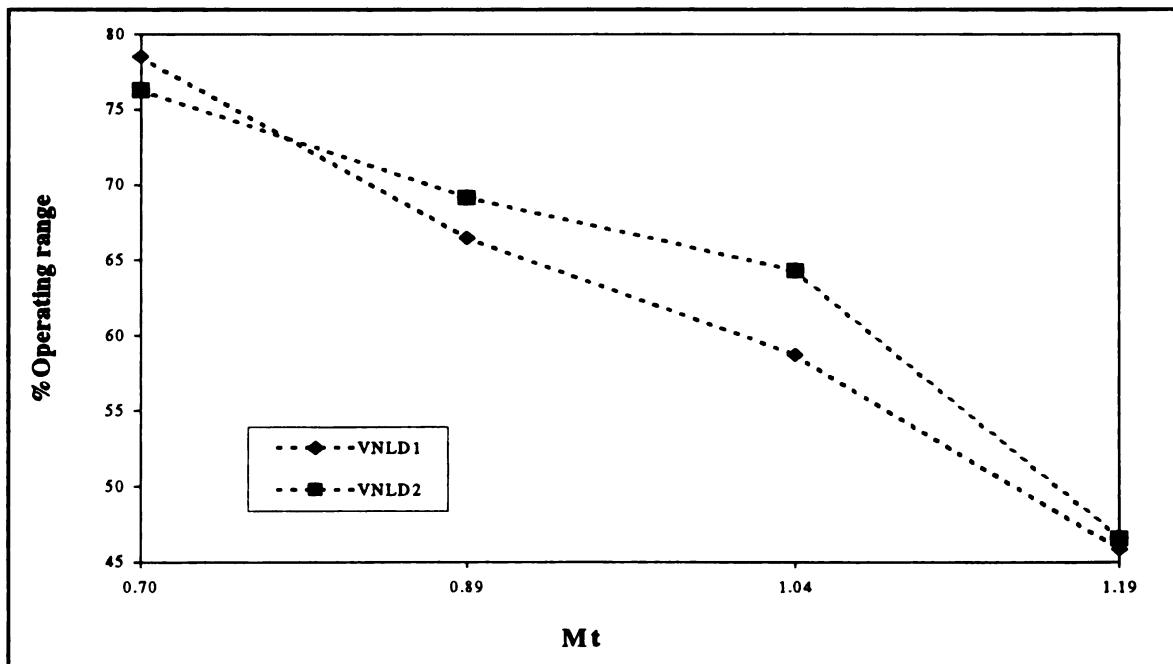


**Figure 5.3 Total operating range of the compressor stage with VNLD1 and VNLD2 vs. impeller tip Mach number  $M_t$**

### 5.1.3 At Peak Efficiency

The variation of the peak efficiency of the compressor stage at each impeller speed is shown in Figure 5.4. At impeller tip mach number of 0.7, 0.89, and 1.04; VNLD2 has 2 to 3 percent higher normalized peak efficiency than VNLD1. This difference in the normalized peak efficiency is almost constant at all three speeds. At  $M_t=1.19$ , VNLD1 has a higher normalized peak efficiency by approximately 2 percent, which indicates that VNLD1 has a better performance at higher impeller speeds while VNLD2 have better results at lower to medium speeds.

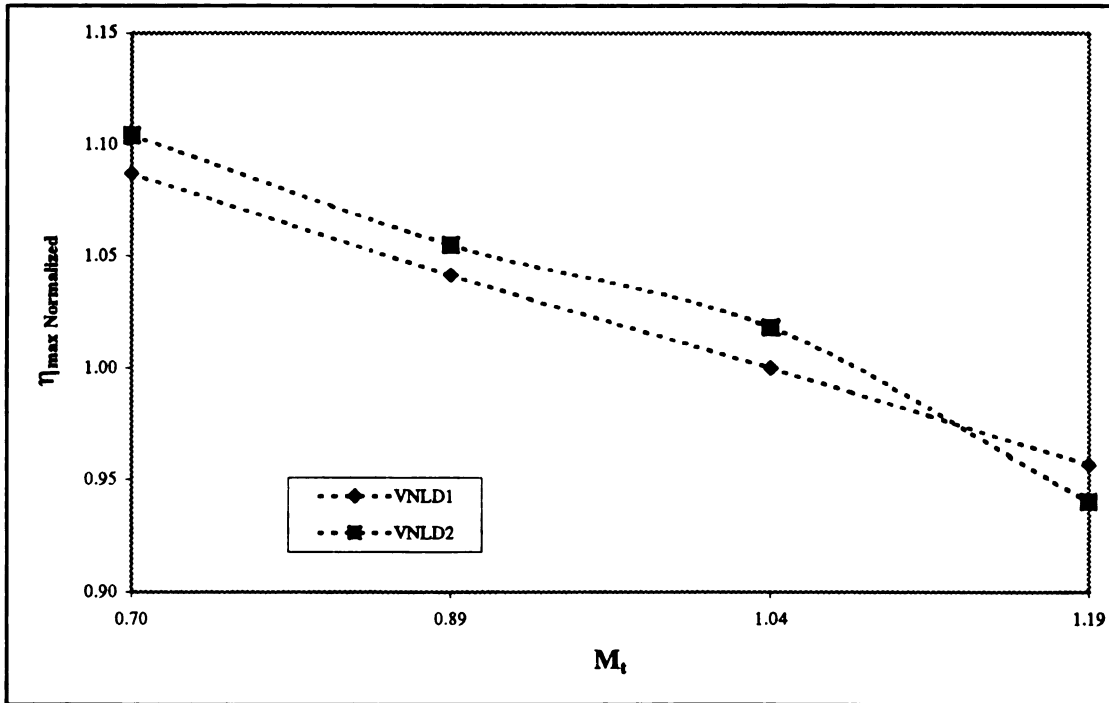


**Figure 5.4 Compressor stage at peak efficiency vs. impeller tip Mach number  $M_t$  for VNLD1 and VNLD2**

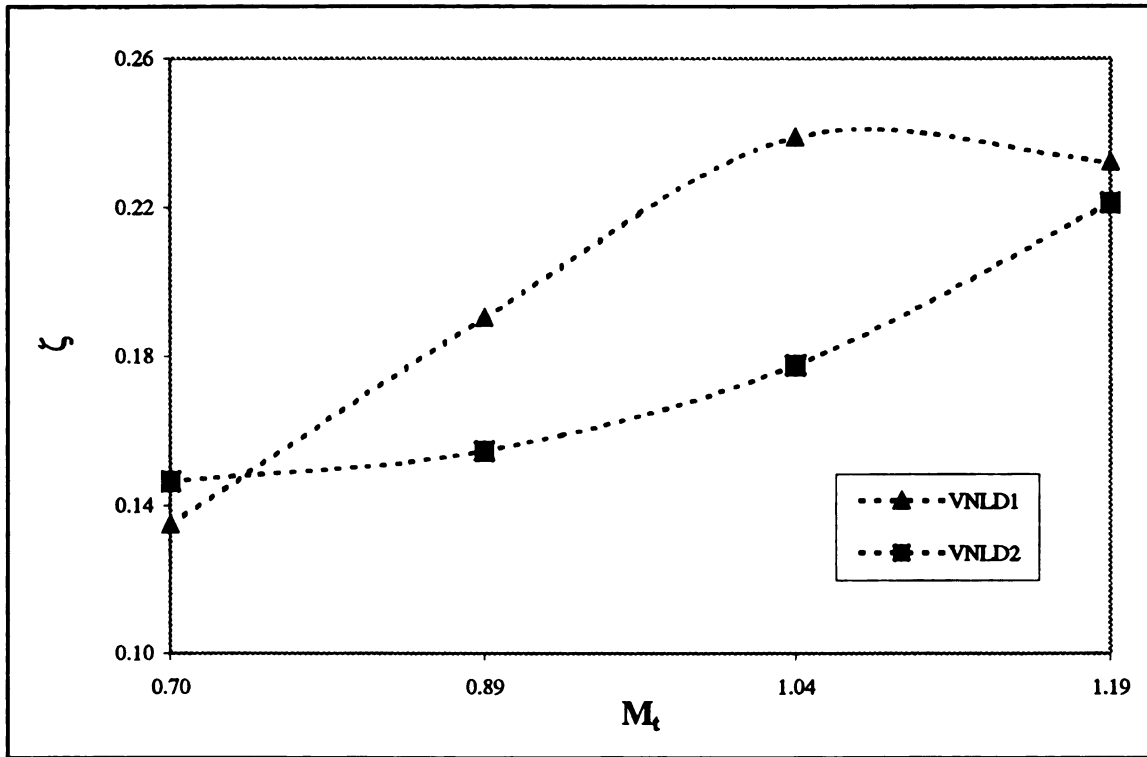


**Figure 5.5 Loss coefficient at peak efficiency vs.  $M_t$  for VNLD1 and VNLD2**

With respect to Figure 5.5 the normalized loss coefficient at peak efficiency for both VNLD1 and VNLD2 along with the downstream volute is shown at each impeller speed. As expected, the loss coefficient increases as the impeller speed increases. VNLD1 has higher losses at medium to high speeds, which are at an impeller tip Mach number of 0.89, 1.04, and 1.19. VNLD2 has higher losses at  $M_t=0.7$ , which is due to compressor stall at a higher flow rate. Also the total pressure measurements at station 3 is not reliable, which could cause that VNLD2 has higher losses at  $M_t=0.7$ . From these results, it could be noted that the centrifugal compressor stage with VNLD2 (the wider vaneless diffuser) has slightly a better stage efficiency and lower losses than VNLD1 (the

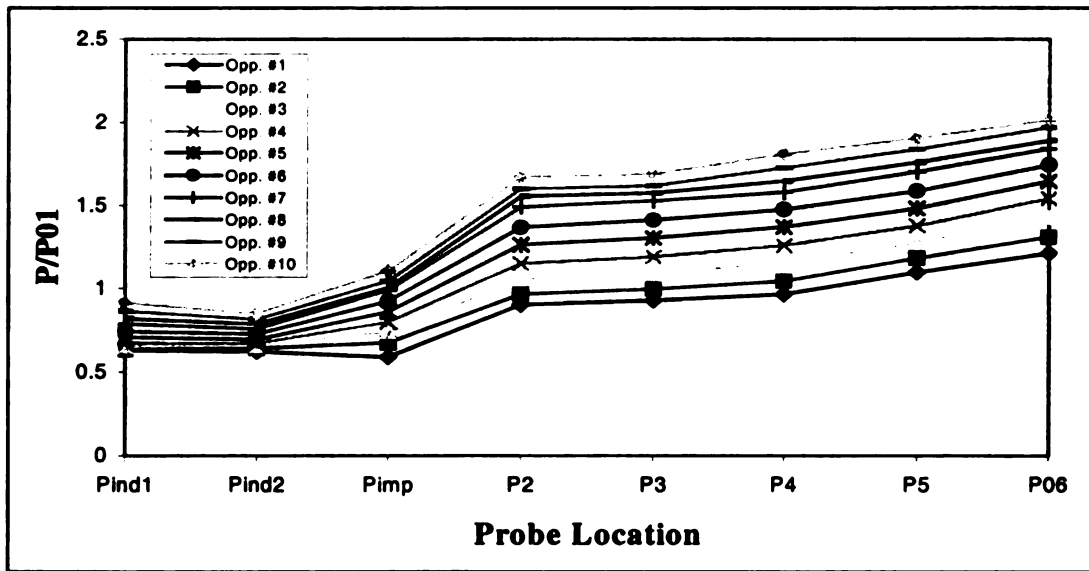
narrow one). But a very wide spacing of the vaneless diffuser walls should not be recommended and this conclusion should be limited by an optimum value of the vaneless diffuser width because of only a small gain in stage efficiency and a great risk of boundary layer separation.

## **5.2 Pressure Rise in the Compressor Stage**

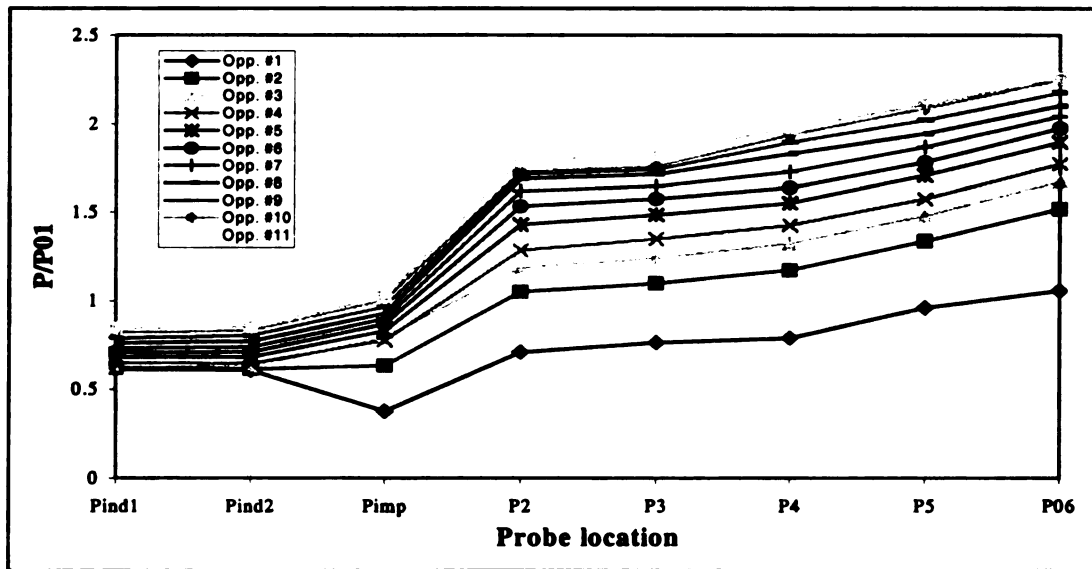
The static pressure from the compressor stage inlet to the compressor stage exit was measured at eight different locations as indicated in chapter four. This is an attempt to understand the effect of changing the vaneless diffuser width on the static pressure rise in the compressor stage. In Figure 5.6 and Figure 5.7, the ratio of the static pressure to the static inlet total pressure has been plotted against the different locations at which the static and total pressures were made. The curves on these figures are for all the different operating points, which range from choked condition (maximum flow) to near compressor stall (minimum flow). The observed differences in terms of pressure ratios for both VNLD1 and VNLD2 were similar for every tested speed. Moreover, the static pressure rise characteristics of each vaneless diffuser were also similar. Thus, the data of impeller speeds 28000 rpm and 32000 rpm for both vaneless diffusers are shown and discussed.

By comparing Figures 5.6 and 5.7, it could be noted that there is no significant differences between them which indicates that by increasing the vaneless diffuser width from that with VNLD1 to that with VNLD2 the static pressure rise in the compressor stage is almost the same and not affected. Thus, by increasing the vaneless diffuser width,



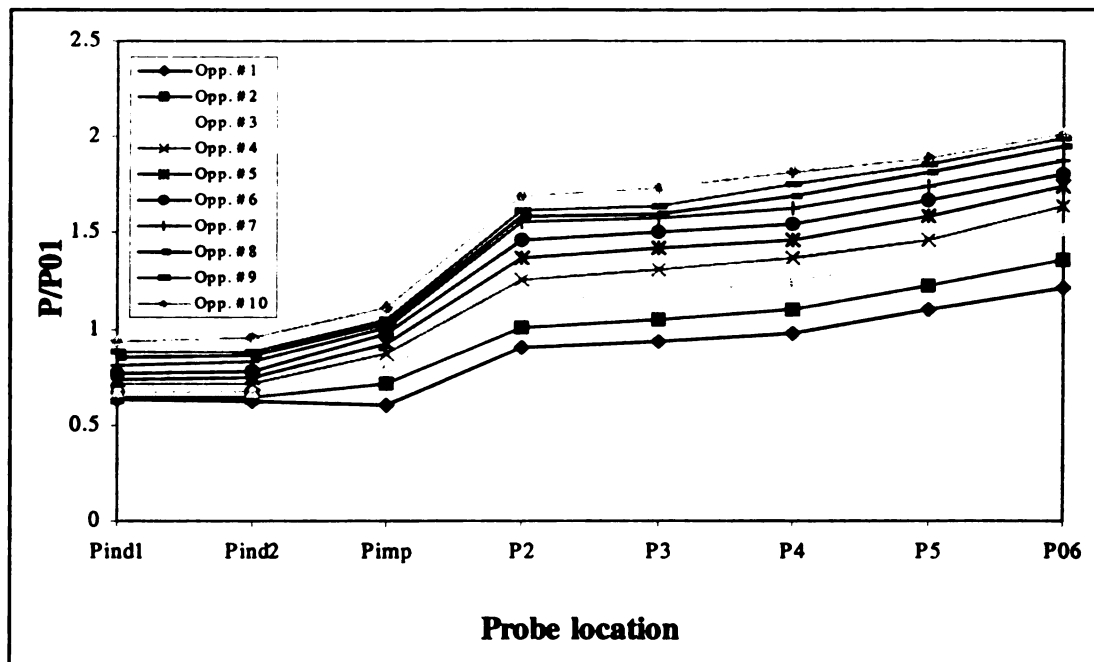


(a) At impeller speed 28000 rpm (Mt=1.04)

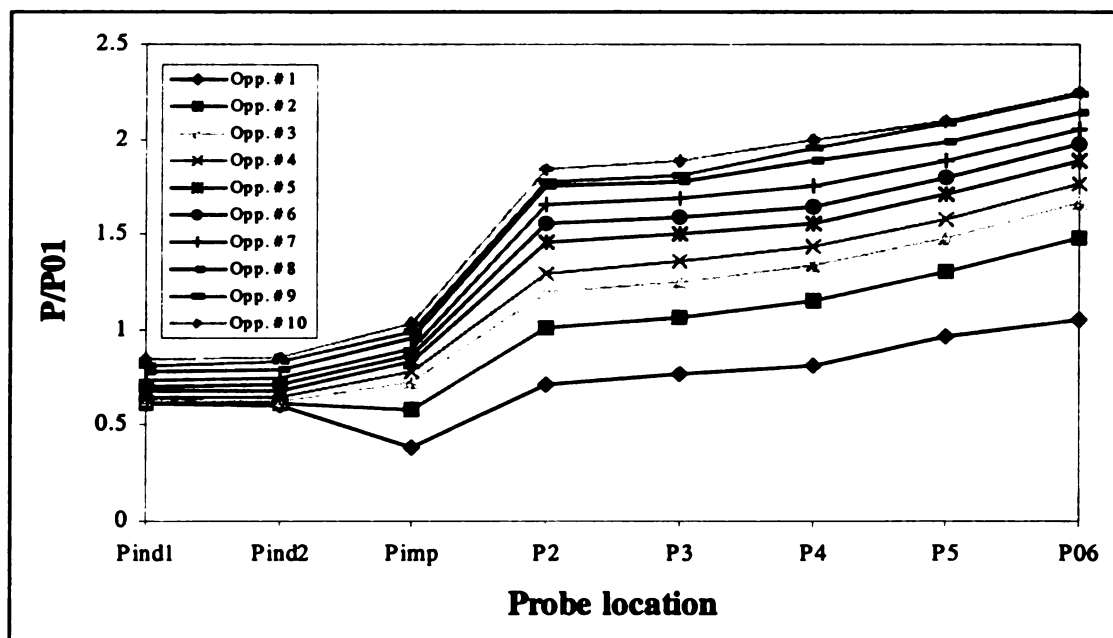


(b) At impeller speed 32000 rpm (Mt=1.19)

**Figure 5.6 Influence of diffuser type on the compressor stage pressure history with VNLD1**



(a) At impeller speed 28000 rpm ( $M_t=1.04$ )



(b) At impeller speed 32000 rpm ( $M_t=1.19$ )

**Figure 5.7 Influence of diffuser type on the compressor stage pressure history with VNLD2**

a better efficiency and a lower loss coefficient could be attained without affecting the pressure rise in the compressor stage. Again that is a restricted conclusion by an optimum width value.

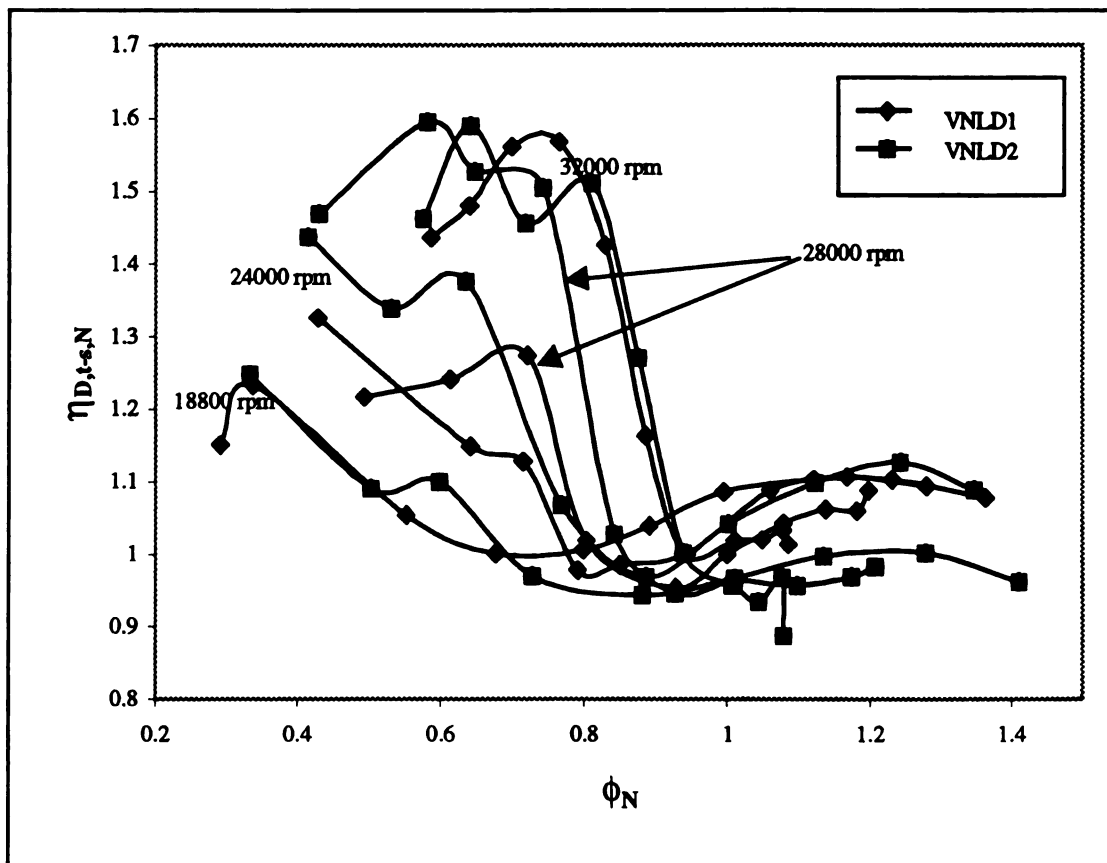
From the static pressure rise in the compressor stage with VNLD1 and VNLD2, the flow in both vaneless diffusers is stable. Moreover, the highest-pressure gain in both VNLD1 and VNLD2 seems to occur at maximum mass flow rates. This could be because at high mass flow rates the flow leaves the impeller more radially than at low mass flow rates. Since the flow angles are higher at high mass flow rates, the flow path in the diffuser is shorter leading to lower flow losses. On the other hand, the volute contributes in the compressor pressure rise at all mass flow rates.

Figure 5.6(b) and Figure 5.7(b) clearly show that the limiting component for maximum flow through the compressor stage is the inducer not the vaneless diffuser. This could be seen from the sudden pressure drop in the impeller at high mass flow rate (Op#1). The inducer choking causes the pressure drop. However, as the mass flow rate is decreased, this phenomenon vanishes.

### **5.3 Overall Vaneless Diffuser Performance Characteristics**

#### **5.3.1 Vaneless Diffuser Efficiency**

The diffuser efficiency defined earlier as a measure of the diffuser performance between the diffuser inlet at  $r_3$  and the diffuser outlet at  $r_5$ . The total-to-static efficiency and static-to-static efficiency for VNLD1 and VNLD2 are shown in Figure 5.8 and Figure 5.9.



**Figure 5.8 Vaneless diffuser performance characteristics: diffuser efficiency total-to-static for VNL D1 and VNL D2**

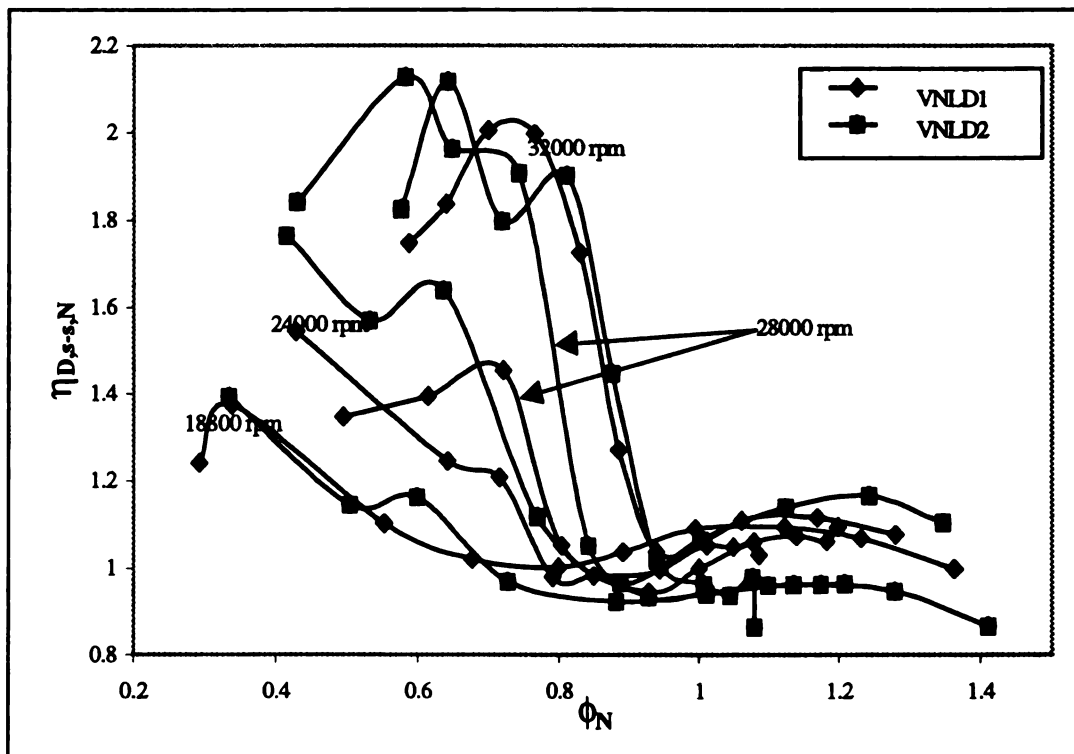


**Figure 5.9 Vaneless diffuser performance characteristics: diffuser efficiency static-to-static for VNLD1 and VNLD2**

Both figures showed that the diffuser efficiency increased as the flow coefficient decreased. Stanitz (1952) has also got this finding. This could be explained by the relationship between the mass flow rate and the velocity. As the flow coefficient decreased, the velocity vectors becomes more tangential so that the flow path in the vaneless diffuser will be longer. This will make the flow diffuses more, and the pressure will rise more in which gives a better performance.

Also, it could be noted from Figure 5.8 and Figure 5.9 that the increase in diffuser efficiency is smooth as the impeller speed low and becomes rapid and sharp as the impeller speed increased. Both cases will be as the flow coefficient decreased. This could be explained by knowing that the diffuser efficiency generally is a ratio of the pressure ratio to the Mach number square of the flow. Generally what is happen is a combination of the numerator increase (pressure ratio) and the denominator decrease (Mach number or velocity), which results in an efficiency increase; and this becomes rapid and sharp as the impeller speed increases.

Regarding increasing the diffuser width, as expected that the diffuser efficiency improved by spacing the diffuser walls farther apart. Both figures show that the diffuser efficiency for VNLD2 is better than that of VNLD1 at all impeller speeds. Until now the wider diffuser (VNLD2) showed a better performance in terms of stage and diffuser efficiencies, and the next step is to check the pressure recoveries.

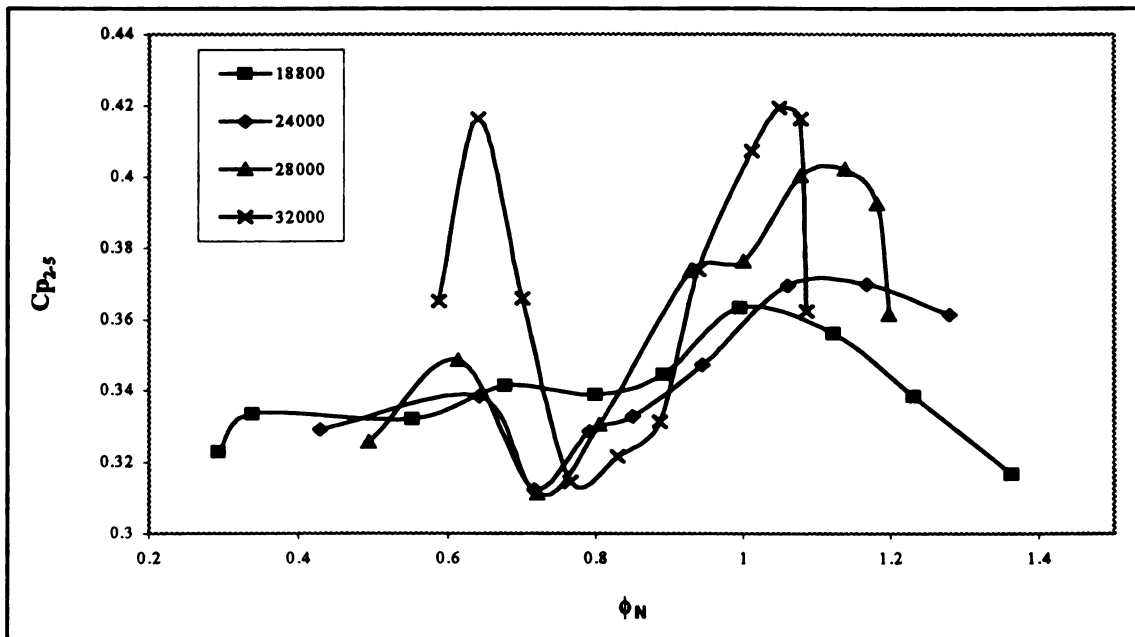
### **5.3.2 Pressure Recovery of the Vaneless Diffusers**

Through this section, the pressure recovery through VNLD1 and VNLD2 will be discussed in details to get more information regarding the differences between the two vaneless diffusers.

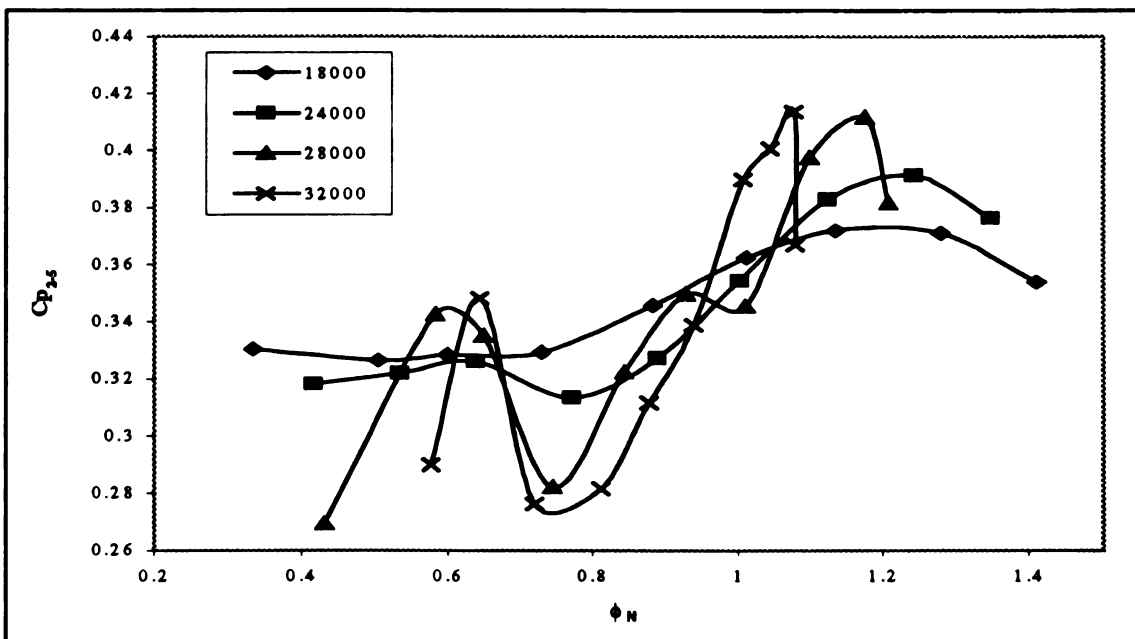
#### **5.3.2.1 Total Pressure Recovery $C_{p_{2-5}}$**

Figure 5. 10 and Figure 5. 11 show the total pressure recovery  $C_{p_{2-5}}$ , from diffuser inlet to diffuser exit, for VNLD1 and VNLD2 at all impeller speeds. As shown on these two figures, there are two peaks with each curve. One of these peaks is near choked condition (maximum flow) and the other near stall (minimum flow). Also it could be noted that all curves have the same trend in which the total pressure recovery decreased as the flow coefficient decreased and increased as the impeller speed increased. At low impeller speed, the  $C_{p_{2-5}}$  curves are smooth and become more disturbed as the impeller speed increased.

By comparing Figure 5. 10 and Figure 5. 11 , it can be seen that VNLD2 has a better  $C_{p_{2-5}}$  than VNLD1 at high flow coefficient and at impeller speeds of 18800 rpm, 24000 rpm, and 28000 rpm. As the flow coefficient decreased, both vaneless diffusers show the same  $C_{p_{2-5}}$  except at high impeller speed where VNLD1 leading VNLD2. Also as the impeller speed increased,  $C_{p_{2-5}}$  becomes more stable with VNLD2 than with VNLD1. Accordingly, increasing the width of the vaneless diffuser from VNLD1 to VNLD2 will improve slightly the pressure recovery  $C_{p_{2-5}}$  in general. This needs to be investigated more by breaking the pressure recovery of the diffuser  $C_{p_{2-5}}$  into the pressure recovery of three different regimes across the diffuser, which will be discussed in the next section.



**Figure 5.10 Variation of Total Diffuser Pressure Recovery  $C_{p2-5}$  for VNLD1**



**Figure 5.11 Variation of Total Diffuser Pressure Recovery  $C_{p2-5}$  for VNLD2**



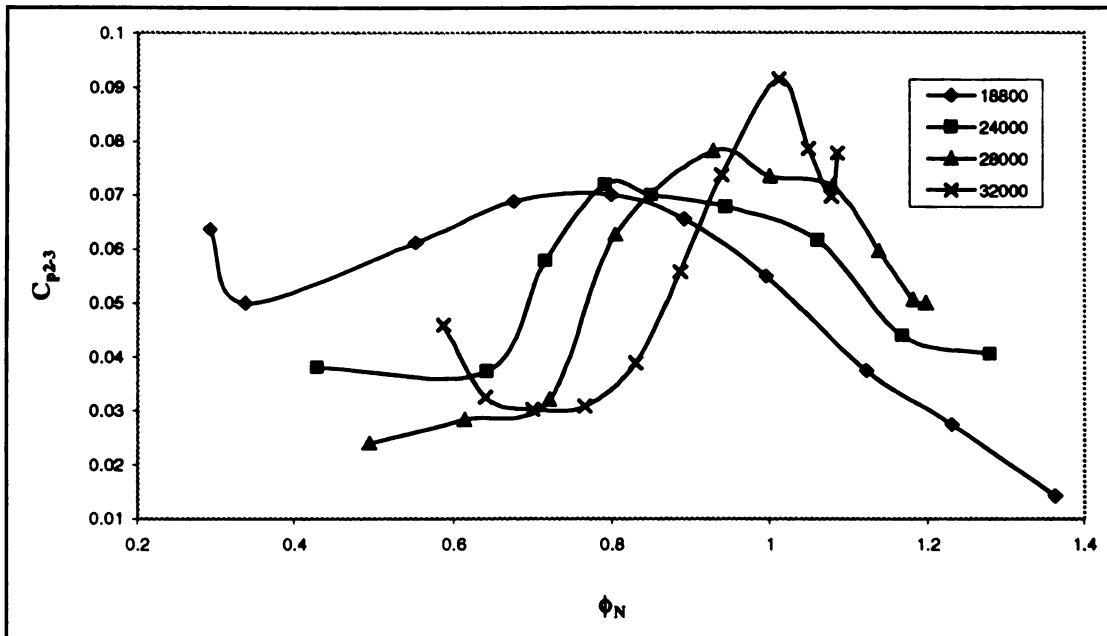


**Figure 5.12 Pressure Recovery  $C_{p2-3}$  for VNLD1**

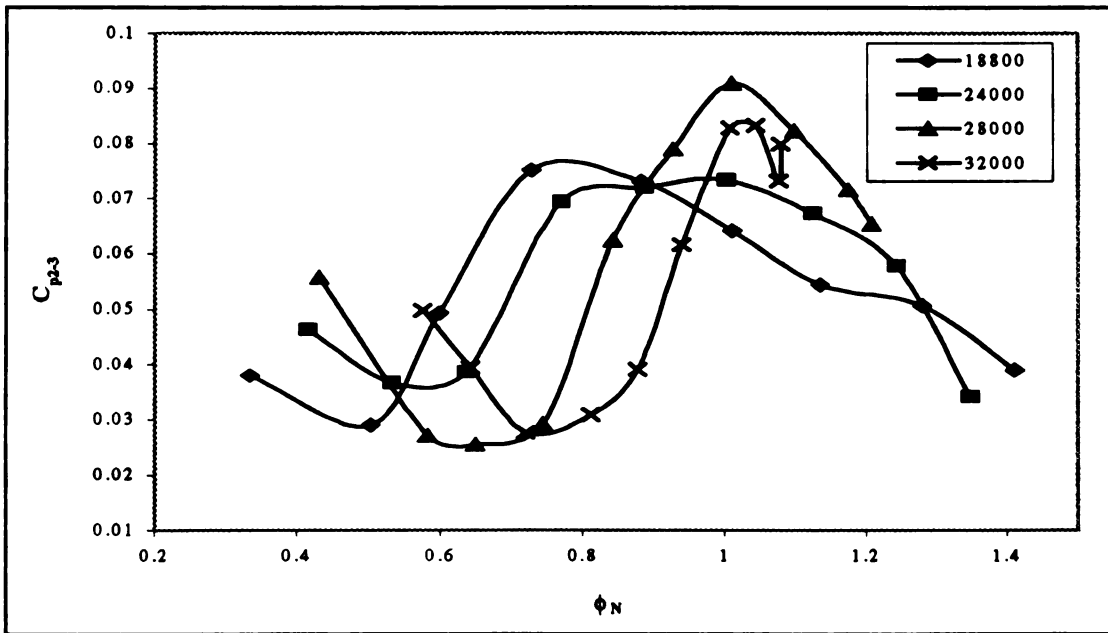


**Figure 5.13 Pressure Recovery  $C_{p2-3}$  for VNLD2**

### 5.3.2.2 Subdivided Pressure Recoveries

Through this section, three different pressure recoveries across the vaneless diffuser will be discussed. They are as follows:

- the pressure recovery in the vaneless space between the impeller exit and the vaneless diffuser inlet ( $C_{p_{2-3}}$ )
- the pressure recovery between the inlet and the middle of the vaneless diffuser ( $C_{p_{3-4}}$ )
- the pressure recovery from the middle to the exit of the vaneless diffuser ( $C_{p_{4-5}}$ )

Figure 5.12 and Figure 5.13 show the pressure recovery in the vaneless space between the impeller exit and the diffuser inlet  $C_{p_{2-3}}$  at all impeller speeds for VNLD1 and VNLD2. As it is shown in these two figures,  $C_{p_{2-3}}$  has a general trend in which it increases smoothly to a peak then it decreased as the flow coefficient decreased. This shows the effect of the width reduction from impeller width to the vaneless diffusers width. The width at the impeller exit is reduced to the vaneless diffuser width in this region due to which there is a flow acceleration in addition to the diffusion by area decrease. The narrower the diffuser, the greater is the flow acceleration and the lower the area decrease. By comparing these two figures, Figure 5.12 and Figure 5.13, it could be seen that  $C_{p_{2-3}}$  increases as the impeller rotational speed increases for both vaneless diffusers. VNLD2 leading VNLD1 at impeller speeds of 18800 RPM, 24000 RPM, and 28000 RPM while VNLD1 leading at 32000 RPM. For both vaneless diffusers and at all impeller speeds,  $C_{p_{2-3}}$  increases again as the flow moving through toward the vaneless diffuser.

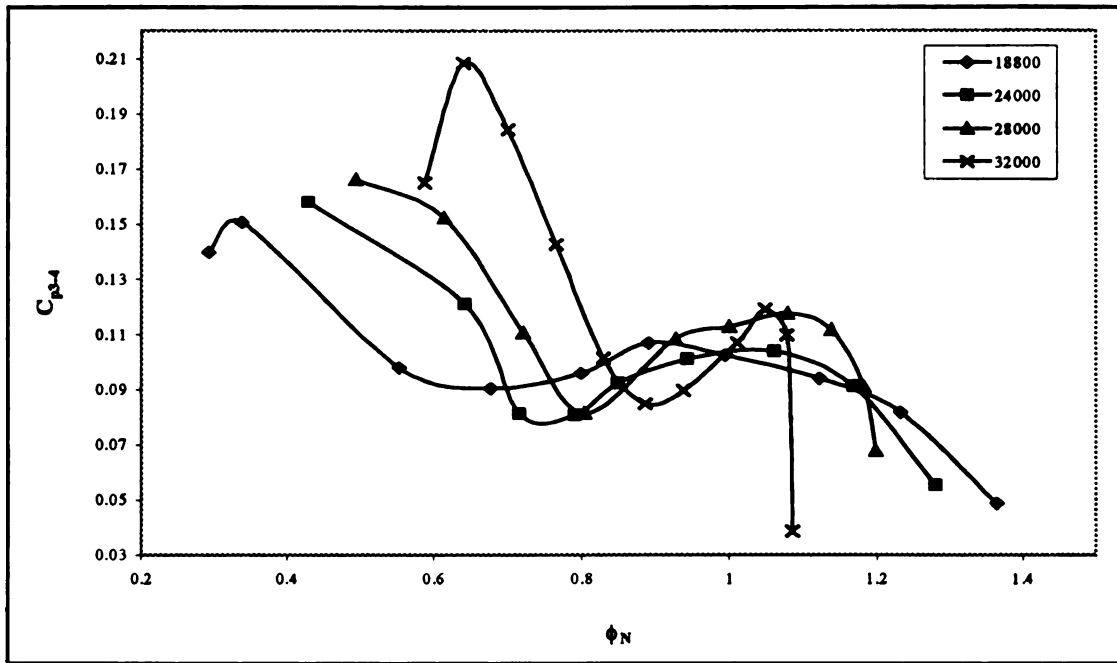


**Figure 5.14 Pressure Recovery  $C_{p3-4}$  for VNLD1**

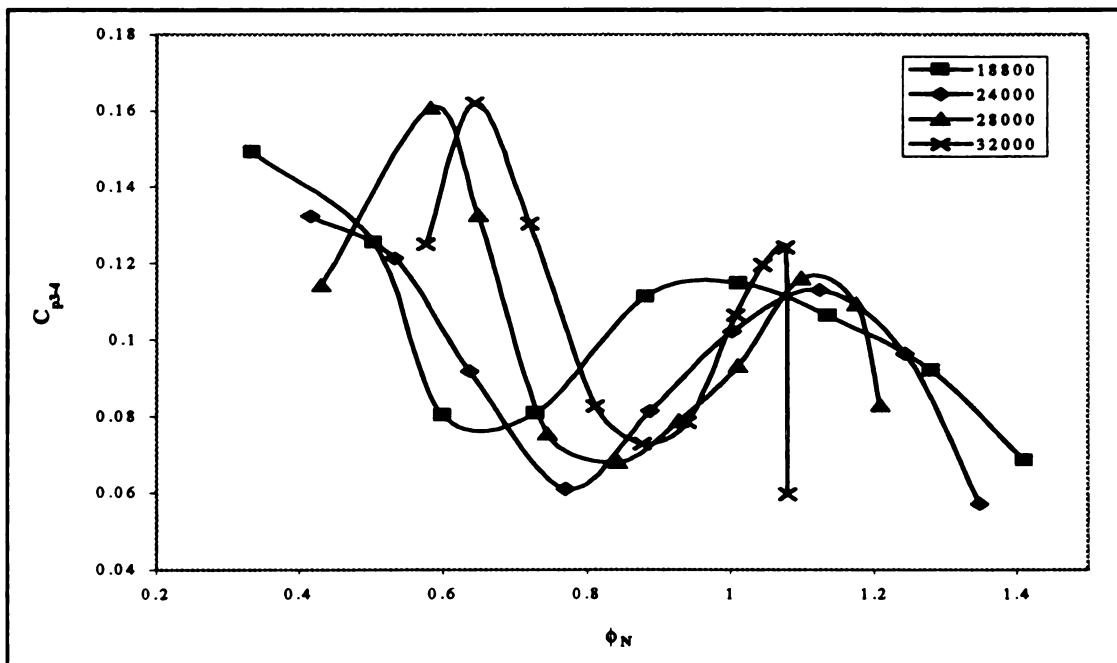


**Figure 5.15 Pressure Recovery  $C_{p3-4}$  for VNLD2**

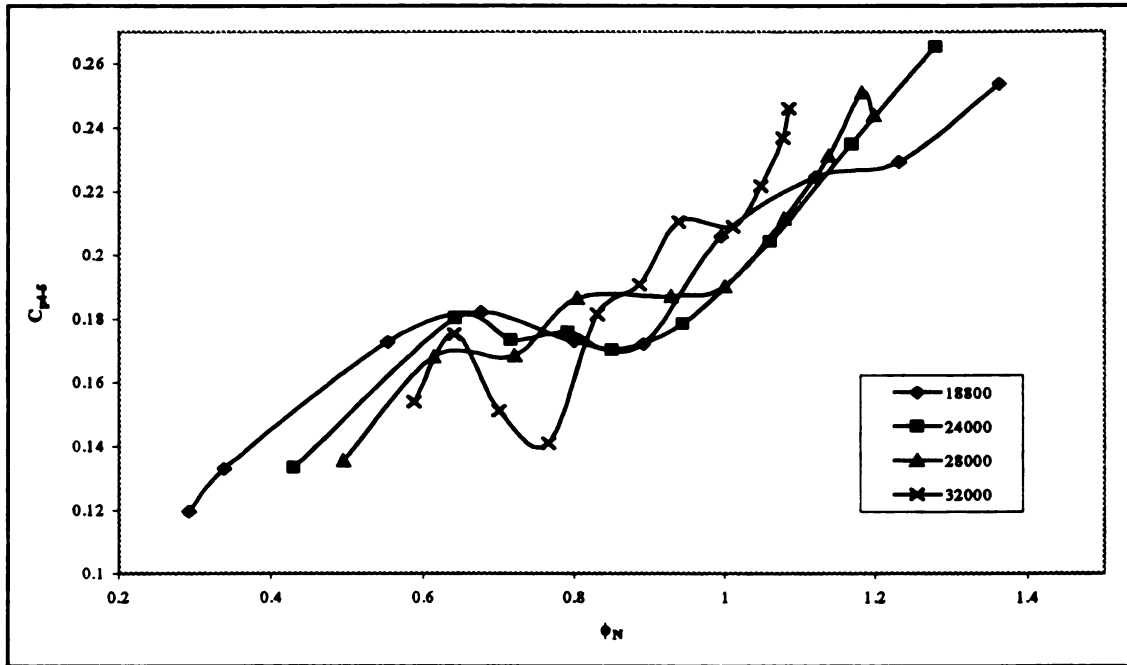


**Figure 5.16 Pressure Recovery  $C_{p4-5}$  for VNLD1**

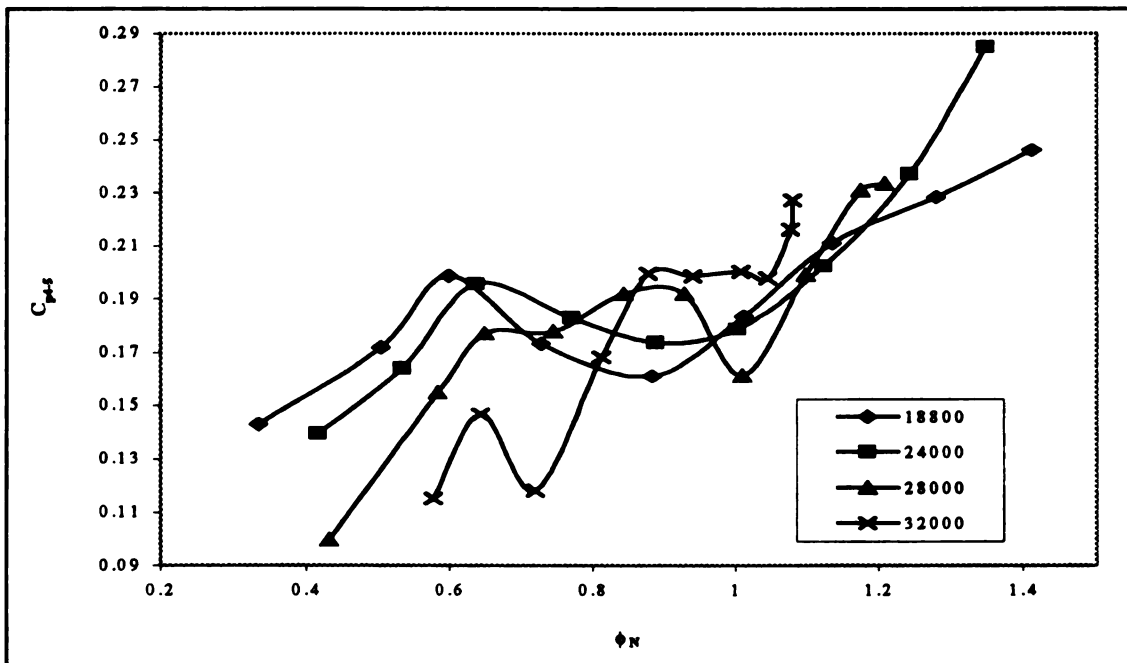


**Figure 5.17 Pressure Recovery  $C_{p4-5}$  for VNLD2**

The pressure recovery between the vaneless diffuser inlet radius and the radius of the middle of the vaneless diffuser  $C_{p3-4}$  is given in Figure 5.14 and Figure 5.15 for both vaneless diffusers and at all impeller rotational speed. For both vaneless diffusers, the  $C_{p3-4}$  increases as the impeller speed increases. Also the  $C_{p3-4}$  increases as the flow coefficient decreases, which is expected because as the velocity decreases the pressure increases as the flow move toward the middle of the vaneless diffuser. The amount of pressure recovery gained through  $C_{p3-4}$  is higher than that by  $C_{p2-3}$  that indicates the effect of the diffuser on pressure recovery as the flow entering the vaneless diffuser. As in  $C_{p2-3}$ , the  $C_{p3-4}$  for VNLD2 is higher than that of VNLD1 for impeller speeds 18800 RPM, 24000 RPM, and 28000 RPM. By comparing the plots for  $C_{p2-3}$  and  $C_{p3-4}$ , it could be noted that these two pressure recoveries are exchanging between each other depending on the flow coefficient. At high flow coefficient,  $C_{p2-3}$  is maximum while  $C_{p3-4}$  is minimum and at low flow coefficient  $C_{p2-3}$  is minimum while  $C_{p3-4}$  is maximum.

As the flow passes the middle of both vaneless diffusers, it gains higher pressure recovery. This could be seen through the plots for the pressure recovery from the middle to the exit of the vaneless diffuser  $C_{p4-5}$ . Figure 5.16 and Figure 5.17 show that the  $C_{p4-5}$  is higher than  $C_{p3-4}$  over the whole range. As shown on these figures that the  $C_{p4-5}$  for both vaneless diffusers is higher at high flow coefficient and decreases as the flow coefficient decreased. This is at all impeller rotational speeds. This could be explained as that at high flow coefficient the flow angles are higher and thus the flow path is small and losses are lower. For both vaneless diffusers, the change in this pressure recovery  $C_{p4-5}$  with impeller rotational speed depends on the flow coefficient.

At high flow coefficient the  $C_{p4-5}$  increases as the impeller speed increased, and at low flow coefficient the  $C_{p4-5}$  decreased as the impeller speed increased. Both vaneless diffusers, VNLD1 and VNLD2, achieved nearly the same  $C_{p4-5}$  at all speeds except at the highest speed of 32000 RPM where VNLD1 is better.

#### **5.4 Comparison Between the Experimental and Theoretical Results**

A comparison between the experimental and the theoretical results in terms of static pressure ratio and the squared of the local flow Mach number  $M^2$  across both vaneless diffusers is presented. The theoretical results presented conclude the assumptions of compressible and incompressible fluid flow. This is to investigate more, experimentally and theoretically, the effects of increasing the diffuser width on the flow in a vaneless diffuser. Because of the similar patterns at all impeller rotational speeds for both vaneless diffusers, only the results for impeller rotational speed of 32000 RPM are presented here.

Figure 5.18 shows the variation in static pressure ratio with the vaneless diffuser radius ratio while Figure 5.19 shows the variation in the squared of the local flow Mach number with the vaneless diffuser radius ratio for both VNLD1 and VNLD2. As shown in both figures that in general the static pressure ratio increased across both vaneless diffusers, while the squared local flow Mach number decreased as expected.

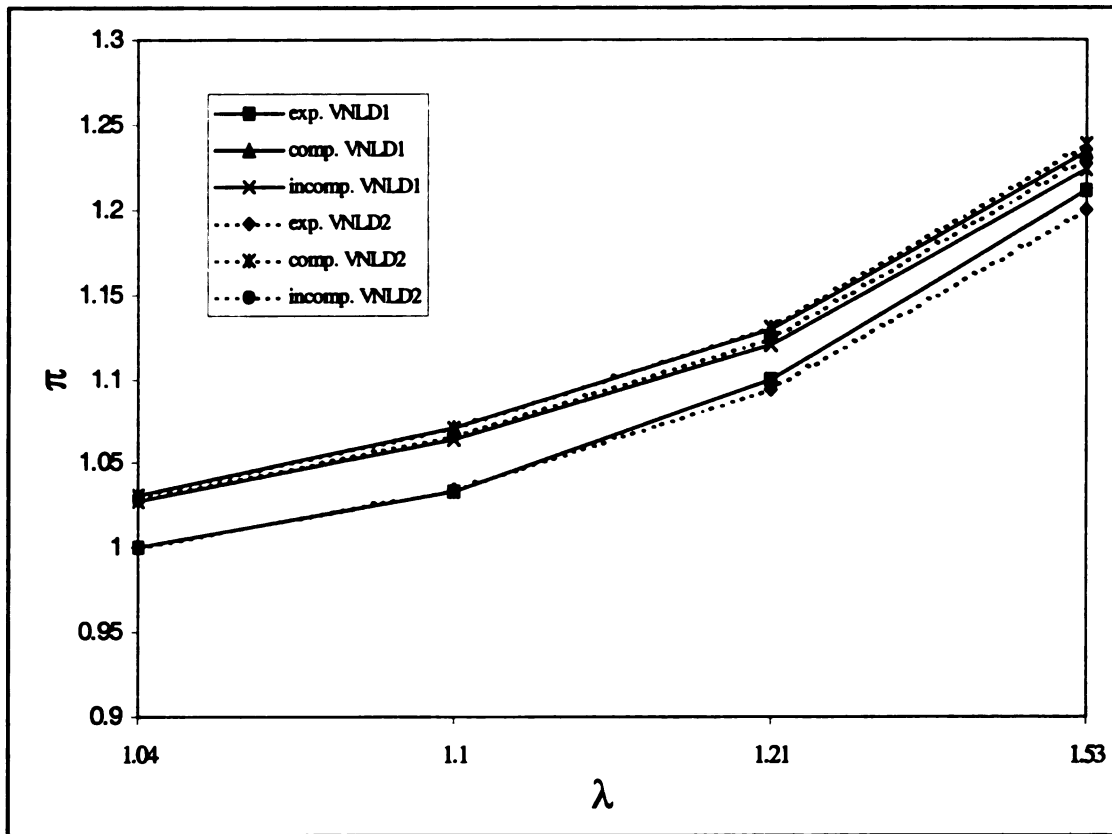


**Figure 5.18 Variation in the Static Pressure Ratio with the Radius ratio for VNLD1 and VNLD2**

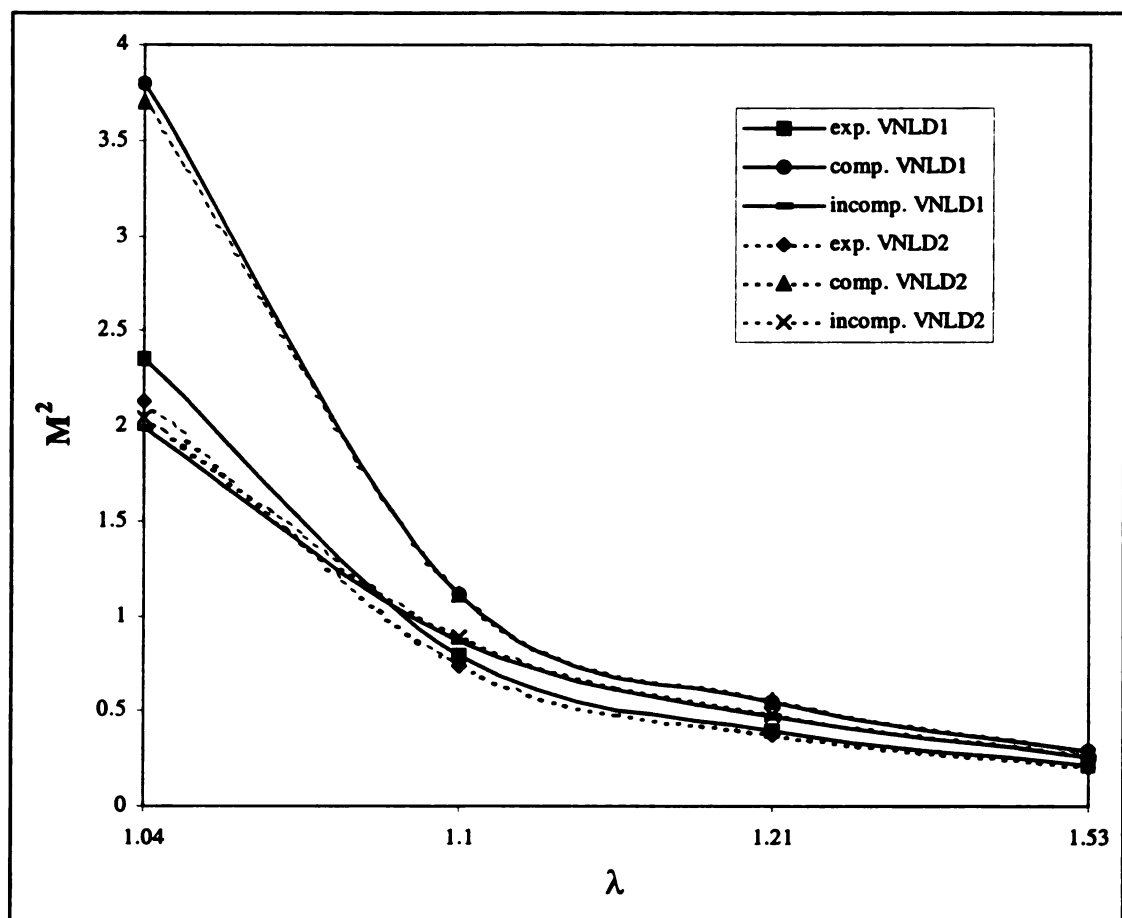


**Figure 5.19 Variation in the squared of Local Flow Mach Number with the Radius ratio for VNLD1 and VNLD2**



The effect of increasing the vaneless diffuser width is to decrease  $M^2$  as shown in Figure 5.19 where the VNLD2 curve is lower than that of VNLD1. This decrease in  $M^2$  results primarily from the decrease in the radial velocity component as a result from the increase flow area that occurs when the diffuser width increased. This decrease in  $M^2$  resulted in an increase in the static pressure ratio as shown in Figure 5.18 where the VNLD2 curves are higher than that of VNLD1. In both figures and for both diffusers, the theoretical results show higher values than the experimental one, which is expected because the theoretical ones are more ideal than the experimental ones, which are the actual. According to these results, increasing the vaneless diffuser width will slightly improve the static pressure rise across the vaneless diffuser.

## **5.5 Unsteady Performance of the Compressor Stage**

Through this section, the unsteady performance of the centrifugal compressor stage with VNLD1 and VNLD2 will be presented and discussed in an attempt to investigate the causes of instability through the compressor stage. This could be done through the four dynamic pressure probes installed in the inducer (Transducer A), the impeller (Transducers B and C), and the diffuser (Transducer D) to measure the pressure fluctuations through the compressor stage.

This unsteady performance analysis has been determined for both vaneless diffusers at each operating point and for every speed. Because of the similar patterns at all impeller rotational speeds, the data of the maximum impeller speed which is 32000 RPM are presented here for VNLD1 and VNLD2. The outputs from transducer B are left out because its signals are almost the same as transducer C. Both transducer B and transducer C were located in the impeller at the same radius but different circumferential position for the purpose of relative effects.

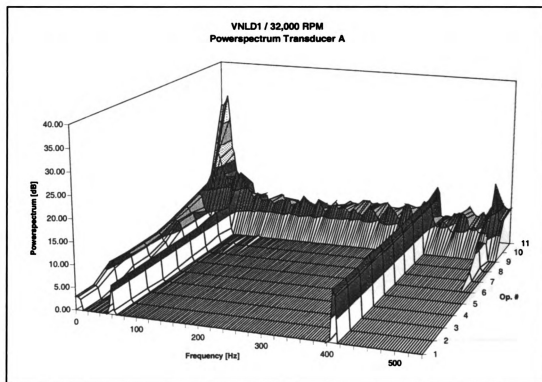
Most rotating stall signals reported in the literature were below the rotational speed of the impeller. For this reason, the data in the range 0-540 Hz are plotted here. Through the centrifugal compressor stage and with both vaneless diffuser and at each transducer, a three-dimensional plot of the power spectrum is presented.

### **5.5.1 Unsteady Flow in the Inducer**

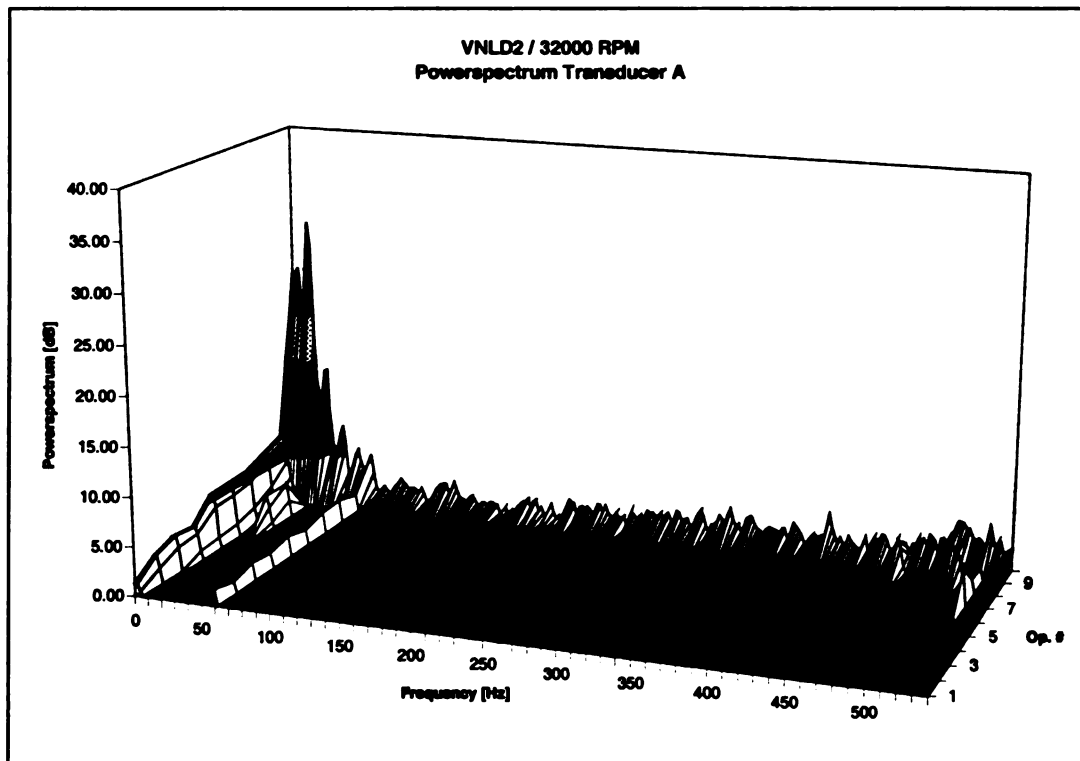
Figure 5.20 and Figure 5.21 show the power spectra of the signal from transducer A at the maximum impeller speed (32000 RPM) for VNLD1 and VNLD2. As shown on this figure and the following figures, the energy level of the unsteady signals at low frequencies is generally larger than at high frequencies. This tendency is common with both vaneless diffusers, at every operating point, at all transducers, and at every impeller rotational speed.

Figure 5.20 shows a rotational frequency of 408 Hz in all four transducers through the compressor stage. The energy level for this peak keeps constant through all the operation points. Also by comparing the two figures (Figure 5.20 and Figure 5.21) it could be seen that one weak peak is present with both vaneless diffusers configuration at a rotational frequency of 60 Hz. This peak is common in all transducers and occurs only at an impeller speed of 32000 RPM. The energy level for this peak is constant for all operating points. Therefore, the 408 Hz with VNLD1 and 60 Hz with both vaneless diffusers are suspected of being caused by either electrical distortions or mechanical vibrations and not in flow phenomena.

No significant pressure fluctuations are found in the inducer at high mass flow rates. However, at low mass flow rates the pressure fluctuations grow at approximately operating point number nine for VNLD1 and VNLD2. These pressure fluctuations indicate the onset of inducer stall. The energy level of these pressure fluctuations with VNLD1 is higher than that with VNLD2, which indicates that the inducer is more stable with VNLD2. The surge phenomena will be discussed through the next section.



**Figure 5.20 Power spectrum of the compressor stage with VNLD1 at 32000 rpm  
Transducer A**



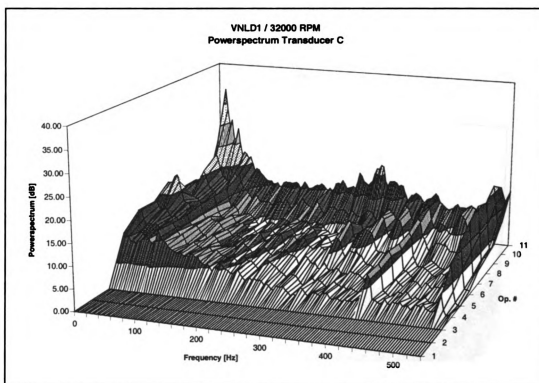
**Figure 5.21 Power spectrum of the compressor stage with VNLD2 at 32000 rpm  
Transducer A**

### **5.5.2 Unsteady Flow in the Impeller**

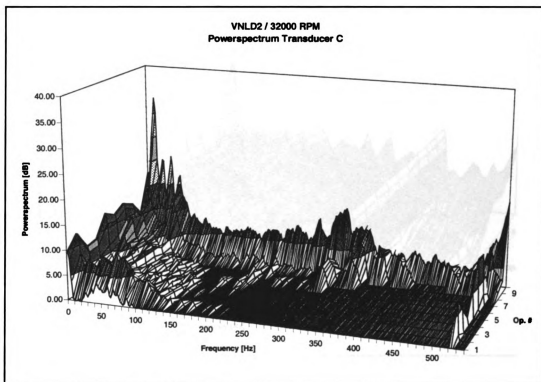
Figure 5.22 and Figure 5.23 shows the power spectra from transducer C at impeller rotational speed of 32000 RPM for VNLD1 and VNLD2. The transducer C is located in the impeller. The energy of the unsteady signals in the impeller is generally higher than in the inducer. For both vaneless diffusers the peak at a frequency of approximately 533 Hz, which corresponds to the impeller rotational speed, is much higher in the impeller than in the inducer.

Figure 5.22 shows that at the first three operating points, VNLD1 is stable in the whole frequency range. The level of energy in the unsteady signals begins to increase after point three to a medium level and constant over approximately the frequency range. On the other hand, VNLD2 in Figure 5.23 shows high energy level at low frequencies in the whole frequency range and through all the operating points. This could be due to the inducer choke and the associated losses. At operation number nine for VNLD1 and number seven for VNLD2 the fluctuations begin to increase. At the last operation for both vaneless diffusers one peak has been found. A strong peak is present with both VNLD1 and VNLD2 at frequency of 12 Hz but with slightly different energy level. The energy in this peak is between 29 and 36 dB. It is much higher than all other signals. Since the peak occurred at the same frequency in all transducer signals, it can be classified as stage surge.

Table 5.1 summaries the characteristic data of the surge phenomena detected with both VNLD1 and VNLD2. Surge is always the responsible phenomena for the operating range limit at low mass flow.



**Figure 5.22 Power spectrum of the compressor stage with VNLD1 at 32000 rpm  
Transducer C**



**Figure 5.23 Power spectrum of the compressor stage with VNLD2 at 32000 rpm  
Transducer C**



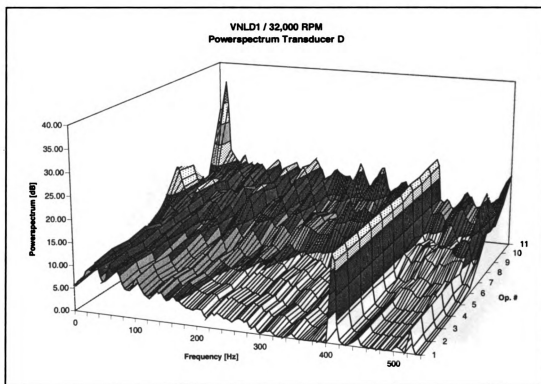


**Figure 5.24 Power spectrum of the compressor stage with VNLD1 at 32000 rpm  
Transducer D**

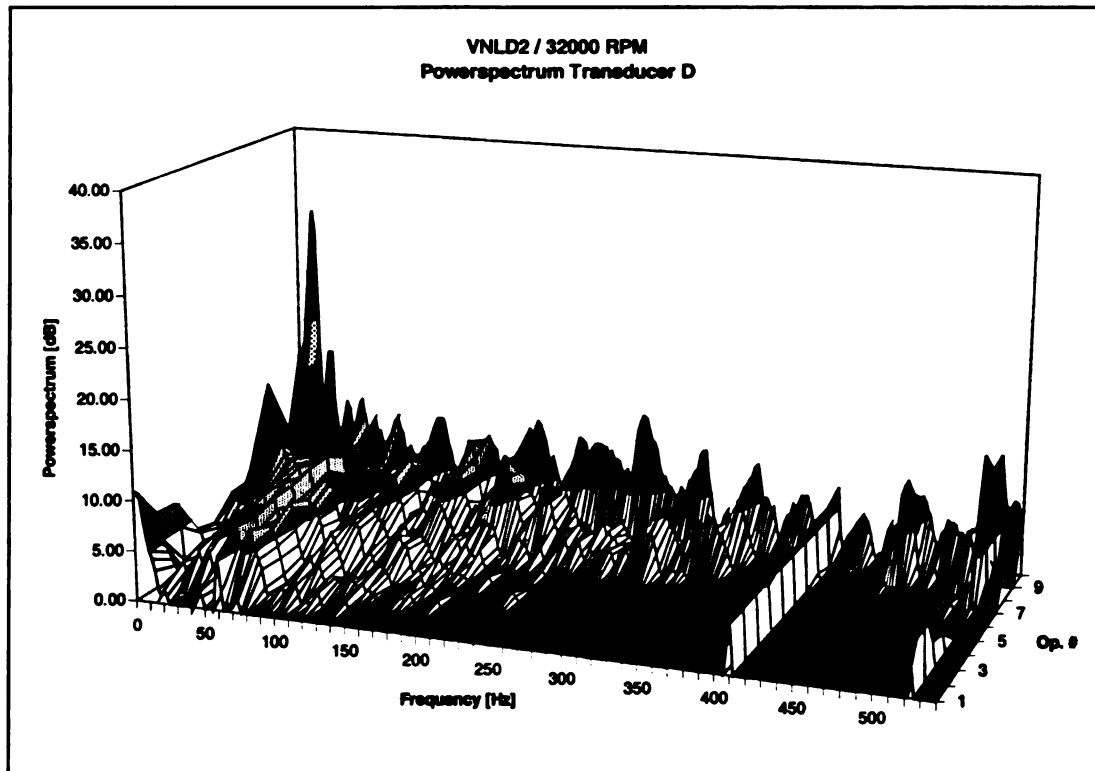


**Figure 5.25 Power spectrum of the compressor stage with VNLD2 at 32000 rpm  
Transducer D**

### 5.5.3 Unsteady Flow in the Diffuser

In Figure 5.5 and 5.6 the power spectra from transducer D at impeller rotational speed of 32000 RPM for VNLD1 and VNLD2 are presented. The transducer D is located in the diffuser.

For VNLD1 in Figure 5.5, the pressure fluctuations are low in the first five operating points. The VNLD1 operates stable in this region, and the fluctuations increase from operation five and on over the whole frequency range. At operation point number eleven, a peak of frequency 12 Hz is found with the highest energy level. This is expected because transducer D is located in the diffuser, and the static pressure is highest in the diffuser.

In Figure 5.6, VNLD2 show a similar trend but with more stability with no pressure fluctuations was detected until operation number seven. After this point, the pressure fluctuations increased and a peak was found at a frequency of 12 Hz.

**Table 5-1 Surge Characteristics through the Compressor Stage with VNLD1 and VNLD2 at all Impeller speeds Using Transducer D**

Diffuser type		18800	24000	28000	32000
		RPM	RPM	RPM	RPM
VNLD1	Surge freq.	6 Hz	6 Hz	8 Hz	12 Hz
	Energy level	26 dB	23 dB	15 dB	35 dB
	Flow coeff.	0.292	0.428	0.494	0.586
VNLD2	Surge freq.	6 Hz	6 Hz	8 Hz	12 Hz
	Energy level	17 dB	16 dB	17 dB	31 dB
	Flow coeff.	0.333	0.414	0.430	0.575

As shown in Table 5-1, the surge frequency increases from 6 Hz to 12 Hz as the impeller rotational speed increased. As shown in this table that the diffuser width has no influence on the surge frequencies while there is a difference in the energy level of the unsteady signals and the surge flow coefficient. VNLD2 show a better stability in which the energy level of the unsteady signals is lower than for VNLD1. Also, the occurrence of surge has been shifted to a lower flow rate with VNLD2 in which it has a wider flow range than VNLD1.

## 6. CONCLUSIONS AND RECOMMENDATIONS

Two vaneless diffusers, VNLD1 and VNLD2, that differ in their passage widths are tested experimentally downstream of the same centrifugal impeller to investigate the effect of this variation on the overall stage performance. Each diffuser was tested at four different impeller speeds: 18800 rpm, 24000 rpm, 28000 rpm, and 32000 rpm. These speeds corresponds to impeller tip Mach numbers of  $M_t = 0.7, 0.89, 1.04, \text{ and } 1.19$ . A theoretical analysis was also carried out from the diffuser inlet radius to the diffuser outlet radius using different values of radius ratio. The results of this theoretical analysis were compared to the measured performance curves of both vaneless diffusers. In addition to that, unsteady analysis was carried out by measuring the pressure fluctuations through the centrifugal compressor components with both vaneless diffusers.

The overall performance of the compressor stage with VNLD2 showed a better performance than with VNLD1 at impeller tip speeds of 18800 RPM, 24000 RPM, and 28000 RPM. It has been found also that the centrifugal compressor stage with VNLD2 had a wider flow range than with VNLD1 at each impeller speed. This has been attained as the choke flow shifted to a higher flow coefficient and the surge point to a lower flow coefficient for the compressor stage with VNLD2. In addition to stage efficiency, the diffuser efficiencies, total-to-static and static-to-static, have been compared for both vaneless diffusers. For both VNLD1 and VNLD2 the efficiencies increased as the flow coefficient decreased. It has been found that the diffuser efficiency slightly improved by spacing the diffuser walls farther apart.

In addition to studying the overall performance of the compressor stage and the vaneless diffuser, the pressure recovery of VNLD1 and VNLD2 was studied from the diffuser inlet radius to the diffuser exit through the total pressure recovery and the subdivided pressure recoveries. For both vaneless diffusers, it was found that the major part of the pressure recovery through the vaneless diffuser occurred between the middle to the exit radii. It was also found that the pressure recovery between the impeller exit and the diffuser inlet contributes in the total pressure recovery Cp2-5. Similar findings to the stage performance have been found with the pressure recovery in which VNLD2 gives better pressure recovery at impeller speeds of 18800 RPM, 24000 RPM, and 28000 RPM. The variation in the static pressure ratio and the square of the local Mach number has been carried out with the radius ratio from the diffuser inlet to the diffuser outlet radii for both vaneless diffusers. The experimental and theoretical results were similar. As expected it has been found that across the diffuser, the pressure ratio increased and the velocity decreased. Also, it has been found that increasing the diffuser wall spacing will result in a decreased the velocity and, as a result an increased pressure ratio.

The unsteady results showed that with increasing the diffuser width the impeller rotating stall was shifted to lower flow rates at all impeller rotating speeds. At the same time, the frequencies of the rotating stalls decreased as the diffuser width increased.

According to these results, it could be concluded that increasing the vaneless diffuser width would improve the compressor stage efficiency, attain wider operating range, and give more stable operation at low to medium impeller speeds. At the same time, as the vaneless diffuser width increased, the length of the flow path increased, which should result in increased losses. A very wide spacing of the diffuser walls should

not be recommended because of a small gain in efficiency and a great risk of separation. The overall performance results for the stage, which have been found through this work, may show that the difference between these two vaneless diffusers, which is approximately 17 %, is within the optimum width. However, according to these results, increasing the diffuser width is not recommended at high impeller rotating speeds (more than 28000 RPM). Therefore the effects at high impeller speeds should be the subjects of further investigation. Through this work the results were related to the flow coefficient through the compressor stage. For future investigations, it will also be helpful to investigate the results not only to the flow coefficient but also to the flow angle at the vaneless diffuser inlet. During these experiments, the total pressure  $P_{03}$ , which has been used to calculate the flow angle at the diffuser inlet, was measured by Kiel type probe located in the middle of the flow channel. This probe is suspected to be too large relative to the channel height, resulting in incorrect values at lower mass flow rates.

## **BIBLIOGRAPHY**



## **BIBLIOGRAPHY**

Amineni, Naresh K, 1996, "Design and Development of Advanced Vaned Diffusers for Centrifugal Compressors," Ph.D. thesis, Michigan State University.

Aungier, R. H., 1988, "A Systematic Procedure for the Aerodynamic Design of Vaned Diffusers," Flow in Non Rotating Turbomachinery Components, ASME FED - Vol. 69, pp. 27-34.

Bammert, K., Jansen, M., and Rautenberg, M., 1983, "On the Influence of the Diffuser Inlet Shape on the Performance of a Centrifugal Compressor Stage," ASME Paper No. 83-GT-9.

Barina, F. J., 1947, "Comparative Performance of Two Vaneless Diffusers Designed With Different Rates of Passage Curvature for Mixed-Flow Impellers," NASA 1490.

Bradshaw, G. R. and Laskin, E. B., 1948, "Experimental Study of Effects of Vaneless-Diffuser Diameter on Diffuser Performance," NACA TN 1713.

Brown, W. B., 1947, "Friction Coefficients in A Vaneless Difuser," NACA TN 1311.

Brown, W. B. and Bradshaw, G. R., 1947, "Method of Designing Vaneless Diffusers and Experimental Investigation of Certain Undetermined Parameters," NACA TN 1426.

Camatti, M., Betti, D., and Giachi, M., 1995, "Vaned Diffusers Development Using Numerical and Experimental Techniques," ASME Paper No. 95-WA/PID-4.

Clements, W. W., and Artt, D. W., 1987, "The Influence of Diffuser Channel Geometry on the Flow Range and Efficiency of a Centrifugal Compressor," Proceedings Institute of Mechanical Engineers, Vol. 201, pp. 145-152.

Clements, W. W., and Artt, D. W., 1988, "The Influence of Diffuser Channel Length - Width Ratio on the Efficiency of a Centrifugal Compressor," Proceedings Institute of Mechanical Engineers, Vol. 202, pp. 163-169.

Conrad, O., Raif, K., and Wessels, M., 1980 "The Calculation of Performance Maps for Centrifugal Compressors with Vane - Island Diffusers," Performance Prediction of Centrifugal Pumps and Compressors, ASME, pp. 135-147.

Dean, R. C., and Senoo, Y., 1960, "Rotating Wakes in Vaneless Diffusers," ASME Journal of Basic Engineering, Vol. 82, pp. 563-574.

Dixon, S. L., "Fluid Mechanics, Thermodynamics of Turbomachinery," University of Liverpool, 3<sup>rd</sup> edition, Pergamon Press, London.

Eckadt, D., 1976, "Detailed Flow Investigations Within a High-Speed Centrifugal Compressor Impeller," Journal of Fluid Engineering, Trans. ASME.

Engeda, A., 1996, "ME 940 Class Notes Advanced Turbomachinery," ME Dept., MSU.

Engeda, A., 1995-1, "Numerical Flow Prediction of the Diffusion Process in a Radial Vaneless Diffuser," ASME, Numerical Simulation in Turbomachinery, FED-Vol. 227, pp. 153-158.

Engeda, A., 1995-2, "Simple Theoretical Analyses of the Diffusion Process in a Radial Vaneless Diffuser," ASME, Complex and Separation Flows, FED-Vol 217, pp. 61-66.

Frigne, P. & al, 1980, "Rotating Non Uniform Flow in Radial Compressors," AGARD CP 282.

Hintelmann, M., 1994, "A design Method for Airfoil Vaned Diffusers for Centrifugal Compressors" Diploma Thesis, MSU, East Lansing.

Holman, J. P., "Experimental Methods for Engineers," 6<sup>th</sup> edition, McGraw-Hill, Inc., New York.

Inoue, M and Cumpsty, N. A., 1984, "Experimental Study of Centrifugal Impeller Discharge Flow in Vaneless and Vaned Diffusers," *Journal of Engineering of gas Turbines and Power*, Vol. 106, pp. 455-467.

Jansen, W., 1964, "Steady Fluid Flow in a Radial Vaneless Diffuser," *ASME, Journal of Basic Engineering*, Vol. 86, pp. 607-619.

Japikse, D., 1984, "Turbomachinery Diffuser Design Technology," *The Design Technology Series (DTS-1)*, Concepts ETI, Inc., Norwich, Vermont.

Jiang, T., and Yang, T., 1982, "Improved Vane Island Diffusers at High Swirl," *ASME Paper No. 82-GT-68*.

Johnston, J. P., and Dean, R. C., 1966, "Losses in Vaneless Diffusers of Centrifugal Compressors and Pumps: Analysis, Experiment, and Design," *ASME Journal of Engineering for Power*, Vol. 88, pp. 49-60.

Kenny, D. P., 1972, "A Comparison of the Predicted and Measured Performance of High Pressure Ratio Centrifugal Compressor Diffusers," *Advanced Radial Compressors, VKI Lecture Series 50*.

Kim, Won J., 1998, "Design and Development of Low Solidity Vaned Diffusers for Centrifugal Compressors," *Ph.D. thesis, Michigan State University*.

Kline, S. J., Abbott, D. E., and Fox, R. W., 1959, "Optimum Design of Straight Walled Diffusers," *ASME Journal of Basic Engineering*, Vol. XXX, pp. 321-331.

Ligrani, P.M. & al, 1982, "Rotating Stall Measurements in the Vaneless Diffuser of a Radial Flow Compressor *ASME Paper 82-GT-257*.

Logan, E., 1993, "Turbomachinery: basic theory & applications," 2<sup>nd</sup> edition, Arizona State University, Tempe, Arizona.

Miller, R. W., 1992, "Flow Measurement Engineering Handbook," Second Edition, Mc Graw Hill.

Nishida H. & al, 1995, "A Study on the Rotating Stall of Centrifugal Compressors," Hitachi Ltd., Ibaraki, Japan Achieved by personal correspondence with Jean - Luc Di Liberti.

Pampreen, R.C., 1993, "Compressor Surge and Stall Concept," ETI, inc.

Polikovsky, V. and Nevelson, M., 1942, "The Performance of a Vaneless Diffuser Fan," NACA TM 1038.

Reeves, G. B., 1977, "Estimation of Centrifugal Compressor Stability With Diffuser Loss Range System," ASME Journal of Fluid Engineering, Vol. 99, pp. 76-83.

Reneau, L.R., Johnston, J. P., and Kline, S. J., 1967, "Performance and Design of Straight, Two - Dimensional Diffusers", ASME Journal of Basic Engineering, Vol. 89, pp. 141-150.

Rhoden, H.G., 1956, "Effects of Reynolds Number on the Flow of Air through a Cascade of Compressor Blades," Aeronautical Research Council R. & M. No 2919.

Rodgers, C., 1982, "The Performance of Centrifugal Compressor Channel Diffusers," ASME Paper No. 82-GT-10.

Runstadler, P.W., and Dean, R. C., Jr., 1969, "Straight Channel Diffuser Performance at High Mach Numbers," Journal of Basic Engineering.

Runstadler, P.W., Jr., Dolan, F. X., and Dean, R. C., Jr., 1975, "Diffuser Data Book," Creare TN-186.

Schlichting, H., 1987, "Boundary-Layer Theory", translated by J. Kestin, McGraw-Hill, Inc., 7<sup>th</sup> edition.

Senoo, Y. & al, 1978, "Limits of Rotating Stall and Stall in Vaneless Diffuser of Centrifugal Compressor," ASME Paper No. 78-GT-19.

Senoo, Y. & al., 1979, "Experimental Study on Flow in a Supersonic Centrifugal Impeller," Journal of Engineering for Power, pp.32-41.

Stanitz, J. D., 1952, "One-Dimensional Compressible Flow in Vaneless Diffusers of Radial- and Mixed-Flow Centrifugal Compressors, Including Effects of Friction, Heat Transfer, and Area Change," NACA TN 2610.

Stein, W., and Rautenberg, M., 1985, "Flow Measurements in Two Cambered Vane Diffusers With Different Passage Widths," ASME Paper No. 85-GT-46.

Stuart, D.J.K., 1955, "Analysis of Reynolds Number Effects in Fluid through Two-Dimensional Cascades," Aeronautical Research Council R. & M. No 2920.

Vavra, M.H., 1960, "Aero Thermodynamics and Flow in Turbomachines," John Wiley & Sons, Inc.

Whitfield, A. and Roberts, D. V., 1983, "Alternative Vaneless Diffusers and Collecting Volute for Turbocharger Compressors," ASME, 83-GT-32.

Wilmsen, B., 1996, "Design and Development of an Unsteady Data Acquisition System for Centrifugal Compressor," Master Thesis, Michigan State University.

Wilson, D.G., 1991, "The Design of High-Efficiency Turbomachinery and Gas Turbines," The MIT Press, 5<sup>th</sup> edition, Cambridge.

Yoshinaga, Y., Gyobu, I., Mishina, H., Koseki, F., and Nishida, H., 1980, "Aerodynamic Performance of a Centrifugal Compressor With Vaned Diffuser," ASME Journal of Fluid Engineering, Vol. 102, pp. 486-493.

Yingkang, Z. and Sjolander, S. A., 1987, "Effect of Geometry on the Performance of Radial Vaneless Diffusers," ASME, Journal of Turbomachinery, Vol. 109, pp. 550-556.